

Development of high-performance thiazolothiazole-based semiconducting polymers for organic solar cells

(有機太陽電池の高効率化に向けたチアゾロチアゾール系半導体ポリマーの開発)

Masahiko Saito

2015

Department of Applied Chemistry, Graduate School of Engineering
Hiroshima University

Contents

1. General Introduction

2. Application of thiophene-thiazolothiazole copolymers originally designed for field effect transistor for organic photovoltaic device.

3. Thiophene-thiazolothiazole copolymers: drastic change of molecular orientation by molecular-weight control and blending with PC₆₁BM lead to high efficiencies in solar cells

4. Thiophene-thiazolothiazole copolymers: significant impact of side chain composition on backbone orientation and solar cell performance

5. Thiophene-thiazolothiazole copolymers: effect of side chain position on crystallinity and solar cell performance

6. Synthesis and Photovoltaic Properties of Thiophene-Thiazolothiazole Copolymers with Oxygen Containing Functional Groups as The Side Chain

7. OPV Characteristics of Semiconducting Polymer with Thiazolothiazole and Naphthobisthiadiazole in the Backbone

8. Closing Remarks

9. List of Publications

Acknowledgement

Chapter 1

General Introduction

1-1. Organic Photovoltaics

Due to the potential application to next generation ultra-thin, large-area, and/or flexible devices, organic field-effect transistors (OFETs),^[1] organic light-emitting diodes (OLEDs),^[2] and organic photovoltaics (OPVs),^[3] have been intensively studied in the last two decades. In particular, OPVs have drawn much attention as a new renewable energy source.

One of the largest breakthrough in OPVs was reported by Tang and coworkers in 1986,^[4] in which a bilayer structure of copper (II) phthalocyanine (CuPC) and anthra[9,1,2-c,d,e:10,5,6-c',d',e']bis[benzimidazolo[2,1-a]-isoquinoline]-10,21-dione (PTCBI) (**Figure 1.1**) was fabricated by vapor deposition. Although the power conversion efficiency (PCE) the cell was 1%, the report triggered the wave of OPV reserches. Since then, various approaches have been conducted to improve PCE, for example, modification of the device structure,^[5] and device process,^[6] and the development of the materials.^[7] which raised PCEs > 10% in single junction and > 11% in multi-junction OPVs.^[8]

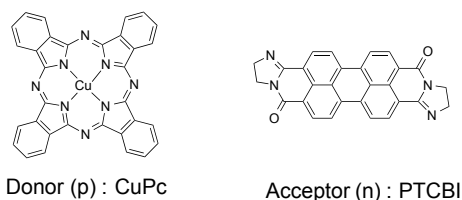


Figure 1.1 Chemical structure of CuPc and PTCBI

1-2. Fundamental mechanism of OPV

Main parameters of solar cells are short-circuit current density J_{SC} (mA/cm^2), fill factor FF, open-circuit voltage V_{OC} (V) and power conversion efficiency PCE (%). Current density and voltage at the maximum output are represented by J_{max} and V_{max} , respectively (**Figure 1.2a**). FF is determined by the following relationship.

$$FF = (J_{max} \times V_{max}) / (J_{SC} \times V_{OC}) - (1)$$

PCE is determined by the following relationship, where the energy of incident light (P_{inc}) is usually 100 (mW) *i.e.*, 1 sun, in case of AM 1.5G.

$$\text{PCE} = \{(J_{\text{max}} \times V_{\text{max}}) / P_{\text{inc}}\} \times 100 = J_{\text{SC}} \times V_{\text{OC}} \times \text{FF} - (2)$$

In OPV cells, sunlight is absorbed by the photoactive layers composed of donor (p-type) and acceptor (n-type) organic semiconducting materials to generate photocurrents. The p-type material donate electrons and transports holes, and the n-type material accept electrons and transports electrons. As shown in **Figure 1.2b** and **1.2c**, fundamental mechanism of photoelectric conversion can be divided roughly into three elementary processes. The active layer absorb sunlight (1-1. light absorption) and generates excitons (1-2. Exciton generation), which can be called light absorption process. The excitons then diffuse to the interface of the p-type and n-type materials (2-1. exciton diffusion) and separate into holes and electrons (2-2. charge separation), which can be called charge generation process. The generated holes and electrons move to the anode and cathode, respectively, through the domains of the corresponding materials (3-1. charge transport) and extracted at the electrodes (3-2. charge injection), which can be called charge carrier collection process.

It is therefore the improvement of the efficiency of these fundamental processes leads to the improvement of overall PCE of the corresponding cell. J_{SC} is determined by the quantity of the collected charge carriers that were generated by the sunlight absorption and thus is largely affected by all the three fundamental processes. In order to obtain high J_{SC} , the active layer must absorb as much sunlight as possible to generate excitons. Since charge separation occurs at the p/n interface in the active layer and the diffusion length of exciton is typically ~ 10 nm, the active layer must have as large interface area as possible. It is noted that for charge separation (electron transfer from the p-type to the n-type material), it is widely accepted that the offset of the lowest unoccupied molecular orbital (LUMO) energy levels between the p-type and n-type materials is required to be more than 0.3 eV (**Figure 1.2d**). Well-developed paths of the materials and high charge carrier mobility are necessary to collect the charge carriers at the electrode. V_{OC} is mostly determined by the energetics between the p-type and n-type materials; V_{OC} is proportional to the difference of the energy level between the highest occupied molecular orbital (HOMO) of the p-type and LUMO of the n-type materials (E_{diff}) (**Figure 1.2d**). Thus, a large E_{diff} is required to obtain a high

V_{OC} . It is important to note that V_{OC} is also affected by charge recombinations that occur in the charge generation process, which is called geminate recombination, and in the charge carrier collection process, which is called bimolecular recombination. FF is roughly determined by resistance of the active layer and thus largely affected by the charge carrier collection processes, including charge recombinations. Thus, as similar to the requirement for high J_{SC} , well-developed paths of the materials and high charge carrier mobility are necessary.

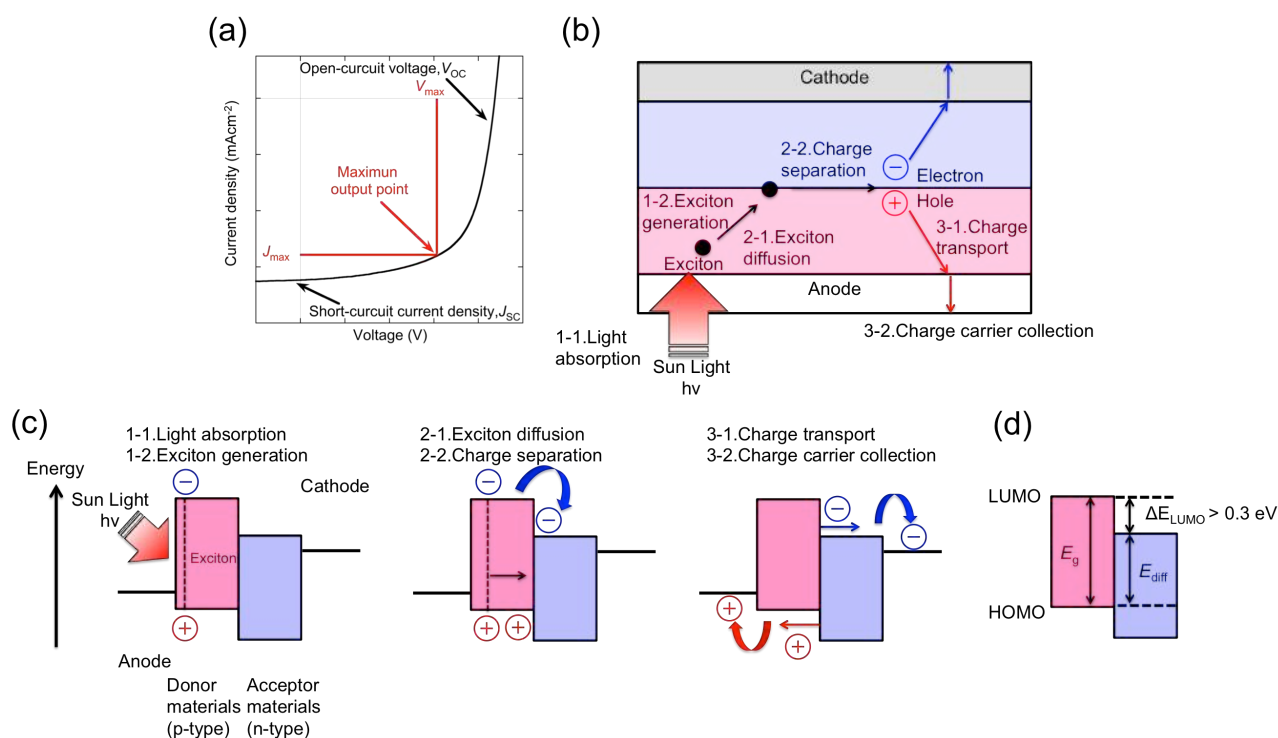


Figure 1.2 (a) J - V curve and relationship of J_{SC} , V_{OC} , and FF. (b) Schematic illustration of photoelectric conversion in organic photovoltaics. (c) Fundamental mechanism of photoelectric conversion using energy diagrams. (d) Important parameters that determine the photovoltaic properties.

1-3. Approaches to improve the PCE

1-3-1. Device structures

There are three representative device structures reported for OPVs. “Bilayer structure”, which is the simplest structure of OPV cells, contains planarly stacked p-type and n-type material layers in between the electrodes (**Figure 1.3a**). Given the mechanism of the charge separation process, the bilayer structure can generate limited amount of charge carriers and thus afford relatively low J_{SC} , since the area of the p/n interface is limited. To

overcome this limitation, “p-i-n structure” (**Figure 1.3b**) was contrived by Hiramoto and co-workers^[9]. The term “i” means an intrinsic layer (mixture of p- and n-type materials). In this structure, the i-layer offer significantly increased area of the p/n interface, which leads to the improvement of J_{SC} . On the other hand, “bulk heterojunction (BHJ) structure” (**Figure 1.3c**) is a cell with a single active-layer that is a mixture of p-type and n-type materials and thus has much larger p/n interface area^[10]. The BHJ structure can be simply fabricated by solution-processes. Most of OPVs that use semiconducting polymers are made with the BHJ structure.

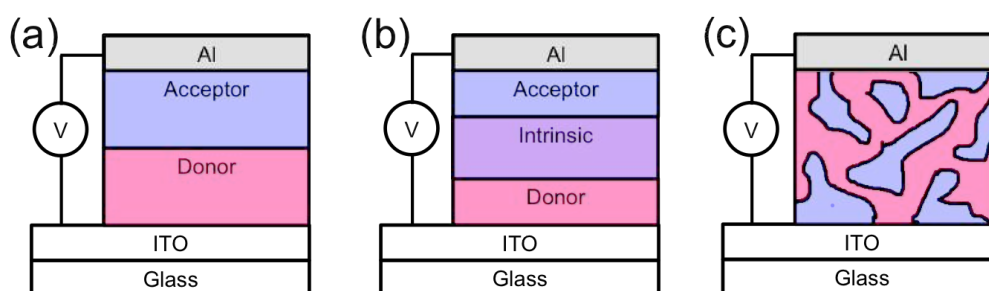


Figure 1.3 Structure of organic photovoltaic cells (a) bilayer syructure, (b) p-i-n structure, (c) bulk heterojunction (BHJ) structure.

1-3-2. Materials

1-3-2-1. Requirements for semiconducting polymers

Materials are fundamental components of OPV cells. Therefore, the development of the materials including p-type and n-type photoactive materials and interlayer materials is a crucial issue. The development of semiconducting polymers that are typically used as the p-type material is of particular importance because the n-type materials used in combination with are mostly fixed to fullerene derivatives, such as [6,6]-phenyl-C₆₁-butyric acid methyl ester (PC₆₁BM) or [6,6]-phenyl-C₇₁-butyric acid methyl ester (PC₇₁BM).

For the development of high-performance semiconducting polymers, the electronic structure and the ordering structure are important properties. The electronic structure is referred to the HOMO and LUMO energy levels and the optical bandgap (E_g). Since the active layer is required to absorb as much sunlight as possible to achieve high J_{SC} , the semiconducting polymer is necessary to have broad absorption range, *i.e.*, narrow E_g . For instance, the absorption spectrum of regioregular poly(3-hexylthiophene) (P3HT), one of the standard semiconducting polymers, is ranged from ca. 400 to 650 nm, which covers only a portion of solar spectrum (**Figure 1.4a**). This

should be broadened to achieve high J_{sc} . As V_{oc} is determined by E_{diff} , the semiconducting polymer is required to have a lower-lying HOMO energy level (**Figure 1.4b**).

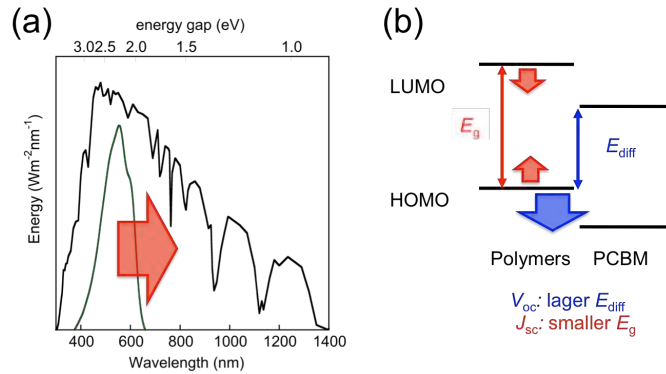


Figure 1.4 (a) AM1.5G solar spectrum and absorption spectrum of P3HT. (b) Relationship of the energy diagrams of the materials and the photovoltaic parameters.

The ordering structure refers to crystallinity and orientation of polymer backbone. The ordering structure mostly determines the transport property of the charge carriers. In general, a dominant carrier transport path at the molecular level is through the π - π stacking of the polymer backbones (**Figure 1.5**). Therefore, the polymer backbone must be highly coplanar, which promotes the close π - π stacking. On the other hand, as OPV has a vertically stacked structure, carrier transport of out-of-plane direction to the substrate plane is necessary. Thus, the direction of the backbone π - π stacking is desired to be normal to the substrate plane, which is so-called “face-on” orientation (**Figure 1.5a**). In addition, a structure with the π - π stacking is parallel to the substrate plane is called “edge-on” orientation (**Figure 1.5b**), which facilitates the in-plane carrier transport and thus suitable for OFETs.

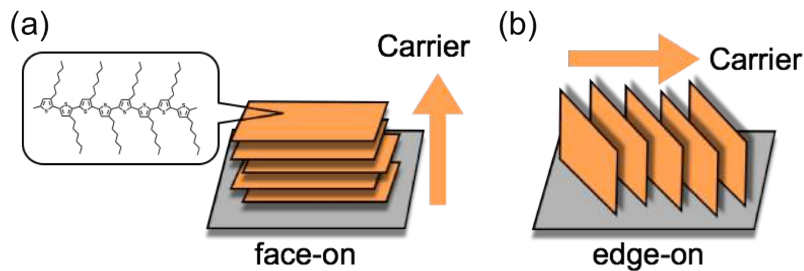


Figure 1.5 Schematic structure of polymer orientation, face-on orientation (a) edge-on orientation (b).

1-3-2-2. Development of semiconducting polymers

The BHJ solar cell was first reported by Yu and co-workers, where a phase-separated polymer blend composite made of poly[2-methoxy-5-(2'-ethyl-hexyloxy)-1,4-phenylene vinylene], MEH-PPV, as a donor and poly(2,5,2',5'-tetrahexyloxy-7',8'-dicyano-di-*p*-phenylene vinylene), CN-PPV was used.^[11] PC₆₁BM, a most widely used fullerene derivative as the n-type materials that is highly soluble in organic solvents was synthesized and applied to OPV in the 1990s by the group of Wudl and Heeger.^[10] The use of PC₆₁BM significantly facilitated the photoinduced electron transfer, resulting in the improvement of PCE. The most widely studied semiconducting polymers are poly[2-methoxy-5-(3',7'-dimethyl-octyloxy)-2,4-phenylene vinylene] (MDMO-PPV) and P3HT. The cells that use MDMO-PPV and P3HT in combination with PC₆₁BM typically afford efficiencies of 2.5%^[12] and 4-5%,^[13-15] respectively.

The largest issue in these polymers was that they do not have sufficiently wide absorption range. Thus, in order to overcome this issue, narrow E_g polymers had been developed. However, narrow E_g polymers synthesized at the early stage of this field had relatively low carrier mobilities and higher HOMO levels, which hindered the improvement of PCEs. This was resolved by carefully choosing the building units introduced in the polymer backbone, resulting in so-called donor-acceptor (D-A) polymers.^[16] The D-A polymer is composed of an electron-rich (donor ; D) unit and an electron-poor (acceptor ; A) unit, in which mixing of the molecular orbitals occurs and in turn affords a narrow E_g . Furthermore, the choice of a weak D unit with less electron donating nature and a strong A unit with high electron accepting nature can afford a polymer with a narrow E_g and a low-lying HOMO energy level. To date, a large number of D-A polymers with various D and A units were reported in order to improve PCE (**Figure 1-6**).

The introduction of fused heteroaromatic rings can bring about rigid and planar structures in the polymer backbones. Furthermore, the use of D-A structure can enhance the intermolecular interaction of the polymer backbones. The combination of these two strategies allows us to create highly crystalline polymers with high carrier mobilities. It should be noted, however, the solubility of polymers is an important factor that determines the ability to miscible with the fullerene derivatives and to be solution-processed. Thus, although most of D-A polymers consist of fused heteroaromatic rings, the branched and long alkyl groups introduced as the solubilizing groups often reduce the crystallinity of the polymers.

1-4 Thiazolothiazole-based Semiconducting Materials

Thiazolothiazole (TzTz), a fused ring of two thiazoles, is an electron deficient heteroaromatic ring. Several semiconducting materials using TzTz have been reported. Yamashita and co-workers reported on small molecules based on TzTz, which showed high field-effect mobility as the active layer for both p- and n-type OFET devices.^[17] Osaka, McCullough and co-workers reported on semiconducting polymers based on TzTz, which demonstrated that the polymers form highly crystalline structure and high hole mobilities in OFET devices.^[18] These results suggest that TzTz-based polymers are also promising as semiconducting materials for OPVs, and prompted me to design and synthesize new TzTz-based polymers in order to achieve high PCE.

1-5 This thesis

In this thesis, I will describe the design and synthesis of a series of thiazolothiazole-based semiconducting polymers and their application to the organic solar cells (OPVs). I will also discuss in-depth structure-properties relationships to understand key parameters that determine the performances of the OPVs.

This thesis consists of nine chapters including the general introduction as Chapter 1 and conclusions as Chapter 8. In Chapter 2, I show the application of TzTz-based semiconducting polymers, which have been originally developed for organic field-effect transistors (OFETs) (PTzQT-14, PTzBT-14HD and PTzBT-HD; **Figure 1-7**), to OPVs. The difference in the trend of the performances between OFETs and OPVs will be discussed.

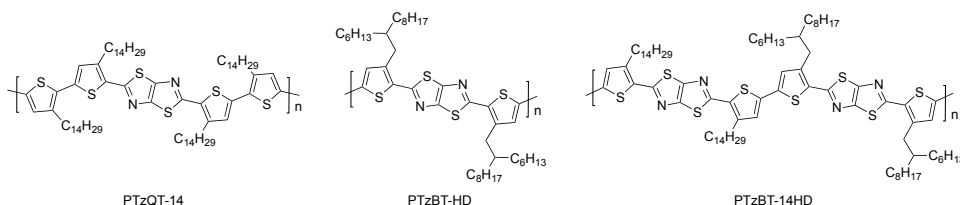


Figure 1-7. Chemical structure of thiophene-thiazolothiazole-based semiconducting polymers

In Chapter 3, I focus on PTzBT-14HD, since this polymer was revealed to be the most promising polymer for OPV among the polymers shown in Chapter 1. I show the importance of the monomer purification for

synthesizing high-molecular-weight polymers. I also discuss the molecular weight dependence of the OPVs using PTzBT-14HD along with the correlation with the ordering structure. In Chapter 4, I synthesized polymers with the same backbone structure as PTzBT-14HD and with various side chains with linear and branched motifs (**Figure 1-8**). I investigated the impact of the side chain composition on the backbone orientation and solar cell performance.

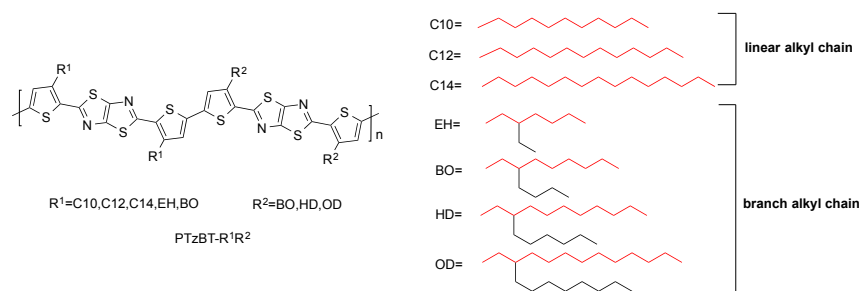


Figure 1-8. Chemical structure of PTzBT- R^1R^2

In Chapter 5, I investigated the effect of the side chain position in PTzBTs, by synthesizing PTzBT- R^1R^2i (**Figure 1-9**). The difference in solubility, crystallinity, orientation and OPV performance is discussed.

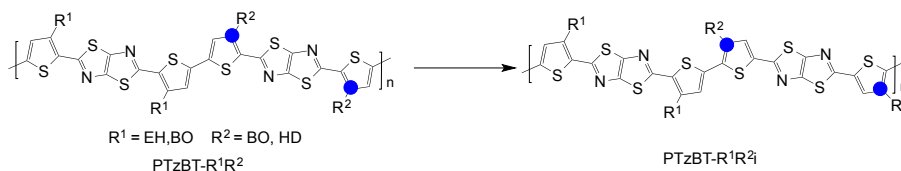


Figure 1-9. Chemical structure of PTzBT- R^1R^2i

In Chapter 6, I show the synthesis of PTzBTs with alkoxy and ester groups as the side chains, namely PTzBT-*o*BOHD, PTzBT-BOeHD and PTzBT-*o*BOeHD (**Figure 1-10**), to obtain broader absorption range and thus high OPV performances. I discuss the effect of these side chains on the physicochemical properties, thin film properties, and OPV performance.

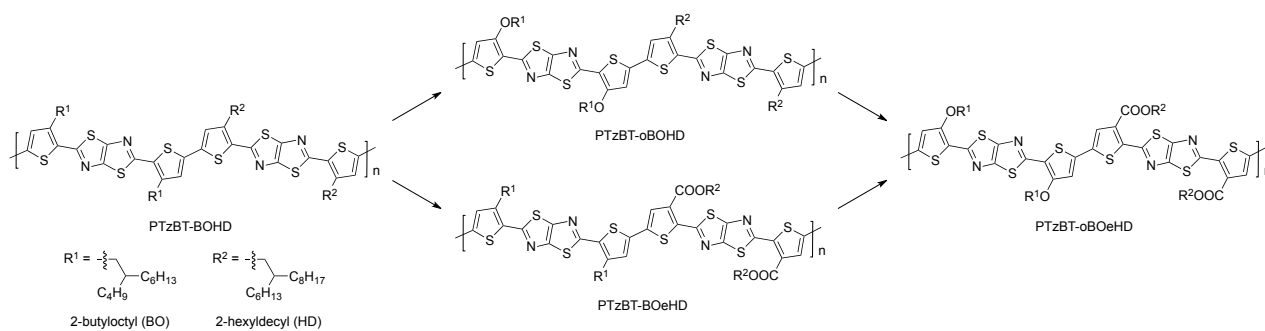


Figure 1-10. Chemical structure of PTzBT-oBOHD, -BOeHD, and -oBOeHD.

In Chapter 7, I show the synthesis of the polymers with thiazolothiazole and naphthobisthiadiazole in the backbone (**Figure 1-11**) to obtain both deep HOMO level and broad absorption range. I investigated the physicochemical properties, crystallinity, orientation and OPV characteristics and stability.

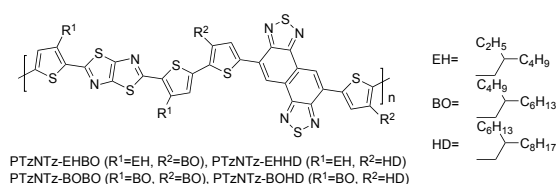


Figure 1-11. Chemical structure of PTzNTz- R^1R^2 .

Reference

- [1] Z. Bao, J. Locklin, *Organic Field-Effect Transistors* 1st, CRC, 2007.
- [2] K. Müllen, U. Scherf, *Organic Light-Emitting Devices: Synthesis, Properties and Applications*, Wiley-VCH, 2005.
- [3] C. Brabec, U. Scherf, *Organic Photovoltaics: Materials, Device Physics, and Manufacturing Technologies*, Wiley-VCH, 2008.
- [4] C. W. Tang, *Appl. Phys. Lett.*, **1986**, 48, 183.
- [5] (a) J. Y. Kim, K. Lee, N. E. Coates, D. Moses, T.Q. Nguyen, M. Dante, A. J. Heeger, *Science* **2007**, 317, 222. (b) J. Gilot, M. M. Wienk, R. A. Janssen, *J. Adv. Mater.* **2010**, 22, E67. (c) G. Li, C. W. Chu, V. Shrotriya, J. Huang, Y. Yang, *Appl. Phys. Lett.* **2006**, 88, 253503. (d) C. Waldauf, M. Morana, P. Denk, P. Schilinsky, K. Coakley, S. A. Choulis, C. J. Brabec, *Appl. Phys. Lett.* **2006**, 89, 233517. (e) J. Huang, G. Li, Y. Yang, *Adv. Mater.*

2008, 20, 415.

[6] (a) C. J. Brabec, N. S. Sariciftci and J. C. Hummelen, *Adv. Funct. Mater.*, **2001**, 11, 15 (b) L. M. Chen, Z. R. Hong, G. Li and Y. Yang, *Adv. Mater.*, **2009**, 21, 1434 (c) K. M. Coakley and M. D. McGehee, *Chem. Mater.*, **2004**, 16, 4533 (d) G. Dennler, M. C. Scharber and C. J. Brabec, *Adv. Mater.*, **2009**, 21, 1323 (e) S. Günes, H. Neugebauer and N. S. Sariciftci, *Chem. Rev.*, **2007**, 107, 1324

[7] (a) P. M. Beaujuge, J. M. J. Frechet *J. Am. Chem. Soc.* **2011**, 133, 20009. (b) J. Mei, Z. Bao, *Chem. Mater.* **2014**, 26, 601. (c) X. Guo, A. Facchetti, T. J. Marks, *Chem. Rev.*, **2014**, 114, 8943.

[8] (a) Y. Liu, J. Zhao, Z. Li, C. Mu, W. Ma, H. Hu, K. Jiang, H. Lin, H. Ade, H. Yan, *Nat. Commun.* **2014**, 5, 5293. (b) C-C chen, W-H Chang, K. Yoshimura, K. Ohya, J. You, J. Gao, Z. Hong, Y. Yang, *Adv. Mater.* **2014**, 26, 5670.

[9] (a) M. Hiramoto, H. Fujiwara, H. Yokoyama, *Appl. Phys. Lett.*, **1991**, 58, 1062. (b) M. Hiramoto, H. Fujiwara, H. Yokoyama, *J. Appl. Phys.*, **1992**, 72, 3781.

[10] (a) J. C. Hummelen, B. W. Knight, F. Lepeq, F. Wudl, J. Yao, C. L. Wilkins, *J. Org. Chem.*, **1995**, 60, 532. (b) G. Yu, J. Gao, J. C. Hummelen, F. Wudl, A. J. Heeger, *Science*, **1995**, 70, 1789

[11] G. Yu, A. J. Geeger, *J. Appl. Phys.*, **1995**, 78, 4510.

[12] S. E. Shaheen, C. J. Brabec, N. S. Sariciftci, F. Padinger, T. Fromherz, J. C. Hummelen, *Appl. Phys. Lett.* **2001**, 78, 841.

[13] P. Schilinsky, C. Waldauf, C. J. Brabec, *Appl. Phys. Lett.* **2002**, 81, 3885.

[14] W. Ma, C. Yang, X. Gong, K. Lee, A. J. Heeger, *Adv. Funct. Mater.* **2005**, 15, 1617.

[15] G. Li, V. Shrotriya, J. S. Huang, Y. Yao, T. Moriarty, K. Emery, Y. Yang. *Nat. Mater.* **2005**, 4, 864.

[16] (a) D. Mühlbacher, M. Scharber, M. Morana, Z. Zhu, D. Waller, R. Gaudiana, C. Brabec, *Adv. Mater.* **2006**, 18, 2884. (b) J. Peet, J. Y. Kim, N. E. Coates, W. L. Ma, D. Moses, A. J. Heeger, G. C. Bazan, *Nat. Mater.* **2007**, 6, 497.

[17] (a) S. Ando, J. Nishida, Y. Inoue, S. Tokito, Y. Yamashita, *J. Mater. Chem.* **2004**, 14, 1787. (b) S. Ando, J. Nishida, E. Fujiwara, H. Tada, Y. Inoue, S. Tokito, Y. Yamashita, *Chem. Lett.* **2004**, 1170. (c) S. Ando, J. Nishida, H. Tada, Y. Inoue, S. Tokito, Y. Yamashita, *J. Am. Chem. Soc.* **2005**, 127, 5336

[18] (a) I. Osaka, G. Sauvé, R. Zhang, T. Kowalewski, R. D. McCullough, *Adv. Mater.* **2007**, *19*, 4160. (b) I. Osaka, R. Zhang, G. Sauvé, D.-M. Smilgies, T. Kowalewski, R. D. McCullough, *J. Am. Chem. Soc.* **2009**, *131*, 2521. (c) I. Osaka, R. Zhang, J. Liu, D. M. Smilgies, T. Kowalewski, R. D. McCullough, *Chem. Mater.* **2010**, *22*, 4191. (d) J. Peet, L. Wen, P. Byrne, S. Rodman, K. Forberich, Y. Shao, N. Drolet, R. Gaudiana, G. Dennler, D. Waller, *Appl. Phys. Lett.* **2011**, *98*, 043301. (e) M. Zhang, X. Guo, Y. Li, *Adv. En. Mater.* **2011**, *1*, 557. (f) S. Subramaniyan, H. Xin, F. S. Kim, S. Shoaee, J. R. Durrant, S. A. Jenekhe, *Adv. En. Mater.* **2011**, *1*, 854-856; (g) Q. Shi, H. Fan, Y. Liu, W. Hu, Y. Li, X. Zhan, *J. Phys. Chem. C* **2010**, *114*, 16843. (h) M. Yang, B. Peng, B. Liu, Y. Zou, K. Zhou, Y. He, C. Pan, Y. Li, *J. Phys. Chem. C* **2010**, *114*, 17989. (i) L. Huo, X. Guo, S. Zhang, Y. Li, J. Hou, *Macromolecules* **2011**, *44*, 4035. (j) S.-K. Lee, J. M. Cho, Y. Goo, W. S. Shin, J.-C. Lee, W.-H. Lee, I.-N. Kang, H.-K. Shim, S.-J. Moon, *Chem. Commun.* **2011**, *47*, 1791.

Chapter 2

2. Application of thiophene-thiazolothiazole copolymers originally designed for field effect transistor for organic photovoltaic device.

2-1. Introduction

With their great electrical and optical properties and ease of fabrication process using their solutions, semiconducting polymers have been attracting considerable attention for applications in various organic electronic devices such as organic light-emitting diodes (OLEDs), field-effect transistors (OFETs), and solar cells from both academics and industries.^[1] Of particular interest today is bulk heterojunction (BHJ) solar cells using donor-acceptor semiconducting polymers as the photoactive layer materials together with fullerene-based molecules,^[2] where the power conversion efficiency (PCE) has recently reached >7%.^[3] They thus offer great opportunities as new renewable energy sources with light weight and flexibility that differentiates them from conventional inorganic solar cell technologies.^[4] A key to developing high performance semiconducting polymers is to achieve strong π - π stacking structures that determines the transport property of generated charge carriers in the BHJ film.^[5] Therefore the incorporation of π -cores that ensure strong intermolecular interactions with the polymer backbone is an important design strategy. Recently, Osaka, McCullough, and co-workers have reported on the development of a series of donor-acceptor polymers bearing thiazolothiazole (TzTz) as an acceptor unit in the electron-rich polythiophene backbone (**Figure 2-1**).^[5]

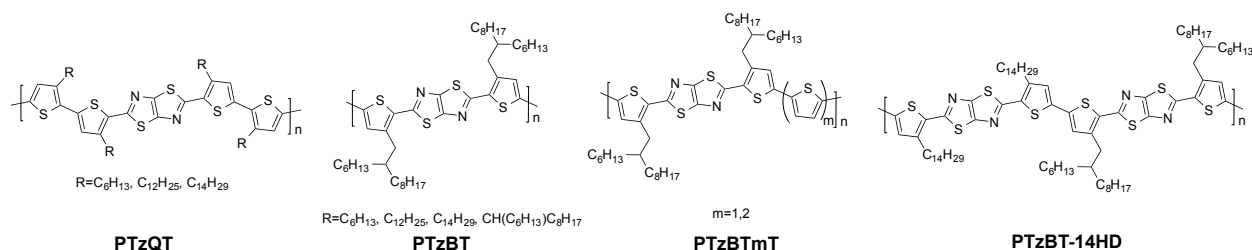


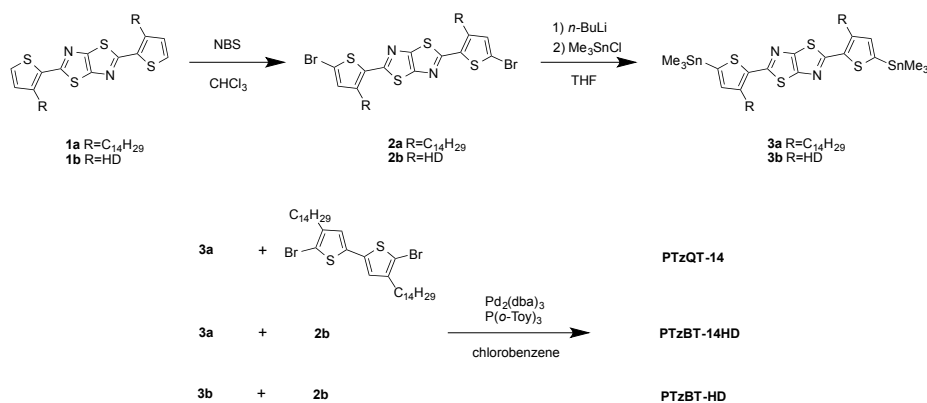
Figure 2-1. Chemical structure of TzTz-based semiconducting polymers

PTzQTs, one of the first examples for the high-performance OFET polymers with a donor-acceptor backbone, form highly ordered and edge-on oriented structures with narrow π - π stacking distances (d_{π}) of 3.5–3.6 Å in the thin film, where the back-bones π -stack parallel to the surface, facilitating the lateral charge carrier transport, in

turn they afford field effect mobilities (μ_{FET}) as high as $0.3 \text{ cm}^2\text{v}^{-1}\text{s}^{-1}$.^[6a,b] These high mobilities in OFETs assured that thiazolothiazole is a promising core unit for semiconducting polymers. Although PTzQTs-based OFETs exhibit high mobilities, their environmental stability is not sufficiently high as they showed some degradation of, in particular, on/off current ratios when the devices were stored in air because of the gradual oxidation with time, most probably as a result of a moderately small ionization potential (IP) of 5.1 eV. Thereafter, PTzBT-HD, PTzBT-14HD, and PTzBTmT (**Figure 2-1**), which possess the lower content ratio of the electron-donating alkylthiophene units in the backbone, were synthesized in order to improve the stability.^[6c] Having larger IPs of 5.2-5.3 eV, the OFET devices based on these polymers were highly stable, maintaining the original OFET performances for several months in air. However, the mobilities for these polymers were lower than that for PTzQT; the μ_{FET} for PTzBT-HD and PTzBT-14HD was 3.0×10^{-4} and $0.1 \text{ cm}^2\text{v}^{-1}\text{s}^{-1}$, respectively. This is apparently because they formed misoriented packing structures, that is, partially face-on oriented structures in the thin film, that could limit the lateral charge transport, most likely owing to the introduction of branched alkyl chains. In addition, far inferior μ_{FET} for PTzBT-HD should be due to the lack of π - π stacking order. From another point of view, however, the partially face-on oriented structure of PTzBT-14HD, with high π - π stacking order, should rather be favorable for the orthogonal charge transport and thus for solar cells,^[7] and besides, its relatively large IP (5.2 eV) should allow higher V_{OC} in solar cells.^[8] In this way, I focused on the series of TzTz based polymers and synthesized these polymers to apply to BHJ solar cells.

2-2. Synthesis

The synthetic route of the monomers and polymers are shown in **Scheme 2-1**. First, **1a** and **1b** were brominated using NBS to give **2a** and **2b**, followed by stannylation via the treatment of *n*-BuLi, which gave the monomer (**3a** and **3b**). All polymers were synthesized via the Stille coupling reaction using a microwave reactor. **3a** was copolymerized with 4,4'-Didoceyl-5,5'-trimethylstannyl-2,2'-bithiophene and **2b** to give PTzQT-14 and PTzBT-14HD, respectively. And **3b** and **2b** were copolymerized to give PTzBT-HD. The polymers were soluble in chloroform (CF) and chlorobenzene (CB) in room temperature, and the molecular weight of polymers evaluated by GPC at 140 °C were ca.10 kDa (M_n).



Scheme 2-1. Synthetic route of TzTz monomer and TzTz-based polymers.

2-3. Solar Cell Characteristics.

Solar cells were fabricated by spin-coating the solutions of polymer and [6,6]-phenyl-C₆₁-butyric acid methyl ester (PC₆₁BM) in chlorobenzene onto the PEDOT:PSS spin-coated ITO glass, followed by vacuum deposition of LiF/Al as the cathode. The optimal polymer-to-PC₆₁BM (p:n) ratio were 1:2 for these polymers. External quantum efficiency (EQE) spectra and current density (J)-Voltage (V) curves of the cells under 1 sun of simulated AM 1.5G solar irradiation (100 mW/cm²) are displayed in **Figure 2-2**, and photovoltaic parameters are summarized in **Table 2-1**. PTzBT-14HD-based cell shows the best PCE of 3.1% with high open-circuit voltage (V_{OC}) of 0.92 V (short-circuit current (J_{SC}) = 6.1 mA cm⁻², fill factor (FF) = 0.56). In the meantime, PTzQT-14 showed low V_{OC} of 0.64 V, along with J_{SC} = 6.0 mA cm⁻², FF = 0.43, resulting in PCEs of 1.6% and PTzBT-HD exhibited PCEs of 0.8% with J_{SC} = 2.3 mA cm⁻², V_{OC} = 0.96 V, FF = 0.37.

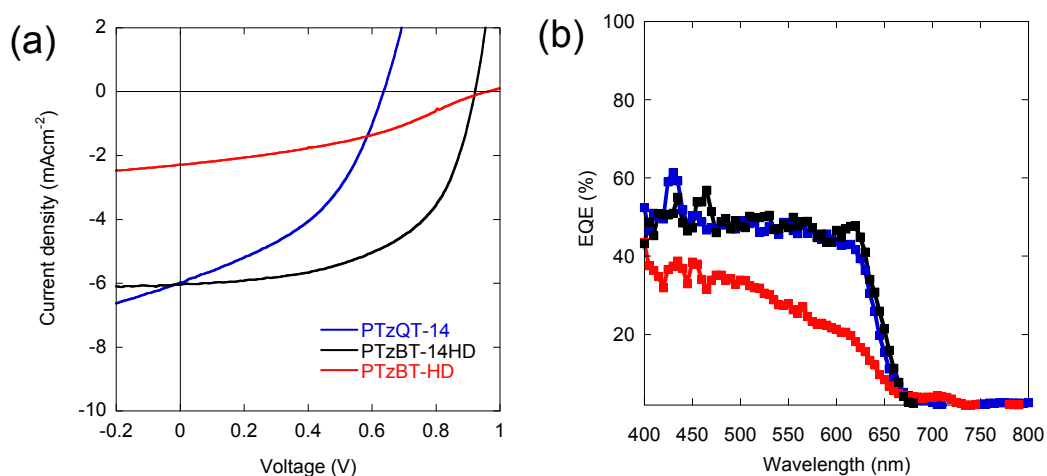


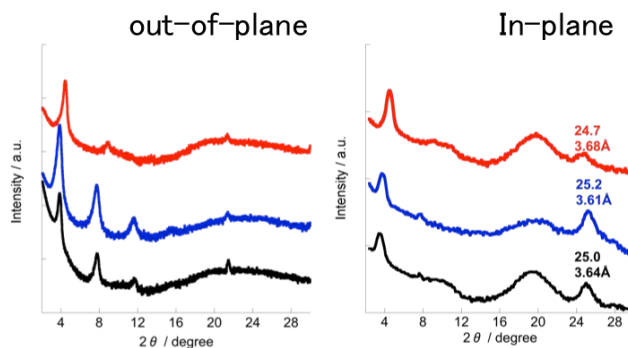
Figure 2-2. J - V curves (a) and EQE spectra (b) of BHJ solar cells (ITO/PEDOT:PSS/polymer:PC₆₁BM/LiF/Al)

Table 2-1. Photovoltaic Properties of the Polymer-Based Solar Cells

Polymer	J_{SC} (mA/cm ²)	V_{OC} (V)	FF	PCE _{max} [PCE _{ave}] (%)
PTzQT-14	6.0	0.64	0.43	1.6 [1.3]
PTzBT-14HD	6.1	0.92	0.37	3.2 [2.8]
PTzBT-HD	2.3	0.96	0.56	0.8 [0.6]

To understand the photovoltaic performances of the cells, polymer ordering structures were investigated by X-ray diffraction studies. X-ray diffraction of polymer/PC₆₁BM blend films on the PEDOT:PSS/ITO substrate, are shown in **Figure 2-3**. In all cases, diffractions assignable to the lamellar structure ($\theta = \text{ca. } 4^\circ$) and the π - π stacking structures ($\theta = \text{ca. } 25^\circ$) appeared along the in-plane and out-of-plane, respectively. π - π Stacking distances of PTzQT-14, PTzBT-14HD and PTzBT-HD were 3.61, 3.64 and 3.68 Å, respectively, and intensity of π - π stacking of PTzBT-HD is low, which means that crystallinity of PTzQT-14 is the highest and PTzBT-HD have weakly ordered π - π stacking structure.

I also investigated the morphology of the polymer/PC₆₁BM blend films by the atomic force microscopy (AFM) (**Figure 2-4**). The PTzQT-14/PC₆₁BM blend and PTzBT-14HD/PC₆₁BM films seems to have formed well-phase-separated morphologies. On the other hands, PTzBT-HD/PC₆₁BM films formed large morphologies and the surface roughness estimated by the root mean square (rms) values of the blend of PTzBT-HD is larger than that of PTzBT-14HD and PTzQT-14.

**Figure 2-3.** X-ray diffraction of TzTz-base polymer/PC₆₁BM blend films

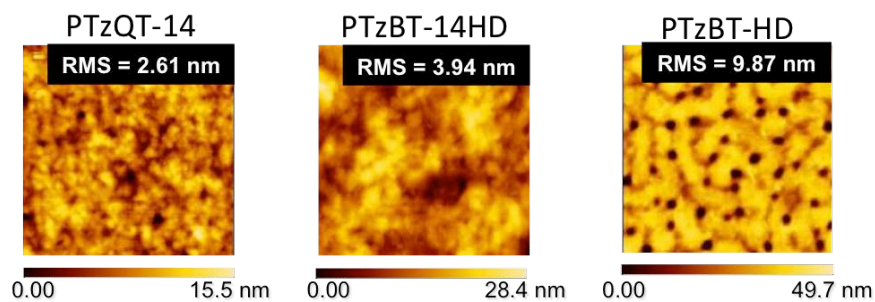


Figure 2-4. AFM image of TzTz-base polymer/PC₆₁BM blend films

2-4. Summary

I used three kind of TzTz-based semiconducting polymers originally developed for OFETs in BHJ solar cells. PTzBT-14HD have both of high crystallinity and morphologies in these polymers. In addition, PTzBT-14HD have large IP lead to obtain high V_{OC} for organic solar cells. Thus, PTzBT-14HD is high potential polymer for crystallinity, morphology and electronic structure in these TzTz-based polymers.

Experimental

General procedure for polymerization

To a reaction tube equipped with a stirring bar, stannylated monomer (0.10 mmol), brominated monomer (0.10 mmol), Pd₂(dba)₃ (1.8 mg, 0.002 mmol), P(*o*-Tol)₃ (2.4 mg, 0.008 mmol), and chlorobenzene (5 ml) were added. Then the tube was purged with argon and sealed. The reaction tube was set into a microwave reactor and heated to 100°C to 200 °C for 5 to 10 min each conditions. After cooling to room temperature, the reaction solution was poured into 200 mL of methanol containing 5 mL of hydrochloric acid, and stirred for 5 hours. Then the precipitated solid was subjected to the sequential Soxhlet extraction with methanol, hexane to remove low molecular weight fractions. The residue was then extracted with chloroform, and reprecipitated in 200 mL of methanol to yield dark purple or dark blue solids (yield = 45-87%).

Instrumentation and Calculations

UV–vis absorption spectra were measured using a Shimadzu UV-3600 spectrometer. Ionization potential (IP) was determined from the onset of photoelectron spectra measured by using a photoelectron spectrometer MODEL AC-2 in air (RIKEN KEIKI CO., LTD). Out- of-plane and in-plane X-ray diffraction specular scans were carried

out using a Rigaku Ultima IV. Samples for the X-ray measurements were prepared by drop-casting the polymer or polymer/PC₆₁BM solution on the PEDOT:PSS spin-coated ITO glass.

Device Fabrication and Measurement

ITO substrates were first precleaned sequentially by sonicating in a detergent bath, deionized water, acetone, and isopropanol at room temperature, and in a boiled isopropanol bath each for 10 min, and then baked at 130° C for 10 min in air, which were then subjected to a UV/ozone treatment at rt for 20 min. The precleaned ITO substrates were coated with PEDOT:PSS (Clevios PVP A14083) by spin-coating (5000 rpm for 30 s, thickness ~50 nm). The photoactive layer was deposited in air by spin coating a CB solution containing 5.0 mg mL⁻¹ PTzBT-14HD with respective amount of PC₆₁BM passed through a 0.45µm PTFE filter at 400 rpm for 20 s and 1500 rpm for 5 s, which were dried in the vacuum for 2 h. The counter electrode, consisting of LiF (0.8 nm) and Al (100 nm), was deposited by vacuum evaporation, where the active area of the cells was 0.0314 cm². The thickness of the film was measured using a surface profiler (Ambios XP-100). *J-V* characteristics were measured using a Keithley 2400 source-measure unit in air without encapsulation of the cells under 1 Sun (AM1.5G) conditions using a solar simulator (Asahi Spectra, HAL-320, JIS class AAA) at 100 mW cm⁻². EQE spectra were measured with a home-built setup consisting of an Asahi Spectra HAL-320 Xe lamp in combination with an Asahi Spectra CMS-100 monochromator. The number of photons incident on the device was calculated for each wavelength by using a calibrated Si diode as the reference.

Reference

[1] a) T. A. Skotheim, J. R. Reynolds, *Handbook of Conducting Polymers*, 3rd ed., CRC Press, Boca Raton, FL **2007**; b) M. Leclerc, J.-F. Morin, *Design and Synthesis of Conjugated Polymers*, Wiley-VCH Verlag GmbH & Co. KGaA, Weinheim, Germany **2010**; c) A. C. Arias, J. D. MacKenzie, I. McCulloch, J. Rivnay, A. Salleo, *Chem. Rev.* **2010**, *110*, 3-24; d) A. Facchetti, *Chem. Mater.* **2011**, *23*, 733–758; e) F. Garnier, R. Hajlaoui, A. Yassar, P. Srivastava, *Science* **1994**, *265*, 1864-1866; f) C. Brabec, V. Dyakonov, U. Scherf, *Organic Photo- voltaics, Materials Device Physics, and Manufacturing Technologies*; Wiley-VCH Verlag GmbH & Co. KGaA, Weinheim, Germany **2008**; g) S. Günes, H. Neugebauer, N. S. Sariciftci, *Chem. Rev.* **2007**, *107*, 1324-1338; h) B. C.

Thompson, J. M. J. Frechet, *Angew. Chem., Int. Ed.* **2008**, *47*, 58-77; i) J. Peet, A. J. Heeger, G. C. Bazan, *Acc. Chem. Res.* **2009**, *42*, 1700-1708; j) J. Chen, Y. Cao, *Acc. Chem. Res.* **2009**, *42*, 1709-1718; k) O. Inganäs, F. Zhang, M. R. Andersson, *Acc. Chem. Res.* **2009**, *42*, 1731-1739; l) Y. Liang, L. Yu, *Acc. Chem. Res.* **2010**, *43*, 1227-1236; m) P.-L. T. Boudreault, A. Najari, M. Leclerc, *Chem. Mater.* **2011**, *23*, 456-469.

[2] a) G. Yu, J. Gao, J. C. Hummelen, F. Wudl, A. J. Heeger, *Science* **1995**, *270*, 1789-1791; b) D. Mühlbacher, M. Scharber, M. Morana, Z. Zhu, D. Waller, R. Gaudiana, C. Brabec, *Adv. Mater.* **2006**, *18*, 2884-2889.

[3] a) Y. Liang, Z. Xu, J. Xia, S. Tsai, Y. Wu, G. Li, C. Ray, L. Yu, *Adv. Mater.* **2010**, *22*, E135-E138; b) H. Y. Chen, J. Hou, S. Zhang, Y. Liang, G. Yang, Y. Yang, L. Yu, Y. Wu, G. Li, *Nature Photon.* **2009**, *3*, 649-653; c) T. Y. Chu, J. Lu, S. Beaupré, Y. Zhang, J. R. Pouliot, S. Wakim, J. Zhou, M. Leclerc, Z. Li, J. Ding, Y. Tao, *J. Am. Chem. Soc.* **2011**, *133*, 4250-4253; d) S. C. Price, A. C. Stuart, L. Yang, H. Zhou, W. You, *J. Am. Chem. Soc.* **2011**, *133*, 4625-4631.

[4] a) C. Brabec, *Sol. Energy Mater. Sol. Cells* **2004**, *83*, 273-292; b) C. J. Brabec, J. R. Durrant, *MRS Bull.* **2008**, *33*, 670-675; c) F. C. Krebs, *Sol. Energy Mater. Sol. Cells* **2009**, *93*, 394-412.

[5] a) J. Hou, H. Y. Chen, S. Zhang, G. Li, Y. Yang, *J. Am. Chem. Soc.* **2008**, *130*, 16144-16145; b) H.-Y. Chen, J. Hou, A. E. Hayden, Y. Yang, K. N. Houk, Y. Yang, *Adv. Mater.* **2010**, *22*, 371-375; c) M. C. Scharber, M. Koppe, J. Gao, F. Cordella, M. A. Loi, P. Denk, M. Morana, H.-J. Egelhaaf, K. Forberich, G. Dennler, R. Gaudiana, D. Waller, Z. Zhu, X. Shi, C. J. Brabec, *Adv. Mater.* **2010**, *22*, 367-370.

[6] a) I. Osaka, G. Sauvé, R. Zhang, T. Kowalewski, R. D. McCullough, *Adv. Mater.* **2007**, *19*, 4160-4165; b) I. Osaka, R. Zhang, G. Sauvé, D.-M. Smilgies, T. Kowalewski, R. D. McCullough, *J. Am. Chem. Soc.* **2009**, *131*, 2521-2529; c) I. Osaka, R. Zhang, J. Liu, D.-M. Smilgies, T. Kowalewski, R. D. McCullough, *Chem. Mater.* **2010**, *22*, 4191-4196.

[7] a) C. Piliago, T. W. Holcombe, J. D. Douglas, C. H. Woo, P. M. Beaujuge, J. M. J. Fréchet, *J. Am. Chem. Soc.* **2010**, *132*, 7595-7597; b) F. He, W. Wang, W. Chen, T. Xu, S. B. Darling, J. Strzalka, Y. Liu, L. Yu, *J. Am. Chem. Soc.* **2011**, *133*, 3284-3287.

[8] a) C. J. Brabec, A. Cravino, D. Meissner, N. S. Sariciftci, T. Fromherz, M. T. Rispen, L. Sanchez, J. C. Hummelen, *Adv. Funct. Mater.* **2001**, *11*, 374-380; b) A. Gadisa, M. Svensson, M. R. Andersson, O. Inganäs, *Appl. Phys. Lett.* **2004**, *84*, 1609-1611.

Chapter 3

3. Thiophene-thiazolothiazole copolymers: drastic change of molecular orientation by molecular-weight control and blending with PC₆₁BM lead to high efficiencies in solar cells

3-1. Introduction

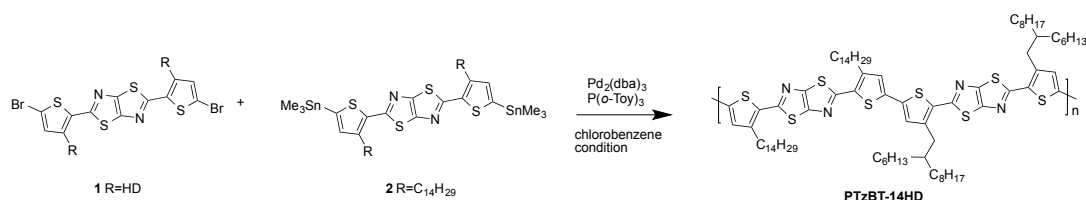
On account of their distinctive potential for fabricating flexible, lightweight, large-area, and low cost devices by solution process, polymer solar cells based on bulk heterojunction (BHJ) have attracted much attention. Especially, in the past decade, the power conversion efficiencies (PCEs) have reached 8% by optimizing optimal structure, carrier mobilities, energy levels and morphologies. PTzBT-14HD-based solar cell shows the best PCE of 3.1% with high open-circuit voltage (V_{OC}) of 0.92 V (short-circuit current (J_{SC}) = 6.1 mA cm⁻², fill factor (FF) = 0.56) in present TzTz-based polymers (Chapter 2).

In these results, it is clear that, with optimal physical and structural properties, such as IP, solubility, molecular ordering, and orientation, arising from the rationally tuned backbone and the alkyl side chain structures, PTzBT-14HD is the best material among the present TzTz-based polymers and is a promising material for solar cells. Taking into account that the molecular weight is low (number averaged molecular weight (M_n) = 13 kDa) the photovoltaic properties of PTzBT-14HD are fairly high and these results prompted us to further investigate PTzBT-14HD. In this paper, I report that PCEs of PTzBT-14HD can be improved to 5.7% with an increase of molecular weight (MW). I also highlight the drastic changes of orientational order in PTzBT-14HD as a function of molecular weight and by blending with PC₆₁BM, which accounts for the high photovoltaic performances. As often seen in many polymer systems, MW affects the photovoltaic properties.^[1]

3-2. Result and discussion

I, therefore, first put our efforts to increase the MW of PTzBT-14HD. Purification of the monomers successfully yielded the polymer samples with higher MW, M_n = 20 kDa with a polydispersity index (PDI) of 3.0, 33 kDa with PDI = 9.1, and 73 kDa with PDI = 19.9, as listed in **Table 3-1**.^[2] Initial PTzBT-14HD, with M_n = 13 kDa, was obtained by a polymerization of monomers **2** and **1** synthesized according to the previously published procedure,^[3] where **2** and **1** were purified by Al₂O₃ and by SiO₂ column chromatography, respectively. However, Al₂O₃ column chromatography carried out for **2** possibly induces cleavage of the C-Sn bond, giving a trace amount of the corresponding monostannylated compound, though it could not be detected by ¹H-NMR spectroscopy in this

case, which may hinder the polymerization. Instead, I purified **2** by recrystallization from hexane, and, in addition, **1** by preparative gel permeation chromatography (GPC), (JAIGEL-1H/2H, CHCl₃ as the eluent) after SiO₂ column chromatography, with which the polymerization gave PTzBT-14HD with $M_n = 20$ kDa. When **2** was further purified by GPC after the recrystallization, M_n of PTzBT-14HD was increased to 33 kDa. An additional recrystallization of **2**, after the sequential purification by recrystallization and GPC, led to the even higher polymer with M_n of 73 kDa. Note that ¹H-NMR spectra of these **2**s were mostly identical, indicating that it could be very difficult to distinguish the purity of distannylated monomers. It should also be mentioned that the same polymerization conditions were employed for all MW-polymers, and repetitive GPC purification of **1** did not affect the MW. The solubility of PTzBT-14HD reduced as the MW increased. While the 13 kDa polymer was soluble in chloroform at room temperature, the 20 and 33 kDa polymers were soluble in hot chloroform and chlorinated benzenes, and the 73 kDa polymer was only soluble in hot chlorinated benzenes. Thus the 73 kDa polymer was collected by Soxhlet extraction with chlorobenzene (CB), whereas other polymers were collected with chloroform. The significantly large PDI for the 33 and 73 kDa polymers is attributed to the relatively low solubility and the higher tendency to aggregate, which could give rise to an artificial peak at a shorter retention time in the chromatogram corresponding to extremely high MW, and thus the overestimation of, particularly, weight-averaged molecular weight (M_w) (**Figure 3-1a**).^[4] It is worth noting that the polymerization of PTzBT-14HD was also employed with using purified **2** and **1** in a microwave reactor, and with certain conditions desired MW samples were reproducibly obtained. For example, polymerization at 100 °C for 5min, 10min, 1h, and at 200°C at 10min gave M_n of ca. 10, 20, 30, and 70 kDa, respectively(**Table 3-1**). UV-vis absorption spectra of the PTzBT-14HD thin films are shown in **Figure 3-1b**. All polymers show well-defined structures, where two peaks appear at 570-575 and 620-630 nm along with a shoulder at ca. 530 nm. The higher MW polymers tend to give a slightly narrower spectrum with a relatively intensified peak at ca. 630 nm, which suggests the improved molecular ordering in the high-MW polymers, being consistent with the phenomena observed in the GPC measurements. IP of the polymers was evaluated by photoelectron spectroscopy in air, and was 5.2 eV for all the samples.



Scheme 3-1. Polymerization of PTzBT-14HD

Table 3-1. Polymerization condition of PTzBT-14HD

	μ -wave condition	fraction	M_n (kDa) ^a	M_w (kDa) ^a	PDI ^a	HOMO (eV)
1	100 °C, 5 min	CF	13kDa	18kDa	1.4	-5.20
2	100 °C, 10 min	CF	20kDa	60kDa	3.0	-5.20
3	200 °C, 10 min	CF	33kDa	290kDa	8.8	-5.20
4		CB	73kDa	1450kDa	19.9	-5.20

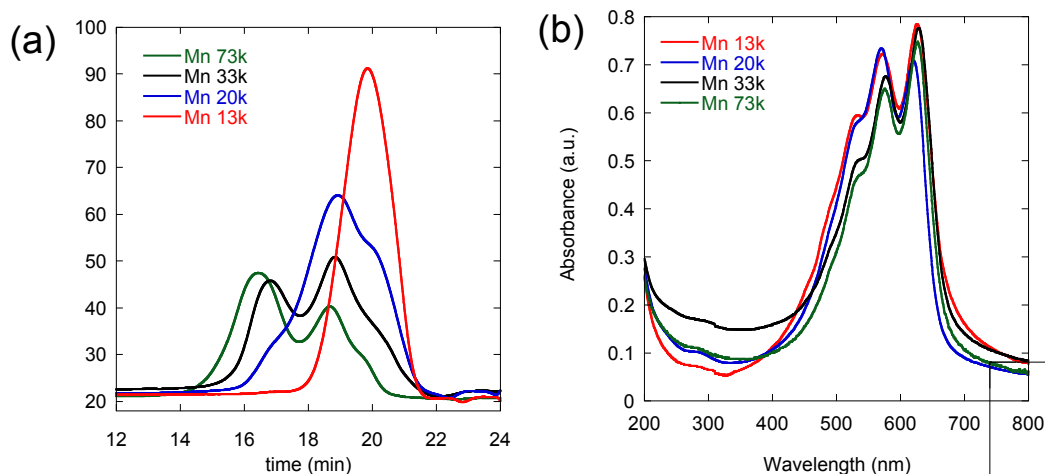


Figure 3-1. GPC chromatograms (a) and UV-vis absorption spectra (b) of PTzBT-14HD

Photovoltaic properties of PTzBT-14HD were examined with BHJ solar cells (ITO/PEDOT:PSS/PTzBT-14HD:PC₆₁BM/LiF/Al). J - V curves of the optimized BHJ solar cells under one sun of simulated AM 1.5G solar irradiation (100 mW cm⁻²) are shown in **Figure 3-2a**. The active-layer thickness of the optimized devices was in the range of 150–170 nm. Although the IP was identical (5.2 eV) regardless of the MW, V_{OC} slightly decreased as the MW increased. J_{SC} , on the other hand, increased gradually and maximized at $M_n = 33$ kDa, and decreased when the MW was further increased to $M_n = 73$ kDa. As a result, PCEs for the polymer with $M_n = 20$ kDa increased to 4.6% ($J_{SC} = 7.8$ mA cm⁻², $V_{OC} = 0.88$ V, FF = 0.67) from 3.1% with $M_n = 13$ kDa, and further increased to 5.7% ($J_{SC} = 10.6$ mA cm⁻², $V_{OC} = 0.84$ V, FF = 0.64) for the polymer with $M_n = 33$ kDa. The $M_n = 73$

kDa polymer gave the PCE of 5.3% with $J_{SC} = 9.2 \text{ mA cm}^{-2}$, $V_{OC} = 0.85 \text{ V}$, $FF = 0.68$, which was slightly reduced from the 33 kDa polymer. While the best PCEs were obtained at p:n = 1:1 for the $M_n = 13$ and 20 kDa polymers, those for the $M_n = 33$ and 73 kDa polymers were obtained at p:n = 1:2 (**Table 1**), which might be due to the difference of the miscibility with PC₆₁BM and possibly the balance of hole and electron mobilities. The average PCEs are also displayed in Table 1. For example, PCEs for the $M_n = 33$ kDa sample were in the range of 5.0-5.7%, with an average of 5.3%. This relatively large variation might be because the film deposition and the measurements are done in air, and the polymer has relatively low solubility, which makes the fabrication process difficult. Nevertheless, PCEs of 5.7%, and even the average number of 5.3%, is among the highest values so far reported for TzTz- containing polymer systems; recently a number of TzTz-based polymers has been reported, where with cyclopentadithiophene (PCE 2.2%),^[5] dithienosilole (PCE 5.6%),^[6] benzodithiophene (PCE 5.2%),^[7] and carbazole (PCE 4.9%)^[8] as the donor unit. The external quantum efficiency (EQE) curves of the optimized devices are shown in **Figure 3-2b**. Consistent with the device performances, the device with the 33 kDa polymer exhibited the highest EQE, ca. 70% at 630 nm, among the four samples. I also prepared the BHJ films processed with 1,8-diiodoctane^[9] or 1-chloronaphthalene^[10] in the polymer/PC₆₁BM solution. However, these solvent additives did not improve the solar-cell performances in this system, suggesting that the phase separation of the BHJ films might already be optimal without the solvent additives. Thermal annealing of the BHJ films led to a large phase separation, perhaps caused by the aggregation of the polymer and/or PC₆₁BM, resulting in a drop in photovoltaic performances. No need of additives or thermal treatment might be of particular importance in terms of the ease of the fabrication process.

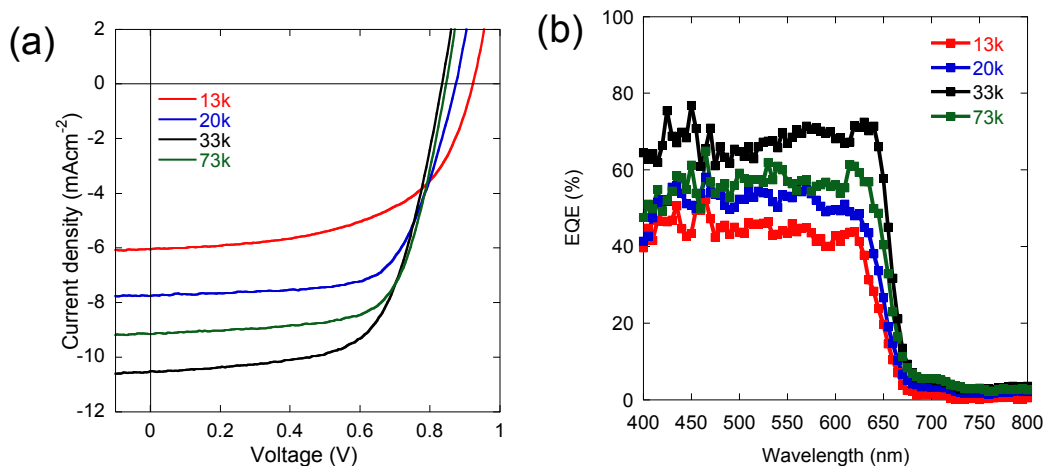


Figure 3-2. J - V curves (a) and EQE spectra (b) of BHI solar cells (ITO/PEDOT:PSS/polymer:PC₆₁BM/LiF/Al)

Table 3-2. Photovoltaic Properties of the Polymer-Based Solar Cells

Molecular weight	p:n	J_{SC} (mA/cm ²)	V_{OC} (V)	FF	PCE _{max} [PCE _{ave}] (%)
13kDa	1:1	6.1	0.92	0.56	3.1 [3.0]
20kDa	1:1	7.8	0.88	0.67	4.6 [4.0]
33kDa	1:2	10.6	0.84	0.64	5.7 [5.3]
73kDa	1:2	9.2	0.85	0.68	5.3 [4.8]

To understand the significant improvement of the photovoltaic performances in the high-MW PTzBT-14HD-based solar cells, the molecular ordering and orientation of the polymers were also studied by 2D grazing incidence X-ray diffraction (GIXD). Polymer-only thin films on the PEDOT:PSS-coated ITO substrate were first measured, and the 2D images are shown in **Figure 3-3a-d**. Reproducing the results of a previous report,^[3] PTzBT-14HD with a low M_n of 13 kDa provides the diffractions corresponding to the lamellar structure at the diffraction vector, q , of 0.2-0.3 Å⁻¹ and the π - π stacking at around $q = 1.7$ Å⁻¹ both as rings, indicating that the crystalline domains do not have preferential orientations such as an edge-on or a face-on orientation.^[11] The d_π was determined to be 3.6 Å by the in-plane X-ray diffraction patterns (**Figure 3-4, 3-5**). Interestingly, when MW increases, the lamellar diffractions tend to appear preferentially on the q_z axis, as arcs for the polymer with $M_n = 20$ kDa and as oval spots for both polymers with $M_n = 33$ and 73 kDa, and the π - π stacking diffraction converges on the q_{xy} axis, indicating a strong tendency to orient edge-on at high MWs. The 73 kDa sample shows slightly lower crystallinity than the 33 kDa sample, as the diffractions of the third order for the lamellar and the π - π stacking appear to be weaker. As has been reported in poly(3-hexylthiophene), the crystallinity can reduce at

extremely high MW.^[12] It should be noted that the μ_{FET} of PTzBT-14HD was 0.10, 0.16, 0.42, and 0.23 $\text{cm}^2\text{V}^{-1}\text{s}^{-1}$ at $M_n = 13, 20, 33,$ and 73 kDa, respectively (**Figure 3-6**), which is quite consistent with the orientational order. This pronounced edge-on orientation on the PEDOT:PSS/ITO substrate with relatively hydrophilic surface should be surprising, since such an orientation of semiconducting polymers is typically achieved on SAM-treated SiO_2 substrates with hydrophobicity and low surface energy.^[13] I then took BHJ films for the GIXD measurements (**Figure 3-3e-f**). The sample with 13 kDa polymer shows very weak π - π stacking crystallinity, and the diffraction appears very weakly as a diffuse ring, indicating that there is no preferential orientation as similar to the polymer-only film. Note that the diffraction ring at ca. $q = 1.4 \text{ \AA}^{-1}$ corresponds to PC_{61}BM crystalites. In BHJ films with the higher MW polymers, interestingly, the polymers show a strong tendency to orient face-on, which is quite contrary to the results observed for the polymer-only film. The π - π stacking diffraction gradually converges toward the q_z axis with changing its texture from a ring to an arc. The increase of MW also leads to the improvement of crystallinity, which is maximized at 33 kDa and slightly reduced at 73 kDa. The high crystallinity and the face-on rich orientation in the high-MW polymers critically rationalize their high PCEs in the solar cells. To our best knowledge, such drastic changes in both molecular ordering and orientation for semiconducting polymer films by increasing MW and by blending with PC_{61}BM have never been observed directly using GIXD. Similar orientational change in regioregular poly(3-hexylthiophene) by mixing PC_{61}BM has recently been reported using field-induced electron spin-resonance measurements (FI-ESR).^[14] Although I do not fully understand the nature of these uncommon phenomena, I speculate that the polymer backbone favors to π - π interact with PC_{61}BM and thus stacks in the face-on manner onto PC_{61}BM on the substrate surface, of which the tendency is likely to be enhanced in the high MW polymers with long-range ordering.

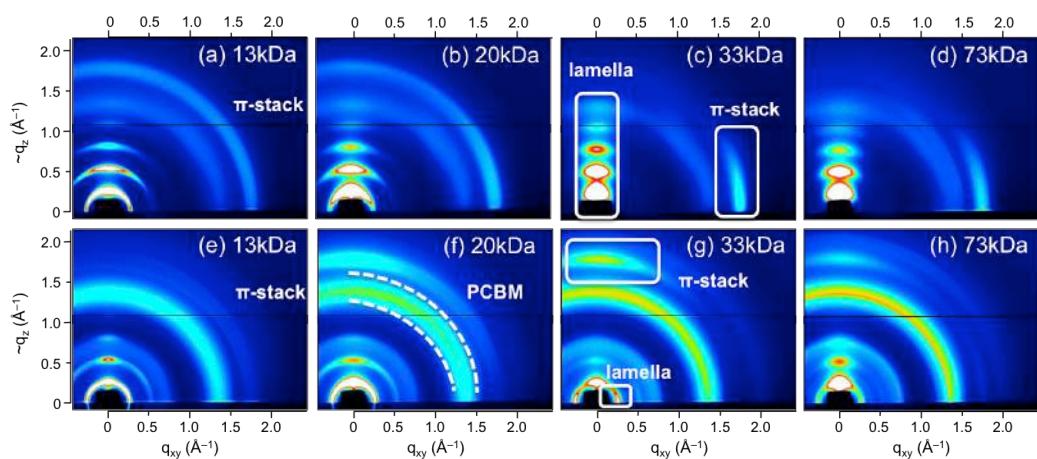


Figure 3-3. 2D-GIXDs images of the PTzBT-14HD thin films (a-d) and PTzBT-14HD/PC₆₁BM blend films (e-h) with different molecular weight on the ITO/PEDOT:PSS substrate.

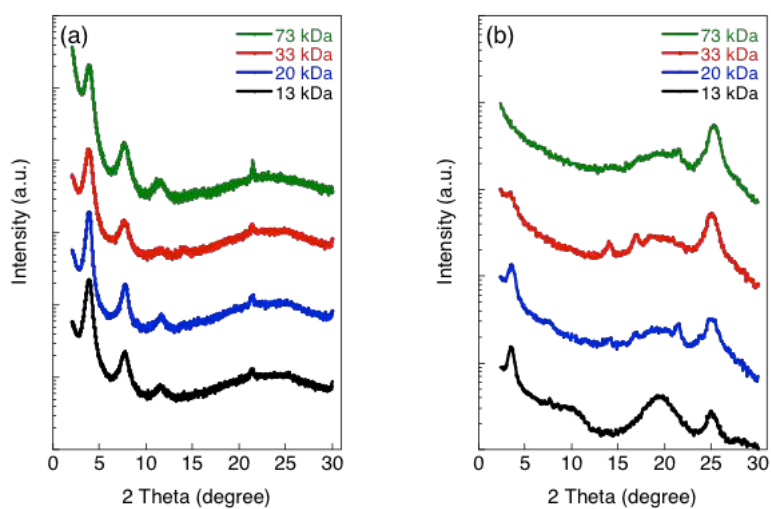


Figure 3-4. Out-of-plane (a) and in-plane (b) XRD pattern of PTzBT-14HD films

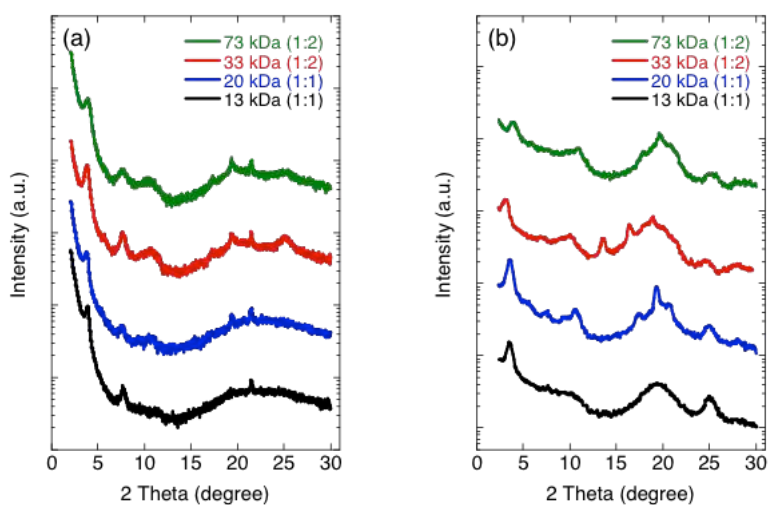


Figure 3-5. Out-of-plane (a) and in-plane (b) XRD pattern of PTzBT-14HD/PC₆₁BM blend films

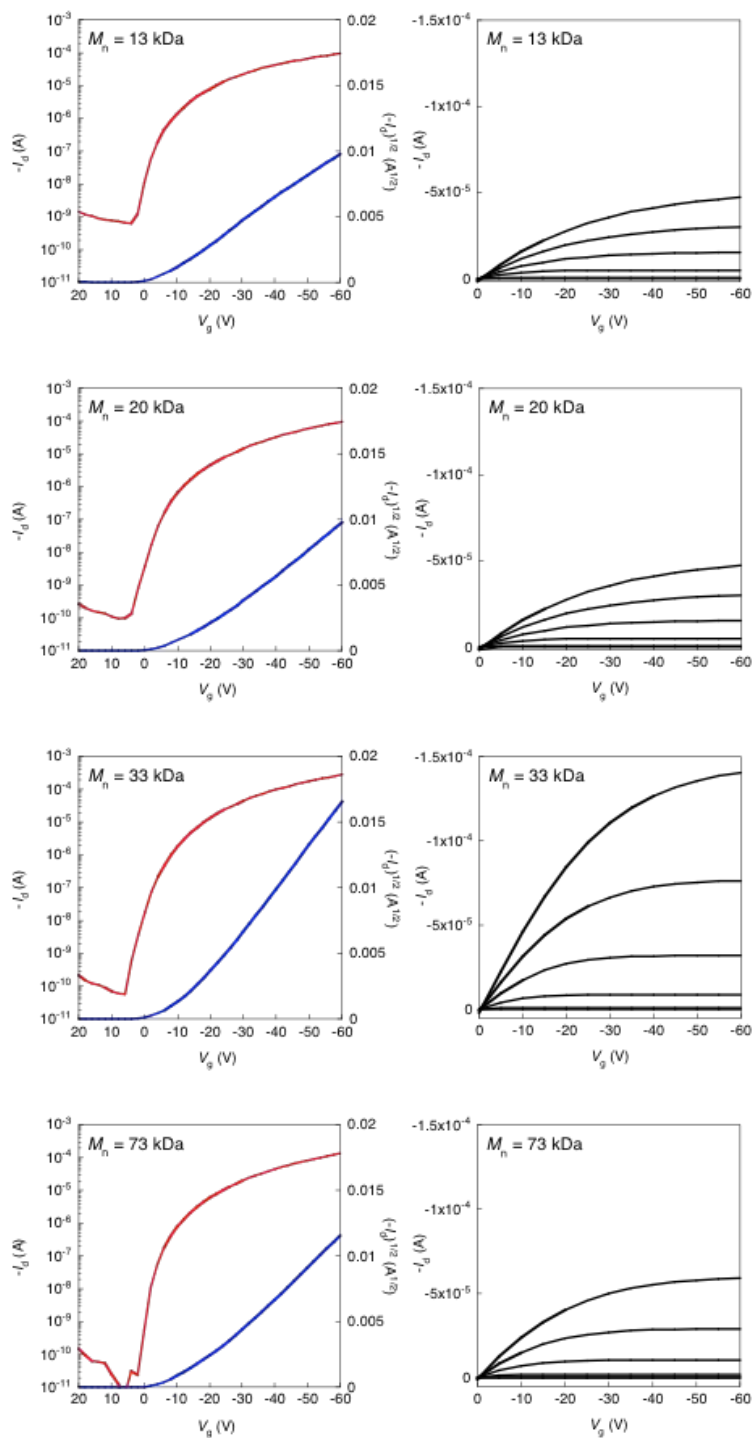


Figure 3-6. Transfer characteristics of the OFET devices based on PTzBT-14HD. Bottom-gate top-contact device on a Si/SiO₂ substrate with a channel length of 50 μm and channel width of 1500 μm are used for OFET characterization; 1H,1H,2H,2H-perfluorodecyltrimethoxysilane (FDTS) was used as the self-assembled monolayer (SAM) material.

3-3. Summary

I highlighted the photovoltaic properties of PTzBT-14HD, and the drastic change in molecular orientation. PTzBT-14HD-based BHJ solar cells, by optimizing MW, exhibited PCEs as high as 5.7%. Considering that the present polymer has an absorption edge of <700 nm and these performances are achieved with PC₆₁BM, there can be room for the improvement of efficiencies in this system. The increase of MW improved the orientational order, which showed a strong correlation with the charge carrier transport property, and blending with PC₆₁BM changed the orientational motif from the edge-on to the face-on, which accounts for the trend in photovoltaic performances. These results show that even polymers that favor an edge-on orientation can orient in a face-on manner in the presence of PC₆₁BM, leading to high PCEs, and might give new insight into understanding the structure–property relationships in BHJ solar cells.

Experimental

General procedure for polymerization

To a reaction tube equipped with a stirring bar, stannylated monomer (0.10 mmol), brominated monomer (0.10 mmol), Pd₂(dba)₃ (1.8 mg, 0.002 mmol), P(*o*-Tol)₃ (2.4 mg, 0.008 mmol), and chlorobenzene (5 ml) were added. Then the tube was purged with argon and sealed. The reaction tube was set into a microwave reactor and heated to 100°C to 200 °C for 5 to 10 min each conditions. After cooling to room temperature, the reaction solution was poured into 200 mL of methanol containing 5 mL of hydrochloric acid, and stirred for 5 hours. Then the precipitated solid was subjected to the sequential Soxhlet extraction with methanol, hexane to remove low molecular weight fractions. The residue was then extracted with chloroform and chlorobenzene, and reprecipitated in 200 mL of methanol to yield dark purple or dark blue solids (yield = 85-94%).

Instrumentation and Calculations

UV-vis absorption spectra were measured using a Shimadzu UV-3600 spectrometer. Thermal analyses were carried out with differential scanning calorimetry (DSC) on a SHIMADZU DSC-60 at 10°C min⁻¹ for both heating and cooling processes. Ionization potential (IP) was determined from the onset of photoelectron spectra measured by using a photoelectron spectrometer MODEL AC-2 in air (RIKEN KEIKI CO., LTD). Grazing incidence X-ray

diffraction (GIXD) experiments were conducted at the SPring-8 on beamline BL19B2. The sample was irradiated at a fixed incident angle on the order of 0.12° through a HUBER diffractometer and the GIXD patterns were recorded with a 2D image detector (PILATUS 100 K). GIXD patterns were recorded with an X-ray energy of 12.39 keV ($\lambda = 1 \text{ \AA}$). Two images were taken in each measurement due to the limited range of the detector, and thus two images are layered to show the entire pattern; a lateral black line in each GIXD image is to show the changeover. Out- of-plane and in-plane X-ray diffraction specular scans were carried out using a Rigaku Ultima IV. Samples for the X-ray measurements were prepared by drop-casting the polymer or polymer/PC₆₁BM solution on the PEDOT:PSS spin-coated ITO glass.

Device Fabrication and Measurement

ITO substrates were first precleaned sequentially by sonicating in a detergent bath, deionized water, acetone, and isopropanol at room temperature, and in a boiled isopropanol bath each for 10 min, and then baked at 130° C for 10 min in air, which were then subjected to a UV/ozone treatment at rt for 20 min. The precleaned ITO substrates were coated with PEDOT:PSS (Clevios PVP A14083) by spin-coating (5000 rpm for 30 s, thickness $\sim 50 \text{ nm}$). The photoactive layer was deposited in air by spin coating a CB solution containing $2.5\text{-}5.0 \text{ mg mL}^{-1}$ PTzBT-14HD with respective amount of PC₆₁BM passed through a $0.45\text{ }\mu\text{m}$ PTFE filter at 400 rpm for 20 s and 1500 rpm for 5 s, which were dried in the vacuum for 2 h. The counter electrode, consisting of LiF (0.8 nm) and Al (100 nm), was deposited by vacuum evaporation, where the active area of the cells was 0.0314 cm^2 . The thickness of the film was measured using a surface profiler (Ambios XP-100). *J-V* characteristics were measured using a Keithley 2400 source-measure unit in air without encapsulation of the cells under 1 Sun (AM1.5G) conditions using a solar simulator (Asahi Spectra, HAL-320, JIS class AAA) at 100 mW cm^{-2} . EQE spectra were measured with a home-built setup consisting of an Asahi Spectra HAL-320 Xe lamp in combination with an Asahi Spectra CMS-100 monochromator. The number of photons incident on the device was calculated for each wavelength by using a calibrated Si diode as the reference.

Reference

- [1] a) P. Schilinsky, U. Asawapirom, U. Scherf, M. Biele, C. J. Brabec, *Chem. Mater.* **2005**, *17*, 2175-2180; b) M. Koppe, C. J. Brabec, S. Heiml, A. Schausberger, W. Duffy, M. Heeney, I. McCulloch, *Macromolecules* **2009**, *42*, 4661-4666; c) J. C. Bijleveld, A. P. Zoombelt, S. G. J. Mathijssen, M. M. Wienk, M. Turbiez, D. M. de Leeuw, R. A. J. Janssen, *J. Am. Chem. Soc.* **2009**, *131*, 16616-16617; d) R. C. Coffin, J. Peet, J. Rogers, G. C. Bazan, *Nature Chem.* **2009**, *1*, 657-661; e) C. Müller, E. Wang, L. M. Andersson, K. Tvingstedt, Y. Zhou, M. R. Andersson, O. Inganäs, *Adv. Funct. Mater.* **2010**, *20*, 2124-2131.
- [2] I also attempted to increase the MW for PTzBT-HD and PTzQT-14, but a high-MW sample of PTzBT-HD could not be obtained and PTzQT-14 afforded a barely soluble sample when MW was further increased above $M_n = 20$ kDa.
- [3] I. Osaka, R. Zhang, J. Liu, D.-M. Smilgies, T. Kowalewski, R. D. McCullough, *Chem. Mater.* **2010**, *22*, 4191-4196.
- [4] a) J. C. Bijleveld, V. S. Gevaerts, D. Di Nuzzo, M. Turbiez, S. G. J. Mathijssen, D. M. de Leeuw, M. M. Wienk, R. A. J. Janssen, *Adv. Mater.* **2010**, *22*, E242-E246; b) H. Bronstein, Z. Chen, R. S. Ashraf, W. Zhang, J. Du, J. R. Durrant, P. S. Tuladhar, K. Song, S. E. Watkins, Y. Geerts, M. M. Wienk, R. A. J. Janssen, T. Anthopoulos, H. Sirringhaus, M. Heeney, I. McCulloch, *J. Am. Chem. Soc.* **2011**, *133*, 3272-3275.
- [5] I. H. Jung, J. Yu, E. Jeong, J. Kim, S. Kwon, H. Kong, K. Lee, H. Y. Woo, H.-K. Shim, *Chem. Euro. J.* **2010**, *16*, 3743-3752.
- [6] a) J. Peet, L. Wen, P. Byrne, S. Rodman, K. Forberich, Y. Shao, N. Drolet, R. Gaudiana, G. Dennler, D. Waller, *Appl. Phys. Lett.* **2011**, *98*, 043301; b) M. Zhang, X. Guo, Y. Li, *Adv. En. Mater.* **2011**, *1*, 557-560.; c) S. Subramaniyan, H. Xin, F. S. Kim, S. Shoaee, J. R. Durrant, S. A. Jenekhe, *Adv. En. Mater.* **2011**, *1*, 854-856.
- [7] a) Q. Shi, H. Fan, Y. Liu, W. Hu, Y. Li, X. Zhan, *J. Phys. Chem. C* **2010**, *114*, 16843-16848; b) M. Yang, B. Peng, B. Liu, Y. Zou, K. Zhou, Y. He, C. Pan, Y. Li, *J. Phys. Chem. C* **2010**, *114*, 17989-17994; c) L. Huo, X. Guo, S. Zhang, Y. Li, J. Hou, *Macromolecules* **2011**, *44*, 4035-4037.
- [8] S.-K. Lee, J. M. Cho, Y. Goo, W. S. Shin, J.-C. Lee, W.-H. Lee, I.-N. Kang, H.-K. Shim, S.-J. Moon, *Chem. Commun.* **2011**, *47*, 1791-1793.

- [9] J. K. Lee, W. L. Ma, C. J. Brabec, J. Yuen, J. S. Moon, J. Y. Kim, K. Lee, G. C. Bazan, A. J. Heeger, *J. Am. Chem. Soc.* **2008**, *130*, 3619-3623.
- [10] C. V. Hoven, X.-D. Dang, R. C. Coffin, J. Peet, T.-Q. Nguyen, G. C. Bazan, *Adv. Mater.* **2010**, *22*, E63-E66.
- [11] M. L. Chabinyc, M. F. Toney, R. J. Kline, I. McCulloch, M. Heeney, *J. Am. Chem. Soc.* **2007**, *129*, 3226-3237.
- [12] J.-F. Chang, J. Clark, N. Zhao, H. Sirringhaus, D. Breiby, J. Andreasen, M. Nielsen, M. Giles, M. Heeney, I. McCulloch, *Phys. Rev. B* **2006**, *74*, 115318.
- [13] R. J. Kline, M. D. McGehee, M. F. Toney, *Nat. Mater.* **2006**, *5*, 222-228.
- [14] S. Watanabe, H. Tanaka, H. Ito, S. Kuroda, T. Mori, K. Marumoto, Y. Shimoï, *Org. Electron.* **2011**, *12*, 716-723.

Chapter 4

4. Thiophene-thiazolothiazole copolymers: significant impact of side chain composition on backbone orientation and solar cell performance

4-1. Introduction

A numbers of studies on polymer-fullerene bulk-heterojunction (BHJ) solar cells have been made in the last several years.^[1-6] In view of the materials, great advances in the development of semiconducting polymers have brought about significant improvement in power conversion efficiencies (PCEs), which has recently exceeded 8%.^[7-10] Photovoltaic properties of the cells largely depend on the ordering structures of the polymer, i.e., crystallinity and orientation,^[11-14] which would determine the exciton diffusion, charge separation, and charge transport properties. It is thus crucial to control the ordering structure by molecular design and synthesis. In general, crystallinity of the polymer, which is often interpreted as the strength of π - π stacking, can be enhanced by the introduction of fused heteroaromatic π -cores into the main chain.^[15-21] Meanwhile, driving force to direct the polymer orientation edge-on and face-on is not yet well-understood, and thus the control of orientation is a remaining issue.^[10,13,22-27]

Among the many polymer systems studied so far, thiazolothiazole (TzTz)-based polymers is an interesting system that provides highly crystalline structures, and thus high charge carrier mobilities and good photovoltaic properties.^[24,28-38] Recently, I have reported that PTzBT-14HD ($R^1 = n$ -tetradecyl (C14), $R^2 = 2$ -hexyldecyl (HD)), **Figure 4-1**) showed hole mobilities of $\sim 0.42 \text{ cm}^2/\text{Vs}$ in thin-film transistors, suggesting that this polymer system has a quite superior charge transport property.^[39] PTzBT-14HD also affords good photovoltaic properties; the conventional BHJ solar cells (ITO/PEDOT:PSS/PTzBT-14HD:PC₆₁BM/LiF/Al) showed PCEs of $\sim 5.7\%$.^[39] More interestingly, the polymer orientation was found to be quite sensitive to the internal (molecular weight) and external (addition of PC₆₁BM) factors. When the molecular weight was low ($M_n = 13\text{kDa}$), it randomly oriented on the substrate plane in the polymer-only film, and by an increase of molecular weight ($M_n = 20\text{kDa}$, 33kDa , and 73kDa), orientational order improved to predominantly edge-on. On the other hand, the polymer spontaneously changed the orientational motif into face-on by blending with PC₆₁BM. All of these structural features are quite in good correlation with the device properties.

This sensitivity inspired us to study further on the orientation using this simple polymer platform. I assumed that this sensitivity in PTzBT-14HD is attributed to the introduction of both I linear and branched alkyl side chain, as they have different size and thus different interactions. In this paper, demonstrate that, in fact, the orientational order in the thiophene-thiazolothiazole (TzTz) copolymer system can be altered by tuning of the alky side chain composition. Furthermore, I highlight that the orientational order significantly impact their solar cell efficiency in particular when the thicker active layers are used, which is particularly important for the practical use.^[31] One of the polymers synthesized here demonstrated high PCEs of >6.5% with the use of PC₆₁BM (7.5% with PC₇₁BM) at the thickness of >300 nm and PCEs of close to 6% even at the extraordinarily thick layers of up to 1 μ m.

4-2. Result and discussion

The polymer structure and alkyl side chains used in this study are shown in **Figure 4-1**. Our speculations about the reason why PTzBT-14HD forms the edge-on orientation in the polymer-only film is that the linear alkyl chain, C14, is longer than the trunk part of the branched HD chain, the *n*-decyl (C10), and thus the character of the linear alkyl chain, which often drives the backbone to edge-on orient,^[29,40] could be stronger. I therefore, hypothesized that by shortening the linear or elongating the branched alkyl chain and by replacing the linear alkyl chain with branched chain in PTzBT-14HD can lead to the polymers with a more tendency to form face-on orientation. Based on this hypothesis, shorter linear chains, the C10 and *n*-dodecyl (C12) groups, are selected as R¹ while maintaining HD as R², i. e., PTzBT-10HD and -12HD, in which the length difference between R¹ and R² is smaller than in PTzBT-14HD and thus the character of R² (branched) could be enhanced. These three linear side chains are also combined with the octyldodecyl (OD) side chain as R² (PTzBT-10OD, -12OD, -14OD). The 2-ethylhexyl (EH) and 2-butyloctyl (BO) branched side chains are also introduced as R¹, with HD and OD as R² (PTzBT-EHHD, -BOHD, -EHHD, -EHOD), thereby in these cases, R¹ and R² are both branched. The BO side chain is also introduced as both R¹ and R² (PTzBT-BOBO). All the polymers are synthesized via the Stille coupling reaction with Pd₂(dba)₃ and P(*o*-Tol)₃ as the catalyst system in chlorobenzene (CB) using a microwave reactor. Although most of the polymers were synthesized at 200 °C for 10 min, some polymers with relatively low solubility, such as PTzBT-10HD, -10OD, -EHHD, and -BOBO, were synthesized at 100 °C for 10 min to avoid “over-polymerization”, giving insoluble samples. All the polymers are collected as chloroform fraction at the time of purification by sequential Soxhlet extraction. PTzBT-14OD, -EHOD, -BOHD, and -BOOD showed higher

solubility than the rest, being soluble even in chloroform, CB, and *o*-dichlorobenzene (DCB) at around 50 °C, and can be processed with room temperature solution. Molecular weights of the polymers are mostly above 30 kDa (M_n) (**Table 4-1**). The relatively low molecular weight for PTzBT-10HD, -10OD, -EHHD, and -BOBO (M_n = 16~24 kDa) is due to the lower polymerization temperature as mentioned above, and these molecular weights may be the limitation while the sufficient solubility is ensured.

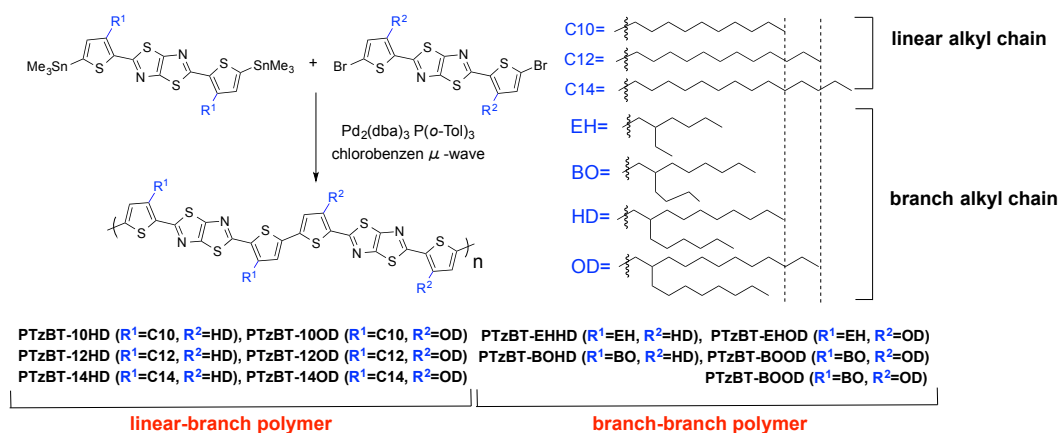


Figure 4-1. Chemical structure and polymerization of PTzBT- R^1R^2

Table 4-1. Polymerization conditions and molecular weights of PTzBT- R^1R^2 .

Side chains	Polymerization conditions	M_n (kDa) ^a	M_w (kDa) ^a	PDI ^a
10HD	100 °C, 10 min	20	60	3.0
10OD	100 °C, 10 min	16	35	2.2
12HD	100 °C, 1 hr	24	29	1.2
12OD	200 °C, 1 hr	41	65	1.6
14HD	100 °C, 1 hr	33	290	8.8
14OD	200 °C, 1 hr	44	130	3.0
EHHD	100 °C, 10 min	22	10985	500
EHOD	200 °C, 1 hr	43	1110	25
BOBO	100 °C, 10 min	16	37	2.3
BOHD	200 °C, 1 hr	35	110	3.1
BOOD	200 °C, 1 hr	28	47	1.7

^a Determined by GPC using polystyrene standard and *o*-dichlorobenzene as the eluent at 140 °C.

UV-vis absorption spectra of the polymers are mostly identical and give absorption maxima at 570-575 and 620-630 nm along with a shoulder at ca. 530 nm in the film (**Figure 4-2a**). The band gaps (E_g) of the polymers are estimated to be ca. 1.8 eV from the absorption onset in the film spectra. HOMO energy levels (E_{HOMO}) were evaluated by photoelectron spectroscopy; typically E_{HOMO} was -5.20 to -5.21 eV and was slightly deeper, -5.23 eV, for PTzBT-BOBO, -BOHD, and BOOD(**Figure 4-2b**).

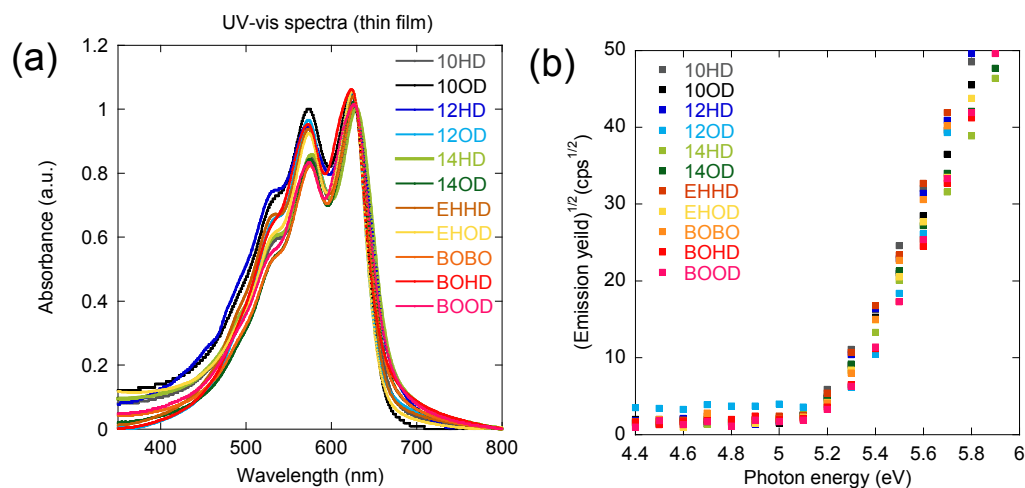


Figure 4-2. UV-vis absorption spectra (a) and Photoelectron spectra (b) of the polymers in the film.

Two-dimensional grazing incidence X-ray diffraction (2D-GIXD) studies were carried out with the polymer films. The experimental 2D-GIXD images of the polymers with linear-branched and all-branched side chains are displayed in **Figure 4-3a** and **4-3b**, respectively. Note that because the diffraction data along the q_z axis ($q_{xy} = 0$) are not true specular scans, the near-specular region is removed from the images.^[41] As has been reported previously,^[39] PTzBT-14HD exhibits the diffraction corresponding to the lamellar structure, ($h00$), on the q_z axis as spots and that corresponding to the π -stacking structure, (010), on the q_{xy} axis as a short arc (**Figure 4-3b**, upper right), in which I assume that the unit cell is orthorhombic. This indicates a predominant edge-on orientation.^[42] This is, again, probably led by the character of the linear C14 side chain (R^1) that is longer than the trunk part of the branched HD side chain (R^2), C10, on the co-unit. When the linear side chain (R^1) becomes shorter such as C12 and C10 (PTzBT-12HD, -10HD), in which the length difference between the HD chain (R^2) and R^1 is smaller or nothing, the lamellar and π -stacking diffractions appear on the q_{xy} and q_z axis (**Figure 4-3b**,

upper middle and left), respectively, corresponding to the face-on crystallite.^[23] In PTzBT-12HD, although the population of the edge-on crystallite is dominant, some face-on crystallites coexist, which I call this bimodal orientation for simplicity. In PTzBT-10HD, the orientation becomes preferentially face-on as the π -stacking diffraction converges toward the q_z axis, though the arcing of the diffraction is relatively large, indicating that there is some misorientation. Similar change in the texture is seen in the case of longer branched side chain, $R^2 = OD$. In PTzBT-14OD (**Figure 4-3b**, bottom right), bimodal orientation is observed as similar to the case in PTzBT-12HD, both of which have the length difference of two carbons between R^1 and R^2 , though population of the face-on crystallite is relatively larger for PTzBT-14OD. By shortening the linear side chain, PTzBT-12OD and 10OD, again the face-on crystallite becomes more dominant (**Figure 4-3b**, bottom middle and left). These results suggest that PTzBT derivatives can form the face-on orientation when the character of the branched side chain is increased, as I expected. In addition, as PTzBT-10HD and -12OD show strong diffractions corresponding to the face-on crystallite, introduction of the linear and branched side chains with the same length could be a key to render the polymer orientation face-on with high crystallinity.

When the linear side chain (R^1) of PTzBT-14HD is replaced with the branched EH or BO side chains (PTzBT-EHHD or -BOHD), the polymers also orient in face-on manners, as the π -stacking diffraction appears on the q_z axis (**Figure 4-3b**, upper left and middle right). In particular, in PTzBT-BOHD, where the length difference between R^1 and R^2 is smaller than in PTzBT-EHHD, the arcing of π -stacking diffraction is less prominent, indicating that PTzBT-BOHD is more preferentially face-on oriented. The texture of PTzBT-BOOD (**Figure 4-3b**, bottom right), where the length difference between R^1 and R^2 is the same as PTzBT-EHHD, appears similar to that of PTzBT-EHHD. When both R^1 and R^2 are BO, PTzBT-BOBO, both the lamellar and π -stacking diffractions appear very strong (**Figure 4-3b**, upper right), suggesting that the face-on orientation is accompanied by the highly crystalline order, which could be understood by the more regular structure than the other PTzBTs. As an exception in the all-branched polymers, PTzBT-EHOD, with the largest length difference between R^1 and R^2 among the present polymers, shows π -stacking diffraction along the q_{xy} axis (**Figure 4-3b**, bottom left), indicative of an edge-on orientation.

In order to quantify the orientation, I calculated the intensity ratio of the out-of-plane (q_z axis) to in-plane (q_{xy} axis) lamellar peaks, which is regarded as the rough estimation of edge-on to face-on crystallite ratio (**Table 4-2**).

Due to the above-mentioned issue in the 2D images, in particular at higher angles along the q_z axis,^[41] I here used lamellar diffractions instead of π - π stacking diffractions. While the ratios of the polymers with face-on orientation are below 1, those of the polymers with edge-on or bimodal orientation are 4-31. PTzBT-BOBO gives the lowest value of 0.2 and PTzBT-14HD give the highest value of 31.0, implying that these polymers have the highest degree of face-on and edge-on, respectively, among the polymers studied here.

π -Stacking distances (d_π) of the polymers are fairly short (**Table 4-2**). Most of the polymers afford d_π of around 3.5 Å, which is quite short for semiconducting polymers, indicating that PTzBTs has strong intermolecular interactions. The slightly wider d_π , by ca. 0.05 Å, is observed for PTzBT-BOBO, -BOHD, and -BOOD, probably as a result of the introduction of long branched side chain for both R¹ and R².

As shown above, the length difference between R¹ and R², in which the length of the trunk part is taken into account in case of branched side chains, seems to play an important role to determine the crystallinity and orientation. When the difference is larger the polymers form an edge-on orientation: note that in the case of the linear-branched system, the linear side chain must be longer. When the difference is smaller, on the other hand, the polymers tend to form a well-ordered face-on orientation with crystalline π - π stacking. Although the real nature of the change in the orientation is yet unclear, it should relate to the intermolecular interactions of the polymers, which would vary according to the difference of length, i.e., size, between R¹ and R².

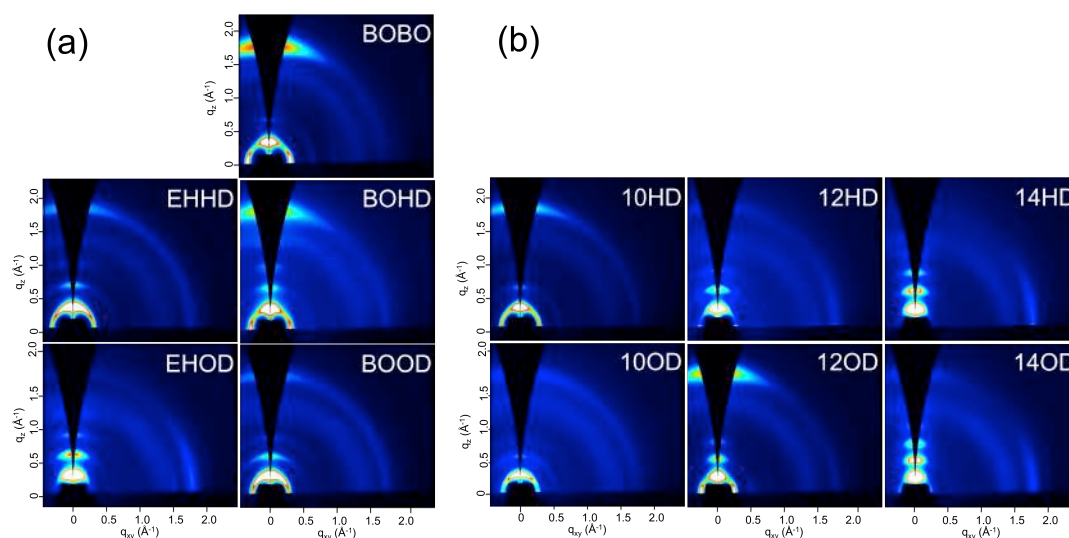


Figure 4-3. 2D-GIXDs images of polymer thin films for PTzBT-R¹R² with the linear and branched side chains (a) and with all branched side chains (b).

Table 4-2. Edge-on and face-on ratios and π stacking distance (d_π) of the polymers

polymer	orientation	$I_{op}/I_{in}^{[a]}$		$d_\pi[\text{\AA}]^{[b]}$	
		polymer-only	blend	polymer-only	blend
10HD	face-on	0.8	0.2	3.49 (3.49)	3.48
10OD	face-on	0.5	0.2	3.54 (3.56)	3.51
12HD	bimodal	4.3	0.4	3.51 (3.54)	3.48
12OD	face-on	0.6	0.1	3.48 (3.48)	3.48
14HD	edge-on	30.1	0.9	NA (3.55)	3.49
14OD	bimodal	11.5	0.2	3.50 (3.51)	3.49
EHHD	face-on	1.0	0.3	3.52 (3.55)	3.46
EHOD	edge-on	8.7	0.9	3.51 (3.54)	3.47
BOBO	face-on	0.2	0.3	3.55 (3.58)	3.52
BOHD	face-on	0.9	0.4	3.54 (3.61)	3.49
BOOD	face-on	0.9	0.5	3.57 (3.61)	3.56

[a] Intensity ratio of out-of-plane (I_{op}) to in-plane (I_{ip}) lamella peaks. The intensity was derived by the curve fitting of the corresponding peaks in the linecuts along the q_z and q_{xy} axis using Pseudo-Voigt function. [b] π -Stacking distances (d_π) are determined from the diffraction profile along the q_z axis (out-of-plane) of the 2D-GIXD image. d_π determined from the in-plane profile (along the q_{xy} axis) are shown in the parenthesis.

In the polymer/PC₆₁BM blend films (**Figure 4-4a and 4-4b**), all the polymers display the texture corresponding to face-on orientation. In other words, while the polymers that form face-on orientation in the polymer-only films, “face-on-polymers”, preserve their orientation, the polymers that form edge-on or bimodal orientation in the polymer-only films, “edge-on-polymers” or “bimodal-polymers”, spontaneously change their orientation into face-on in the blend films, as reported in the previous paper for PTzBT-14HD^[39] and also for other polymers.^[21, 25] This change could be due to the π - π interaction between the polymer and the fullerene,^[43] and/or the weakened π - π stacking of the polymer in the presence of PC₆₁BM. However, the edge-on to face-on ratios of the edge-on polymers (0.9), i. e. PTzBT-14HD and -EHOD, were larger than the others (0.2–0.5) (**Table 4-2**), implying that although the textures in 2D-GIXD can be assigned to the face-on orientation, there may be a certain difference in

the degree of orientation by the primary orientation. Further quantitative analysis will be necessary to confirm this. The π - π stacking diffraction appears weaker in the blend films, suggesting the reduced π - π stacking crystallinity, for the polymers with all-branched side chains compared to those with linear-branched side chains. This might be because the bulky branched side chains would suppress the long-range π - π stacking order particularly in the blend. Nevertheless, most of the polymers are found to preserve the d_π of the primary structure in the polymer-only films. PTzBT-BOOD, with the bulkiest alkyl groups among the present polymers, gives a wider d_π in the blend film than the rest of polymers. Further studies on the change in orientation by the side chain composition and by the addition of PC₆₁BM are currently underway, which will be published separately.

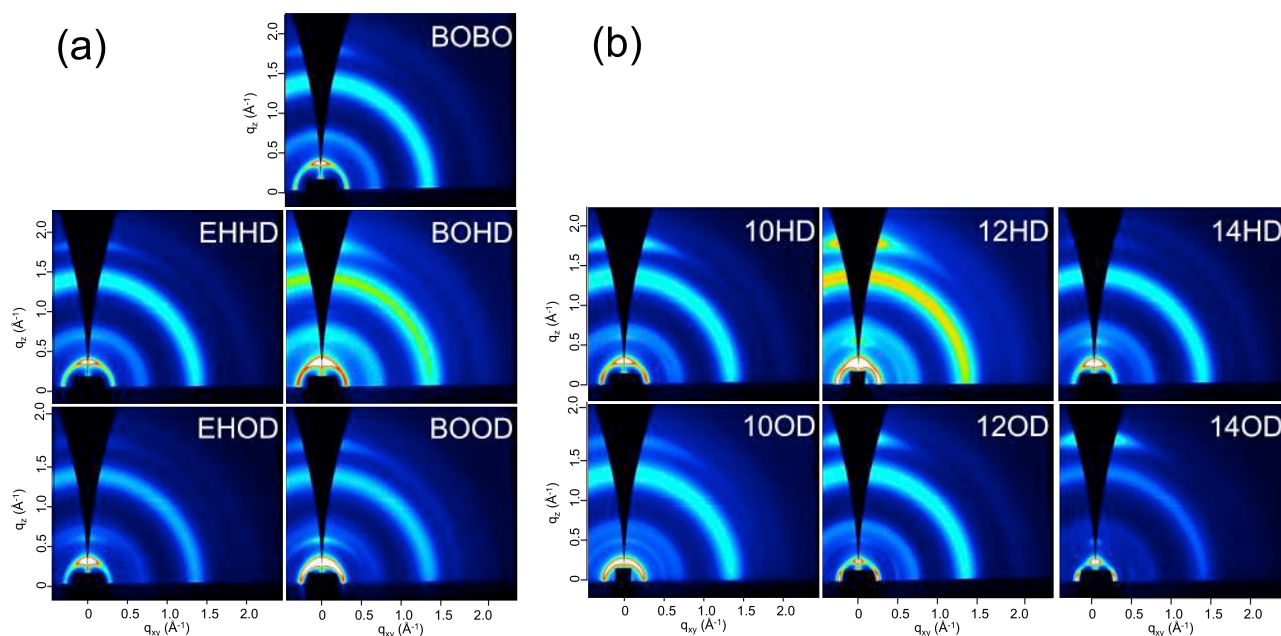


Figure 4-4. 2D-GIXDs images of polymer/PC₆₁BM blend films for PTzBT-R¹R² with the linear and branched side chains (a) and with all branched side chains (b).

Figure 4-5a and **4-5b** depict the current density (J)-voltage (V) curves of the hole-only devices based on polymer-only and polymer/PC₆₁BM blend films (ITO/PEDOT:PSS/active layer/MoO₃/Al), respectively.^[44] The charge carrier mobilities (μ_{SCLC}) listed in **Table 4-3** are those obtained as space-charge-limited-current model for the representative polymers, i.e. PTzBT-14HD, -EHOD (edge-on-polymers), -12HD, -14OD (bimodal-polymers), and -12OD, -BOHD (face-on-polymers), in the polymer-only films and blend films (see **Table S4-1** for the

complete list for all the polymers). As expected, in the polymer-only films, face-on-polymers and bimodal-polymers afford higher μ_{SCLC} , $0.5\text{-}1.9 \times 10^{-4} \text{ cm}^2 \text{ V}^{-1} \text{ s}^{-1}$, whereas edge-on-polymers affords lower μ_{SCLC} , below $0.2\text{-}0.3 \times 10^{-4} \text{ cm}^2 \text{ V}^{-1} \text{ s}^{-1}$. This suggests that the orientation of the polymers largely contributes to the out-of-plane charge transport across the electrodes sandwiching the thin film. Interestingly, in the blend films, although the orientation of all the polymers is face-on regardless of the orientation in the polymer-only films, the face-on-polymers tend to show high μ_{SCLC} as compared to the edge-on-polymers and bimodal-polymers, reflecting the orientation in the polymer-only films.

On the other hands, I fabricated the OFET device and estimated the μ_{FET} , and transfer characteristics of the OFET devices based on PTzBT-R¹R² was shown in **Figure 4-6**. Bottom-gate top-contact device on a 1H,1H,2H,2H-perfluorodecyltrimethoxysilane (FDTS) treated Si/SiO₂ substrate was used. The μ_{FET} of PTzBT-R¹R² was independent of polymer orientation from 2D-GIXDs (**Table 4-3**). And linear-branched polymers were $0.13\text{-}0.28 \text{ cm}^2\text{V}^{-1}\text{s}^{-1}$ and -10HD was 0.0052, which is caused by low molecular weight of -10HD. All-branched polymers were $0.015\text{-}0.11 \text{ cm}^2\text{V}^{-1}\text{s}^{-1}$, all-polymers with EH groups was higher than that of other branched polymers. In these results, vertical direction hole mobilities of face-on polymers were higher than edge-on polymers, though horizontal direction hole mobilities of face-on polymers and edge-on polymers were almost the same.

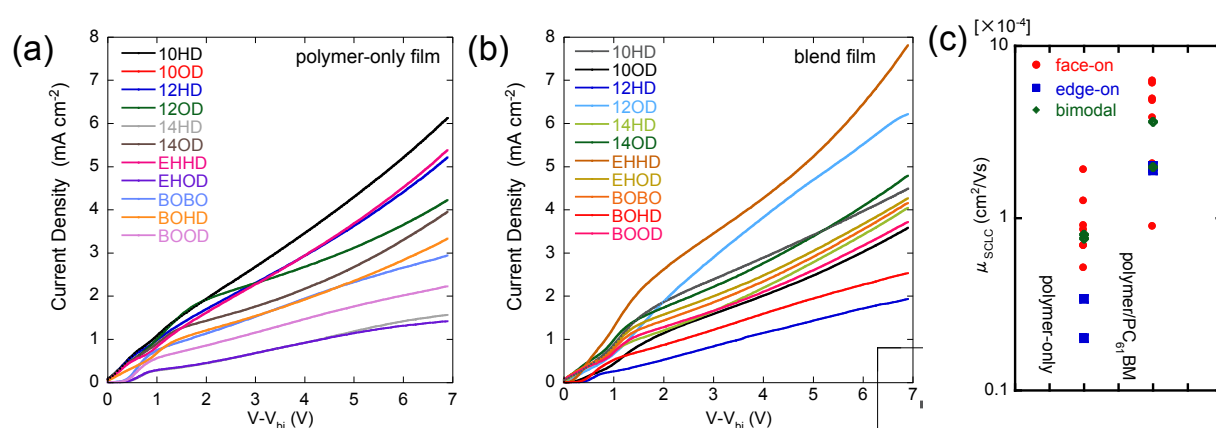


Figure 4-5. *J-V* curves of the hole-only devices with the polymer-only films (a) and polymer/PC₆₁BM blend films (b), and the plot of the mobility evaluated by the space-charge-limited-current model (c).

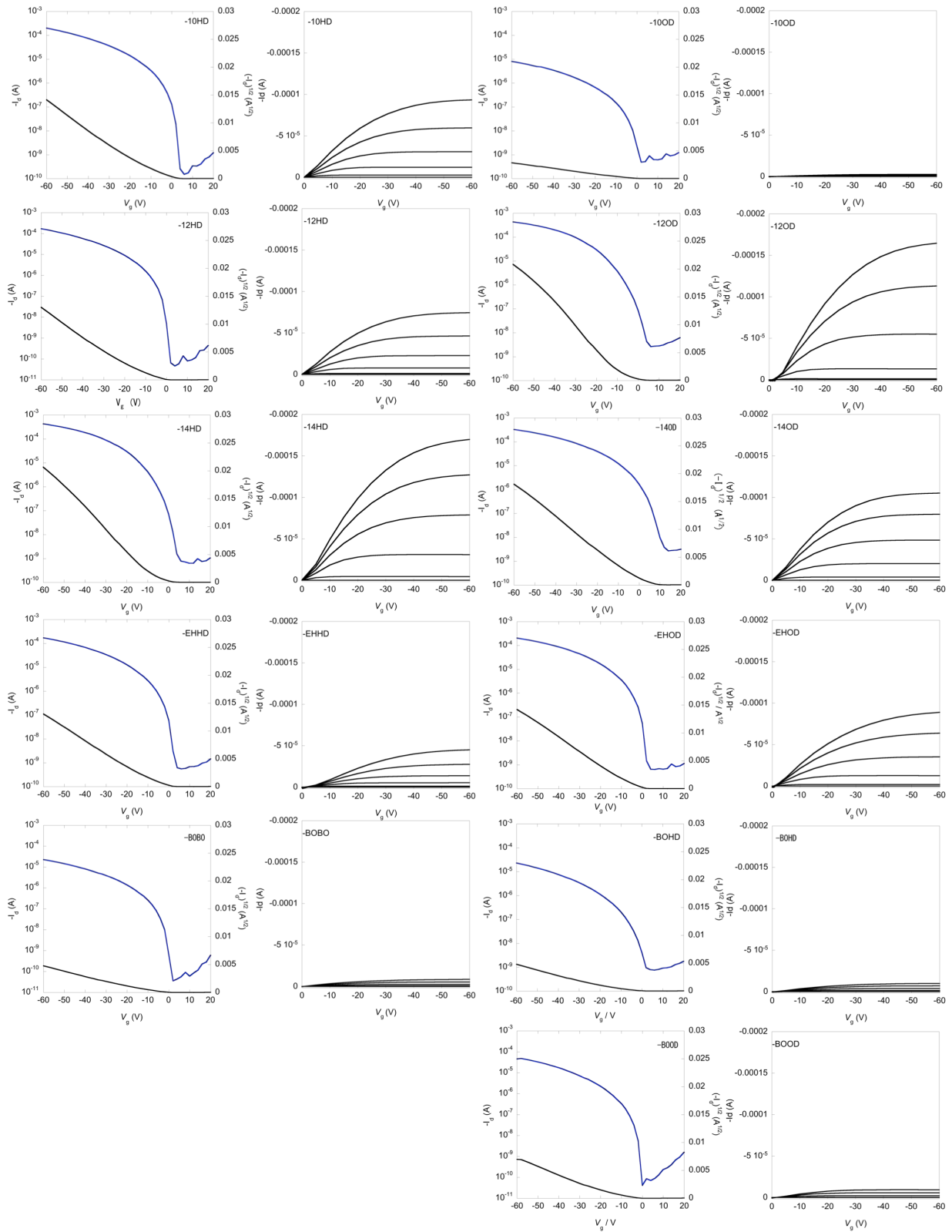


Figure 4-6. Transfer and output characteristics of the OFET devices based on PTzBT-R¹R². Bottom-gate top-contact device on a Si/SiO₂ substrate with a channel length of 50 μm and channel width of 1500 μm are used for OFET characterization; 1H,1H,2H,2H-perfluorodecyltrimethoxysilane (FDTS) was used as the self-assembled monolayer (SAM) material

BHJ solar cells with the device architecture of ITO/PEDOT:PSS/polymer:PC₆₁BM/Ca/Al were fabricated and examined. **Figure 4-7a** and **4-7b** show *J-V* curves and external quantum efficiency (EQE) spectra of the solar cells using roughly 200 nm thickness films, respectively. The optimal polymer (p) to PC₆₁BM (n) ratio was 1:2 for most of the polymers, and 1:1 for PTzBT-BOOD, 1:3 for -BOBO, and 1:4 for -EHHD. Most of the PTzBTs-based cells show good PCEs of >5%, with J_{SC} of ~10 mA/cm², V_{OC} > 0.8 V, FF > 0.6 (**Table 4-3**). **Table 1** summarizes the OPV parameters for the selected polymers due to the limited space. Interestingly, a notable difference in V_{OC} was found between the polymers with the linear-branched and all-branched side chains. The cells with the linear-branched system give V_{OC} of 0.81-0.82 V, whereas the cells with all-branched system give 0.88-0.90 V, despite the fact that E_{HOMO} s of the polymers are almost the same. This difference in V_{OC} on the composition of the side chain is seemingly independent of the orientation or morphology. The V_{OC} difference is possibly due to the different intermolecular interaction between the polymer and PC₆₁BM.^[45,46] The weak π - π stacking crystallinity of the all-branched system compared to the linear-branched system in the presence of PC₆₁BM as described above, which can also be counted as weaker polymer-PC₆₁BM interactions, might reduce the charge recombination, in turn leading to the high V_{OC} .

The fact that J_{SC} and FF of these cells are mostly similar implies that the photovoltaic properties are independent of the polymer orientation and charge transport within the thickness range of < 200 nm. I note that, however, the primary orientation seems to impact the device performance when the active layer is thicker. PTzBT-14HD, -EHOD (edge-on-polymers), -12HD, -14OD (bimodal-polymers), and -12OD, -BOHD (face-on-polymers) were chosen as representative of the polymers with three different orientations, because they have sufficiently high molecular weights, which allows direct comparison of the solar cell properties, and evaluated the OPV properties of their cells with the different thickness (**Table 4-3**).

Figure 4-8a-c depict thickness dependence of J_{SC} , FF, and PCE on the active layer thickness (100-400 nm), respectively, for the cells with these polymers. Clearly, all the polymer-cells increase J_{SC} as a function of thickness, reflecting the increased volume of the light-absorbing layer. On the other hand, while in face-on-polymers, the cells mostly preserve FF above 0.6 even with the 400 nm thickness, in bimodal-polymers and edge-on-polymers, FF drops to < 0.6 when the thickness is above 200 nm. As a result, PCEs increase for face-on-polymers and decrease for bimodal-polymers and edge-on-polymers when the thicker layers (>200 nm)

are used. For example, the cells using a face-on-polymer, PTzBT-BOHD, show a PCE of 6.1% ($J_{SC} = 10.1 \text{ mA/cm}^2$, $V_{OC} = 0.90 \text{ V}$, $FF = 0.67$), which increases to 6.7% ($J_{SC} = 11.4 \text{ mA/cm}^2$, $V_{OC} = 0.89 \text{ V}$, $FF = 0.65$) by increasing the film thickness from 200 nm to 270 nm. On the other hand, those using PTzBT-14HD, with the edge-on orientation in the polymer-only film, show a PCE of 5.4% ($J_{SC} = 9.9 \text{ mA/cm}^2$, $V_{OC} = 0.82 \text{ V}$, $FF = 0.66$), which decreases to 5.0% ($J_{SC} = 11.3 \text{ mA/cm}^2$, $V_{OC} = 0.81 \text{ V}$, $FF = 0.55$) by increasing the film thickness from 200 nm to 270 nm. The reduced FF and PCE for the PTzBT-10OD and -BOOD cells with the thick film (**Table 4-3**), despite the face-on orientation, could be attributed to the relatively large phase separation as seen in the surface morphology (**Figure 4-8**), which is consistent with the low μ_{SCLC} : these polymers showed low OPV performances even with the thin film (<200 nm). The capability to preserve high FF in the thick layer is of particular importance because the thick layers can avoid pinholes and allow good reproducibility in large area processing, and absorb more light and increase J_{SC} .^[31,47,48] One can explain this different trend in the OPV properties in terms of the charge transport properties. Although all the polymers preferentially form the face-on orientation in the blend films, face-on-polymers afford higher out-of-plane mobilities as indicated above, and thereby the charge carrier can travel further through the bulk film, which would presumably contribute to high FF even in the thicker films. On the other hand, in edge-on-polymers and bimodal-polymers, the charge carrier can be trapped or can recombine before reaching the electrode, which gives rise to the loss of FF due to the relatively lower mobility. Bimolecular recombination is an important factor that should be considered to discuss FF for the thick cells,^[49] and therefore the dependence of the recombination rate on the polymer type may be necessary for in-depth understanding of this phenomenon in future.

Having the well-ordered face-on structure, with better solubility than the rest of polymers, PTzBT-BOHD turns out to be the best polymer for the use in OPVs in this series. Notably, PTzBT-BOHD-based cells still demonstrates PCEs of 6.4% with high FF of 0.6 at the thickness of 540 nm and PCEs of 5.8% even at an extraordinarily thick active layers of 1 μm (**Figure 4-7e, 4-7f** and **Table 4-3**). With the use of PC₇₁BM as the n-type material and the optimization of the active layer thickness, the solar cells of PTzBT-BOHD demonstrated a maximum PCE of 7.5% ($J_{SC} = 12.7 \text{ mA/cm}^2$, $V_{OC} = 0.90 \text{ V}$, $FF = 0.65$) at the active layer thickness of 330 nm.

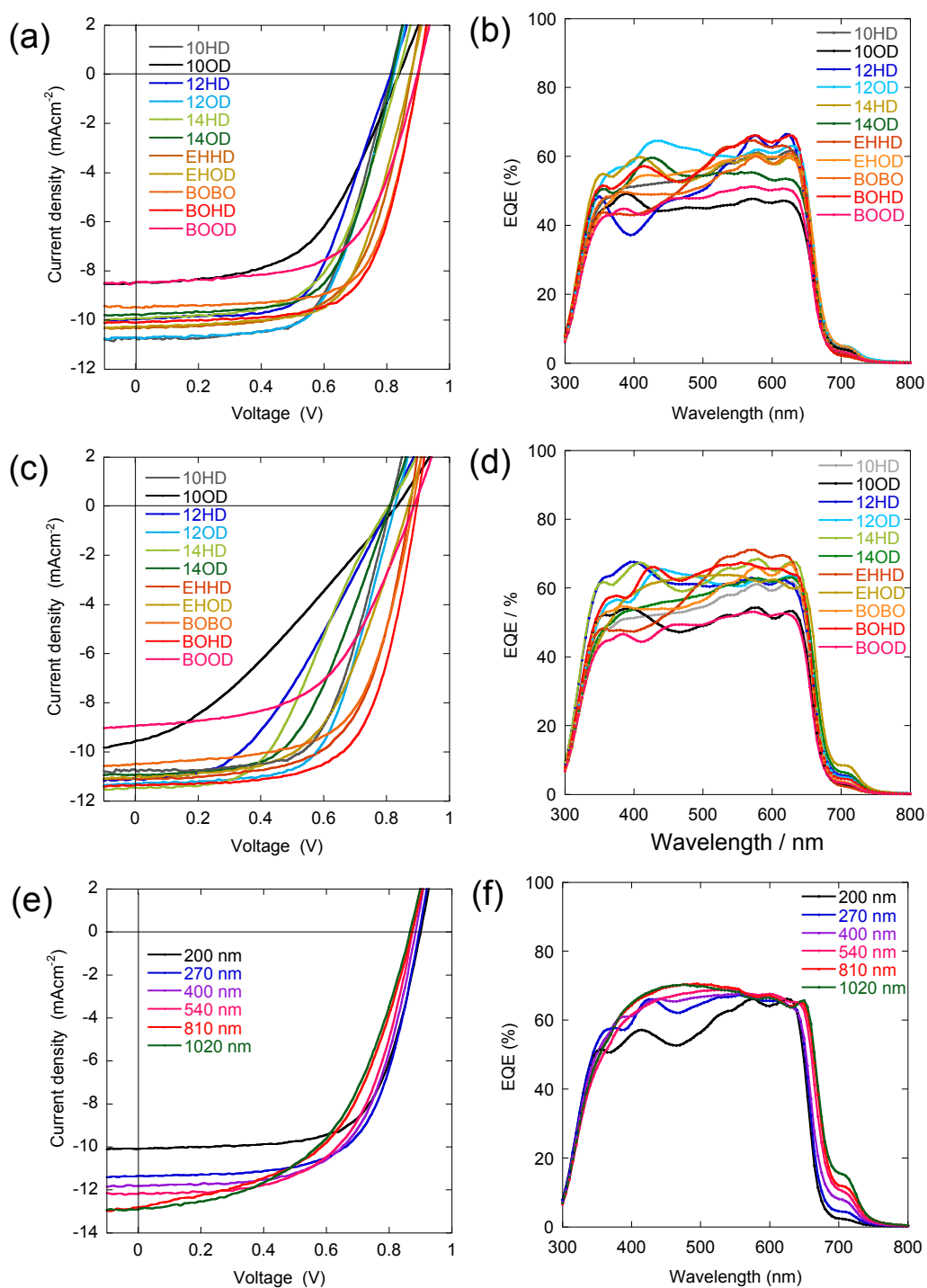


Figure 4-7. (a, b) $J-V$ curves and EQE spectra of the solar cells using PTzBTs/PC₆₁BM as the active layer with the thickness of ca. 200 nm. (c, d) $J-V$ curves and EQE spectra of the solar cell with PTzBT-BOHD/PC₆₁BM with different active layer thickness.

Table 4-3. Polymer orientation, charge carrier mobility, and photovoltaic parameters of polymer-based BHJ cells for PTzBT-R¹R²

Side chains	Orientation [a]	μ_{FET} [cm ² /Vs] [b]	μ_{SCLC} [cm ² /Vs] [c]		Photovoltaic parameters					
			polymer	blend	p:n ratio [d]	thickness [nm]	J_{SC} [mA/cm ²]	V_{OC} [V]	FF	PCE_{max} [%]
10HD	face-on		0.90×10^{-4}	4.91×10^{-4}	1:2	200	9.3	0.82	0.63	4.9 (4.7)
						230	10.2	0.81	0.62	5.2 (4.9)
10OD	face-on		0.69×10^{-4}	2.06×10^{-4}	1:2	190	8.5	0.84	0.54	3.8 (3.6)
						270	9.1	0.83	0.32	2.5 (2.2)
12HD	bimodal	0.11	0.80×10^{-4}	1.98×10^{-4}	1:2	130	7.8	0.81	0.67	4.2 [4.0]
						200	10.0	0.81	0.60	4.8 [4.6]
						270	10.7	0.81	0.53	4.4 [4.2]
						350	11.8	0.80	0.41	3.8 [3.5]
12OD	face-on	0.28	1.25×10^{-4}	6.04×10^{-4}	1:2	130	8.9	0.83	0.66	4.9 [4.7]
						210	10.7	0.82	0.62	5.5 [5.2]
						260	11.3	0.82	0.62	5.8 [5.7]
						370	11.5	0.82	0.61	5.7 [5.5]
14HD	edge-on	0.28	0.20×10^{-4}	1.89×10^{-4}	1:2	110	8.4	0.81	0.67	4.5 [4.2]
						200	9.9	0.82	0.66	5.4 [5.2]
						270	11.3	0.81	0.55	5.0 [4.8]
						360	11.7	0.78	0.52	4.8 [4.5]
14OD	bimodal	0.21	0.76×10^{-4}	3.62×10^{-4}	1:2	120	8.9	0.82	0.67	4.9 [4.7]
						190	9.8	0.82	0.64	5.1 [4.9]
						260	10.9	0.81	0.54	4.8 [4.5]
						370	10.8	0.79	0.53	4.5 [4.2]
EHHD	face-on		1.90×10^{-4}	6.24×10^{-4}	1:4	190	10.3	0.88	0.63	5.8 (5.5)
						250	11.1	0.88	0.62	6.1 (5.9)
EHOD	edge-on	0.13	0.34×10^{-4}	2.01×10^{-4}	1:2	120	8.5	0.89	0.68	5.2 [5.0]
						190	10.3	0.88	0.64	5.8 [5.6]
						260	11.1	0.87	0.56	5.4 [5.2]
						380	11.3	0.88	0.52	5.1 [4.9]
BOBO	face-on		0.69×10^{-4}	3.81×10^{-4}	1:3	190	9.5	0.90	0.68	5.8 (5.6)
						250	10.5	0.89	0.63	5.9 (5.6)
BOHD	face-on	0.015	0.85×10^{-4}	4.79×10^{-4}	1:2	120	8.9	0.91	0.68	5.5 [5.3]
						200	10.1	0.90	0.67	6.1 [5.8]

						270	11.4	0.89	0.65	6.7 [6.5]
						400	11.8	0.89	0.62	6.5 [6.3]
				1:2 [e]		330	12.7	0.90	0.65	7.5 [7.2]
BOOD	face-on	0.51×10^{-4}	0.89×10^{-4}	1:1		190	8.5	0.90	0.62	4.7 (4.4)
						260	9.0	0.89	0.54	4.3 (3.9)

[a] Polymer orientation in the polymer-only film. [b] Charge carrier mobilities evaluated using the Field effect transistor devices (FDTS treated SiO₂/active layer/Au). [c] Charge carrier mobilities evaluated using the hole-only devices (ITO/PEDT:PSS/active layer/MoO₃/Al), in which the active layer is the polymer or polymer/PC₆₁BM blend films. [d] Weight ratio of polymer (p) to PCBM (n) components. [e] PC₇₁BM was used as the n-type material.

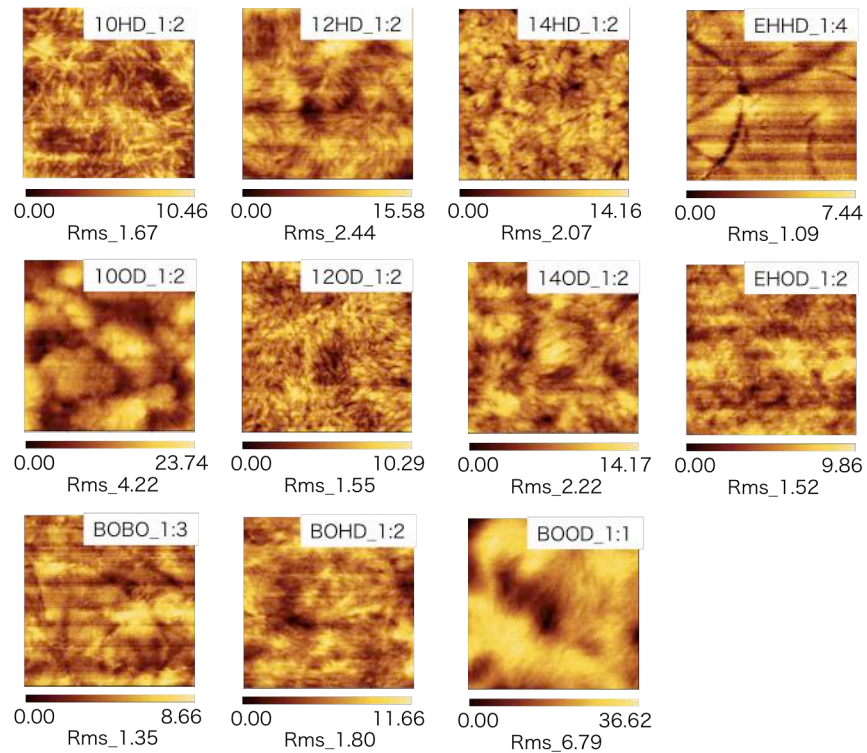


Figure 4-8. AFM images of the polymer/PC₆₁BM blend films. Polymer to PC₆₁BM ratios are shown at the right top.

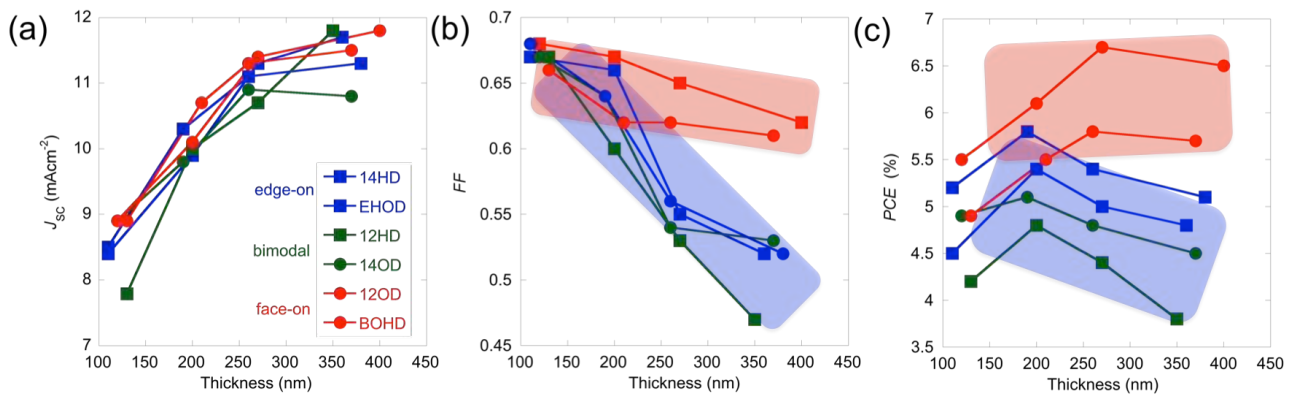


Figure 4-9. Thickness dependence of (a) J_{sc} , (b) FF , and (c) PCE of the solar cells using PTzBT-12HD, -14HD, -12OD, -14OD, EHOD, and -BOHD in conventional cells.

I also fabricated inverted structure device (ITO/ZnO/polymer:PC₆₁BM/MoO_x/Ag) in edge-on polymers (-14HD and -EHOD) and face-on polymers (-12OD and -BOHD) and measured. **Figure 4-10a** and **10b** show J - V curves and external quantum efficiency (EQE) spectra of the solar cells using optimal thickness films, respectively.

The optimal p to n ratio was 1:2 for all polymers, and Most of the PTzBTs-based cells show good PCEs of >7%, with J_{SC} of ~10 mA/cm², V_{OC} > 0.8 V, FF > 0.65. **Table 4-4** summarizes the OPV parameters for these polymers.

And **Figure 4-11a**, **11b** and **11c** depict thickness dependence of J_{SC} , FF, and PCE on the active layer thickness (200-400 nm), respectively, for the inverted cells with these polymers.

In case of conventional structure, the polymers with face-on orientation showed higher performance with thick active layer and the polymers with edge-on orientation showed lower performances as compared to what were observed with 200 nm thickness. Interestingly, in case of inverted structure, both of face-on and edge-on polymers showed higher performance with thick active layer thickness (ca. 300 nm). These results mean that the performances of the solar cells were significantly affected by the orientation when the active layers are thick in conventional structure, however, the performances of solar cells were not affected in inverted structure.

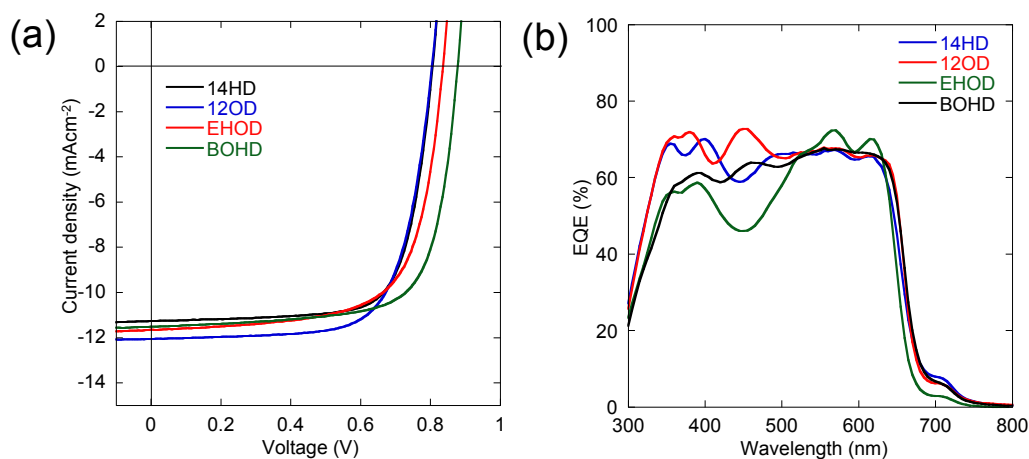


Figure 4-10. (a) J - V curves and (b) EQE spectra of the solar cells using PTzBTs/PC₆₁BM as the active layer with the optimal thickness of 300nm in inverted cells.

Table 4-4. Polymer orientation and photovoltaic parameters of polymer-based BHJ cells for PTzBT-12OD, -14HD, -EHOD, and -BOHD in inverted structure.

Side chains	Orientation [a]	Photovoltaic parameters [b]					
		p:n ratio [d]	thickness [nm]	J_{SC} [mA/cm ²]	V_{OC} [V]	FF	PCE_{max} (PCE_{ave}) [%]
12OD	face-on	1:2	210	10.5	0.81	0.76	6.4 [6.1]
			270	11.3	0.81	0.74	6.8 [6.5]
			310	12.1	0.80	0.70	6.8 [6.6]
			390	11.8	0.80	0.64	6.1 [5.8]
14HD	edge-on	1:2	180	8.6	0.83	0.76	5.5 [5.1]
			240	10.6	0.81	0.75	6.6 [6.3]
			300	11.5	0.81	0.72	6.8 [6.4]
			390	11.1	0.79	0.59	5.2 [5.0]
EHOD	edge-on	1:2	190	10.0	0.84	0.72	6.1 [5.8]
			230	10.6	0.84	0.70	6.3 [6.1]
			300	11.7	0.84	0.68	6.7 [6.5]
			390	11.8	0.83	0.55	5.4 [5.1]
BOHD	face-on	1:2	200	10.0	0.89	0.76	6.7 [6.4]
			250	11.1	0.88	0.76	7.3 [7.0]
			350	11.5	0.88	0.72	7.3 [7.1]
			400	12.5	0.87	0.61	6.7 [6.3]
			1:2 [d]	310	12.7	0.87	0.73

[a] Polymer orientation in the polymer-only film. [c] Weight ratio of polymer (p) to PCBM (n) components. [d] PC₇₁BM was used as the n-type material.

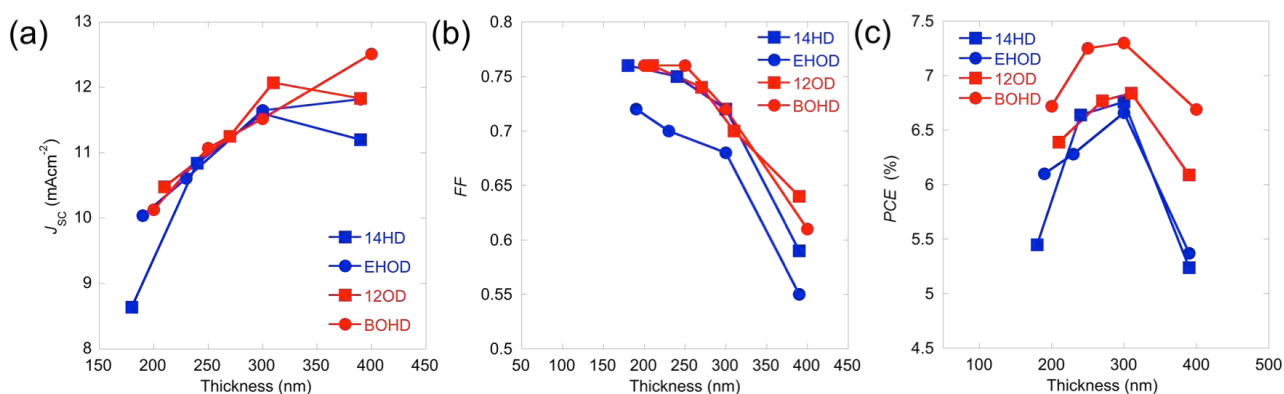


Figure 4-11. Thickness dependence of (a) J_{SC} , (b) FF , and (c) PCE of the solar cells using PTzBT-12HD, -14HD, -12OD, -14OD, EHOD, and -BOHD in inverted cells.

To investigate difference of conventional and inverted structure for polymer orientation, I measured 2D-GIXD and carried out the pole figure analysis of several thicknesses of polymer/PC₆₁BM and polymer-only films. Polymer-only films spun on ITO/PEDOT:PSS and FDTS treated SiO₂ substrate with thickness from ca. 20 nm to 200 nm and polymer/PC₆₁BM blend films spun on ITO/PEDOT:PSS and ITO/ZnO substrate with thickness from ca. 50 nm to 400 nm. I defined the areas integrated with polar angle (χ) of A_z (0-45° and 135-180°) and A_{xy} (55-125°) as corresponding to edge-on and face-on orientation fraction respectively (**Figure 4-12b**). In case of polymer-only films on FDTS treated SiO₂ substrate, whereas the ratio of A_{xy} to A_z (A_{xy}/A_z) of face-on polymers (-12OD and -BOHD) gradually decreased with the decrease of the thin film thickness, A_{xy}/A_z of edge-on polymers (-14HD and -EHOD) were independent of thin film thickness. And in case of polymer-only films on ITO/ZnO substrate, A_{xy}/A_z of all polymers were almost same in several thicknesses (**Figure 4-13b**). These results indicate that orientation was mostly similar in thin film surface, bulk and interface with ITO/ZnO substrate. However, orientation of face-on polymers was edge-on rich in thin film interface with SiO₂ substrate (**Figure 4-13a**). And these have high correlation with OFET characteristics of PTzBT-R¹R². On the other hands, in case of polymer/PC₆₁BM blend films on ITO/PEDOT:PSS substrate (**Figure 4-13c**) and ITO/ZnO (**Figure 4-13d**), A_{xy}/A_z of face-on polymers were independent of thin film thickness. However, A_{xy}/A_z of edge-on polymers gradually decreased with the decrease of the film thickness, indicate that orientation was edge-on rich in thin film interface with ITO/ZnO and ITO/PEDOT:PSS substrate.

Thus, in case of edge-on polymers, it is appropriate to consider that edge-on orientation are rich at the thin film interface with ITO/ZnO and ITO/PEDOT:PSS substrate and face-on orientation are rich in the bulk, but these is not gradient of polymer orientation in face-on polymers.

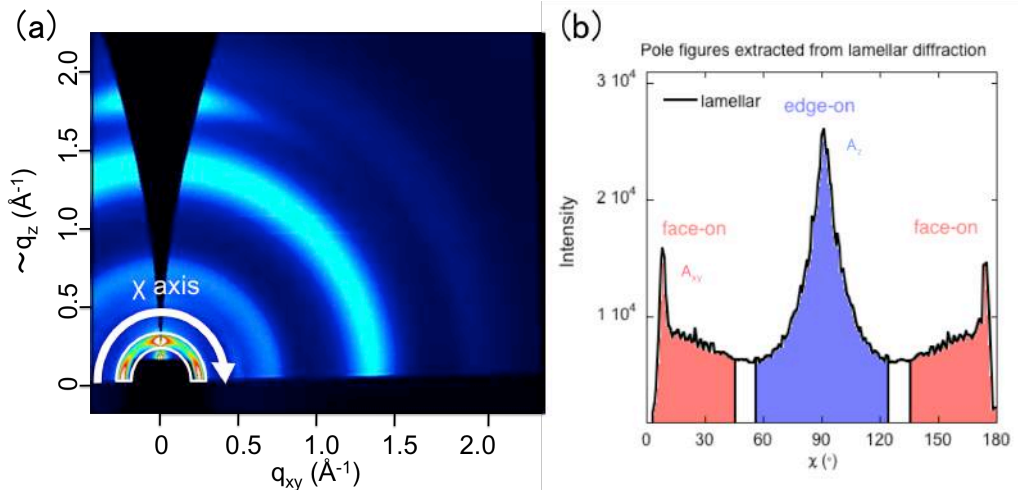


Figure 4-12. (a) Schematic image of diffraction profile pole figure (b) Schematic Pole figure extraction from lamellar diffraction on substrate.

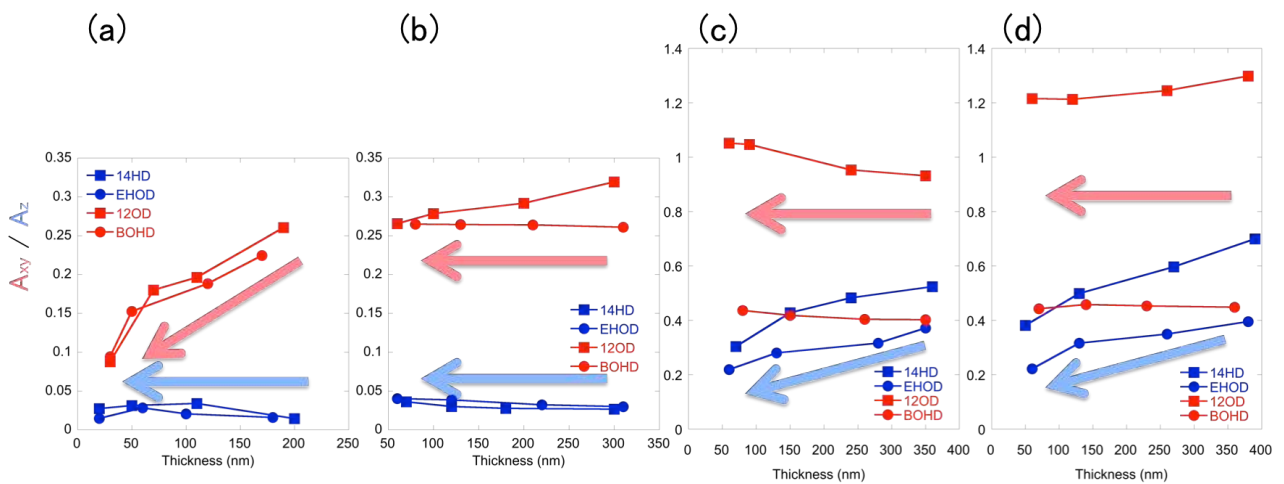


Figure 4-13. Dependence of A_{xy}/A_z on the film thickness : polymer-only films of (a) SiO₂ substrate and (b) ITO/ZnO substrate, polymer/PC₆₁BM blend films of (c) ITO/PEDOT:PSS substrate (d) ITO/ZnO substrate.

Schematic structure of PTzBT-R¹R² films on the Si/SiO₂ substrate is showed in **Figure 4-13**. On the interface of Si/SiO₂ substrate, edge-on polymers were edge-on orientation and orientation is same in the bulk. Whereas face-on orientation polymers orient edge-on on the interface of Si/SiO₂ substrate, orient face-on in the bulk. In the bottom-gate top-contact OFET device, hole transports near the interface of Si/SiO₂ substrate. Thus, hole mobilities of face-on polymers and edge-on polymers are almost the same, because the both of edge-on and face-on polymers orient edge-on on the interface of Si/SiO₂ substrate. And schematic structure of PTzBT-R¹R²/PC₆₁BM

blend films in the solar cell devices is showed in **Figure 4-14**. In these results, in case of conventional device, electron is transport to silver electrode and hole is transport to ITO electrode (**Figure 4-14a**). Thus, electron up to silver and hole down to ITO. Edge-on orientation polymer is disadvantage for hole transport in interface with ITO/PEDOT:PSS substrate. And face-on orientation polymer is advantage for hole transport of vertical direction. On the other hands, in case of inverted cells, Electron is transport to ITO/ZnO substrate and hole is transport to Ag electrode (**Figure 4-15b**), indicate that effect of polymer orientation is low. Because, in interface with substrate, electron transport to ITO/ZnO substrate via PCBM.

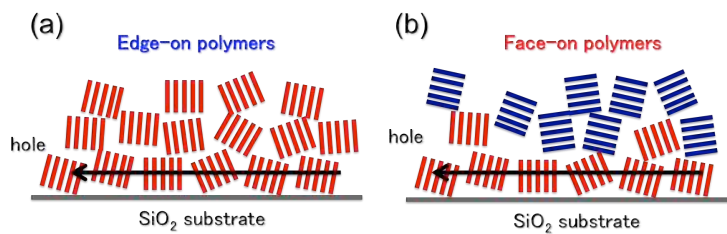


Figure 4-14. Schematic structure of Edge-on and Face-on oriented polymers thin films on SiO_2 substrate

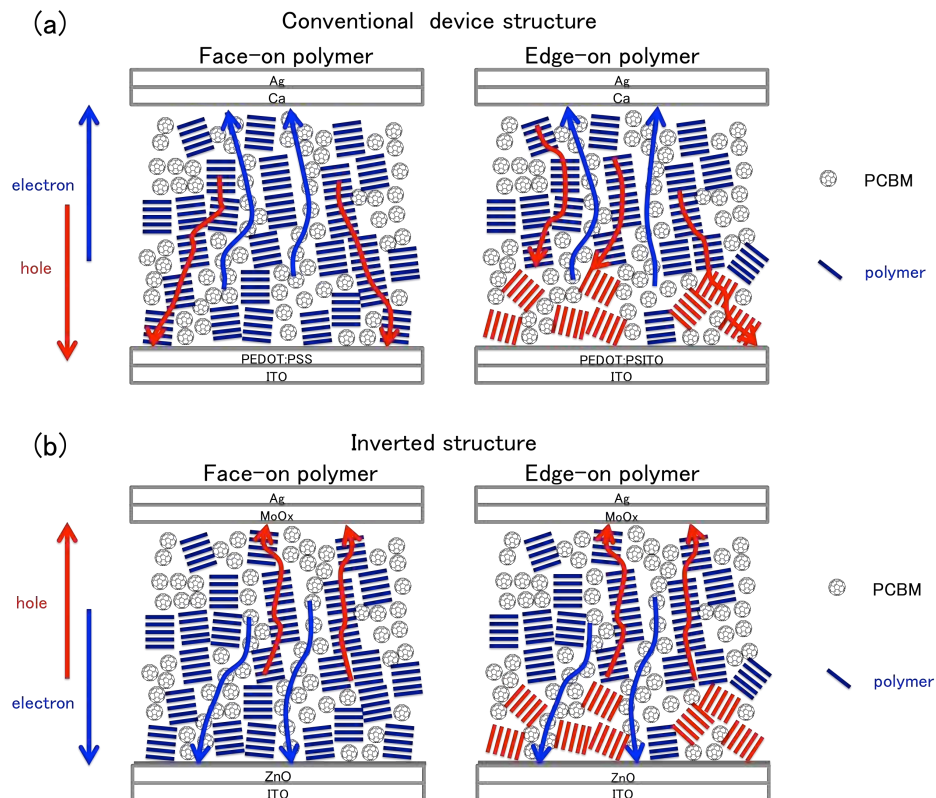


Figure 4-15. Schematic structure of PTzBT- $\text{R}^1\text{R}^2/\text{PC}_{61}\text{BM}$ blend films in the solar cell devices (a) conventional cell with PEDOT:PSS as the bottom layer and Ca as the top layer (b) inverted cell with ZnO as the bottom layer and MoO_x as the top layer.

4-3. Summary

In conclusion, I found that the backbone orientation can be altered through fine-tuning of the side chain composition in a thiophene-thiazolothiazole copolymer system where the length difference between R¹ and R² is an important factor. I demonstrated that the BHJ cells using the polymers with primarily face-on orientation afford high J_{SC} with thicker active layers without a loss of FF, resulting in the increase of PCE, while the cells using the polymers with edge-on or bimodal orientation give a certain drop of FF and thus PCE in conventional device structure. On the other hands, PCE of the cells using the polymers with edge-on, bimodal and face-on orientation were almost the same in inverted cells. These results were caused by distribution of polymer orientation, edge-on polymers were edge-on rich in interface of the ITO substrate.

Experimental

Synthesis.

2,5-Bis(3-alkyl-5-(trimethylstannyl)thiophen-2-yl)thiazolo[5,4-d]thiazoles (**1**) and 2,5-Bis-(5-bromo-3-alkylthiophen-2-yl)thiazolo[5,4-d]thiazoles (**2**) were synthesized according to the reported procedure. Note that **1s** and **2s** with the decyl, dodecyl, tetradecyl, 2-ethylhexyl, and 2-butyloctyl groups were purified by recrystallization using hexane, and **2s** with the 2-hexyldecyl and 2-octyldodecyl groups were purified by column chromatography with silica gel using hexane/chloroform (5:1) as the eluent. All chemicals and solvents are of reagent grade unless otherwise indicated. Toluene was distilled with CaH₂ prior to use. Polymerization was carried out with a microwave reactor, Biotage Initiator. Molecular weights were determined by gel permeation chromatography (GPC) with a TOSOH HLC-8121GPC/HT at 140 °C using *o*-dichlorobenzene (DCB) as a solvent and calibrated with polystyrene standards.

General procedure for polymerization

To a Microwave pressurized vial equipped with a stirring bar, **1** (0.30 mmol), **2** (0.30 mmol), Pd₂(dba)₃ (5.5 mg, 0.006 mmol), P(*o*-Tol)₃ (7.3 mg, 0.024 mmol), and chlorobenzene (12 ml) were added. Then the tube was sealed

and refilled with argon. The reaction tube was put into a microwave reactor and heated to 100 °C for 10 min for (PTzBT-10HD, -10OD, -12HD, -EHHD, and -BOBO), 100 °C for 1 h for (PTzBT-12HD, -14HD), and 200 °C for 10 min (for PTzBT-12OD, -14OD, -EHOD, -BOHD, -BOOD). After cooling to room temperature, the reaction solution was poured into 200mL of methanol containing 5 mL of hydrochloric acid, and stirred for 5 hours. Then the precipitated solid was subjected to sequential Soxhlet extraction with methanol, hexane to remove low molecular weight fractions. The residue was then extracted with chloroform, and reprecipitated in 200 mL of methanol to yield dark purple solid (yield = 85-95%).

Instrumentation.

UV-vis absorption spectra were measured using a Shimadzu UV-3600 spectrometer. Thermal analyses were carried out with differential scanning calorimetry (DSC) on an EXSTAR DSC7020 (SII Nanotechnology, Inc.) at 10 °C/min for both heating and cooling processes. Ionization potential (IP) was determined from the onset of photoelectron spectra measured by using a photoelectron spectrometer, model AC-2, in air (Riken Keiki Co., Ltd). Dynamic force-mode atomic force microscopy study was carried out on a Nanocute scanning probe microscope system (SII Nanotechnology, Inc.). GIXD experiments were conducted at the SPring-8 on beamline BL19B2. The sample was irradiated at a fixed incident angle on the order of 0.12° through a Huber diffractometer, and the GIXD patterns were recorded with a 2-D image detector (Pilatus 300K). GIXD patterns were recorded with an X-ray energy of 12.39 keV ($\lambda = 1 \text{ \AA}$). Although the films for the hole-only devices and the solar cells are prepared by the spin-coating technique, samples for the X-ray measurements were prepared by drop-casting the polymer or polymer/PCBM solution on the PEDOT:PSS-coated ITO substrate, respectively, due to the limitation of the beam time; drop-cast films with typical thickness of around 1 μm reduces the X-ray exposure time. We note that, however, the textures obtained for the drop-cast films were mostly the same as that for the spin-coat films.

Hole-only Device Fabrication and Measurement

ITO substrates were first pre-cleaned sequentially by sonicating in a detergent bath, de-ionized water, acetone, and isopropanol at rt, and in a boiled isopropanol bath each for 10 min, and then baked at 140 °C for 15 min in air,

which were then subjected to a UV/ozone treatment at rt for 20 min. The pre-cleaned ITO substrates were coated with PEDOT:PSS (Clevios PVP A14083) by spin-coating (7000 rpm for 30 sec, thickness: ~50 nm). The active layer (polymer or polymer/PC₆₁BM blend) were then spin coated from a chlorobenzene solution containing 3~5 mg/mL of the polymer (with respective amount of PC₆₁BM) passed through a 0.45 μm PTFE filter at 400 rpm for 20 sec and 1500 rpm for 5 sec, in which the solution was kept heated at 100 °C. The thin films were transferred into a vacuum evaporator connected to the glove box, and the MoO₃ layer (5nm) and the Al layer (100nm) were deposited sequentially. The thickness of the film, which was measured using a surface profiler (Ambios XP-100), was ca. 200 nm for polymer-only films and ca. 300 nm for blend films. *J-V* characteristics were measured in the range of 0–6 V using a Keithley 2400 source-measure unit under nitrogen in the dark, and fitting the results to a space charge limited form, where described as:

$$J = (8/9) \varepsilon_r \varepsilon_0 \mu (V^2/L^3)$$

where ε_r is the dielectric constant of the polymer, ε_0 is the permittivity of free space, μ is the hole mobility, V is the voltage drop across the device ($V = V_{\text{appl}} - V_{\text{bi}}$, where V_{appl} is the applied voltage to the device and V_{bi} is the built-in voltage due to the difference in work function of the two electrodes, which is determined to be 0.1 in this case), and L is the polymer thickness, which was measured with AlphaStep® D-100 profilometer (KLA Tencor). The dielectric constant ε_r is assumed to be 3, which is a typical value for conjugated polymers.

Solar Cell Fabrication and Measurement

ITO substrates were first pre-cleaned sequentially by sonicating in a detergent bath, de-ionized water, acetone, and isopropanol at rt, and in a boiled isopropanol bath each for 10 min, and then baked at 140 °C for 15 min in air, which were then subjected to a UV/ozone treatment at rt for 20 min. The pre-cleaned ITO substrates were coated with PEDOT:PSS (Clevios P VP A14083) by spin-coating (7000 rpm for 30 sec, thickness: ~50 nm). The photoactive layer was deposited in a glove box by spin coating a chlorobenzene solution containing 3~5 g/L of the polymer sample with respective amount of PC₆₁BM or PC₇₁BM passed through a 0.45 μm PTFE filter at 400 rpm for 20 sec and 1500 rpm for 5 sec, in which the solution was kept heated at 100 °C. The thin films were transferred into a vacuum evaporator connected to the glove box, and the Ca layer (20nm) and the Al layer (100nm) were deposited sequentially, where the active area of the cells was 0.16 cm². *J-V* characteristics for the cells were

measured using a Keithley 2400 source-measure unit in nitrogen atmosphere under 1 Sun (AM1.5G) conditions using a solar simulator (SAN-EI Electric, XES-40S1). The light intensity for the $J-V$ measurements was calibrated with a reference PV cell (KONICA MINOLTA AK-100 certified at National Institute of Advanced Industrial Science and Technology, Japan). EQE spectra were measured with a Spectral Response Measuring System (SOMA OPTICS, LTD., S-9241).

Reference

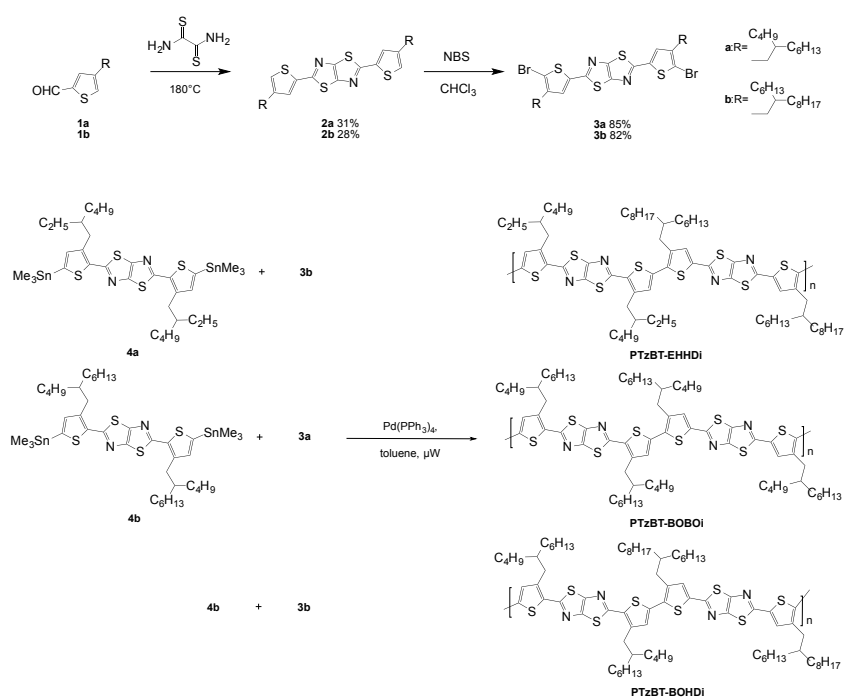
- [1] S. Günes, H. Neugebauer, N. S. Sariciftci, *Chem. Rev.* **2007**, *107*, 1324-1338.
- [2] B. C. Thompson, J. M. J. Fréchet, *Angew. Chem. Int. Ed.* **2008**, *47*, 58-77.
- [3] A. Facchetti, *Chem. Mater.* **2011**, *23*, 733-758.
- [4] P.-L. T. Boudreault, A. Najari, M. Leclerc, *Chem. Mater.* **2011**, *23*, 456-469.
- [5] P. M. Beaujuge, J. M. J. Fréchet, *J. Am. Chem. Soc.* **2011**, *133*, 20009-20029.
- [6] A. Facchetti, *Materials Today* **2013**, *16*, 123-132.
- [7] H.-C. Chen, Y.-H. Chen, C.-C. Liu, Y.-C. Chien, S.-W. Chou, P.-T. Chou, *Chem. Mater.* **2012**, *24*, 4766-4772.
- [8] C. Cabanetos, A. El Labban, J. A. Bartelt, J. D. Douglas, W. R. Mateker, J. M. J. Fréchet, M. D. McGehee, P. M. Beaujuge, *J. Am. Chem. Soc.* **2013**, *135*, 4656-4659.
- [9] L. Dou, C.-C. Chen, K. Yoshimura, K. Ohya, W.-H. Chang, J. Gao, Y. Liu, E. Richard, Y. Yang, *Macromolecules* **2013**, *46*, 3384-3390.
- [10] I. Osaka, T. Kakara, N. Takemura, T. Koganezawa, K. Takimiya, *J. Am. Chem. Soc.* **2013**, *135*, 8834-8837.
- [11] G. Li, V. Shrotriya, J. Huang, Y. Yao, T. Moriarty, K. Emery, Y. Yang, *Nature Mater.* **2005**, *4*, 864-868.
- [12] Y. Kim, S. Cook, S. M. Tuladhar, S. A. Choulis, J. Nelson, J. R. Durrant, D. D. C. Bradley, M. Giles, I. McCulloch, C.-S. Ha, M. Ree, *Nature Mater.* **2006**, *5*, 197-203.
- [13] J. Guo, Y. Liang, J. Szarko, B. Lee, H.-J. Son, B. S. Rolczynski, L. Yu, L. X. Chen, *J. Phys. Chem. B* **2010**, *114*, 742-748.
- [14] E. D. Gomez, K. P. Barteau, H. Wang, M. F. Toney, Y.-L. Loo, *Chem. Commun.* **2011**, *47*, 436-438.
- [15] D. Mühlbacher, M. Scharber, M. Morana, Z. Zhu, D. Waller, R. Gaudiana, C. Brabec, *Adv. Mater.* **2006**, *18*, 2884-2889.

- [16] H.-Y. Chen, J. Hou, A. E. Hayden, H. Yang, K. N. Houk, Y. Yang, *Adv. Mater.* **2010**, *22*, 371–375.
- [17] N. Blouin, A. Michaud, D. Gendron, S. Wakim, E. Blair, R. Neagu-Plesu, M. Belletête, G. Durocher, Y. Tao, M. Leclerc, *J. Am. Chem. Soc.* **2008**, *130*, 732-742.
- [18] Y. Liang, Y. Wu, D. Feng, S.-T. Tsai, H.-J. Son, G. Li, L. Yu, *J. Am. Chem. Soc.* **2008**, *131*, 56-57.
- [19] E. Zhou, M. Nakamura, T. Nishizawa, Y. Zhang, Q. Wei, K. Tajima, C. Yang, K. Hashimoto, *Macromolecules* **2008**.
- [20] M. Wang, X. Hu, P. Liu, W. Li, X. Gong, F. Huang, Y. Cao, *J. Am. Chem. Soc.* **2011**, *133*, 9638–9641.
- [21] I. Osaka, M. Shimawaki, H. Mori, I. Doi, E. Miyazaki, T. Koganezawa, K. Takimiya, *J. Am. Chem. Soc.* **2012**, *134*, 3498-3507.
- [22] H. Sirringhaus, P. Brown, R. Friend, M. Nielsen, *Nature* **1999**.
- [23] J. Rivnay, M. F. Toney, Y. Zheng, I. V. Kauvar, Z. Chen, V. Wagner, A. Facchetti, A. Salleo, *Adv. Mater.* **2010**, *22*, 4359-4363.
- [24] S. Subramaniyan, H. Xin, F. S. Kim, S. Shoaee, J. R. Durrant, S. A. Jenekhe, *Adv. Energy Mater.* **2011**, *1*, 854-860.
- [25] I. Osaka, T. Abe, M. Shimawaki, T. Koganezawa, K. Takimiya, *ACS Macro Lett.* **2012**, 437-440.
- [26] X. Zhang, L. J. Richter, D. M. DeLongchamp, R. J. Kline, M. R. Hammond, I. McCulloch, M. Heeney, R. S. Ashraf, J. N. Smith, T. D. Anthopoulos, B. Schroeder, Y. H. Geerts, D. A. Fischer, M. F. Toney, *J. Am. Chem. Soc.* **2011**, *133*, 15073-15084.
- [27] L. Yang, J. R. Tumbleston, H. Zhou, H. Ade, W. You, *Energy Environ. Sci.* **2013**, *6*, 316-326.
- [28] I. Osaka, G. Sauvé, R. Zhang, T. Kowalewski, R. D. McCullough, *Adv. Mater.* **2007**, *19*, 4160-4165.
- [29] I. Osaka, R. Zhang, G. Sauvé, D. M. Smilgies, T. Kowalewski, R. D. McCullough, *J. Am. Chem. Soc.* **2009**, *131*, 2521-2529.
- [30] I. Osaka, R. Zhang, J. Liu, D.-M. Smilgies, T. Kowalewski, R. D. McCullough, *Chem. Mater.* **2010**, *22*, 4191-4196.
- [31] J. Peet, L. Wen, P. Byrne, S. Rodman, K. Forberich, Y. Shao, N. Drolet, R. Gaudiana, G. Dennler, D. Waller, *Appl. Phys. Lett.* **2011**, *98*, 043301 .

- [32] I. H. Jung, J. Yu, E. Jeong, J. Kim, S. Kwon, H. Kong, K. Lee, H. Y. Woo, H.-K. Shim, *Chem. Eur. J.* **2010**, *16*, 3743-3752.
- [33] M. Zhang, X. Guo, Y. Li, *Adv. Energy Mater.* **2011**, *1*, 557-560. [34] Q. Shi, H. Fan, Y. Liu, W. Hu, Y. Li, X. Zhan, *J. Phys. Chem. C* **2010**, *114*, 16843-16848.
- [35] M. Yang, B. Peng, B. Liu, Y. Zou, K. Zhou, Y. He, C. Pan, Y. Li, *J. Phys. Chem. C* **2010**, *114*, 17989-17994.
- [36] L. Huo, X. Guo, S. Zhang, Y. Li, J. Hou, *Macromolecules* **2011**, *44*, 4035-4037.
- [37] S. K. Lee, J. M. Cho, Y. Goo, W. S. Shin, J.-C. Lee, W.-H. Lee, I.-N. Kang, H.-K. Shim, S.-J. Moon, *Chem. Commun.* **2011**, *47*, 1791.
- [38] M. Zhang, X. Guo, X. Wang, H. Wang, Y. Li, *Chem. Mater.* **2011**, *23*, 4264-4270.
- [39] I. Osaka, M. Saito, H. Mori, T. Koganezawa, K. Takimiya, *Adv. Mater.* **2012**, *24*, 425-430.
- [40] I. McCulloch, M. Heeney, C. Bailey, K. Genevicius, I. MacDonald, M. Shkunov, D. Sparrowe, S. Tierney, R. Wagner, W. Zhang, *Nature Mater.* **2006**, *5*, 328-33.
- [41] J. Rivnay, S. C. B. Mannsfeld, C. E. Miller, A. Salleo, M. F. Toney, *Chem. Rev.* **2012**, *112*, 5488-5519.
- [42] M. L. Chabinyo, M. F. Toney, R. J. Kline, I. McCulloch, M. Heeney, *J. Am. Chem. Soc.* **2007**, *129*, 3226-3237.
- [43] Y. Kobori, R. Noji, S. Tsuganezawa, *J. Phys. Chem. C* **2013**, *117*, 1589-1599.
- [44] V. Shrotriya, Y. Yao, G. Li, Y. Yang, *Appl. Phys. Lett.* **2006**, *89*, 063505.
- [45] M. D. Perez, C. Borek, S. R. Forrest, M. E. Thompson, *J. Am. Chem. Soc.* **2009**, *131*, 9281-9286.
- [46] L. Yang, H. Zhou, W. You, *J. Phys. Chem. C* **2010**, *114*, 16793-16800.
- [47] W. Li, K. H. Hendriks, W. S. C. Roelofs, Y. Kim, M. M. Wienk, R. A. J. Janssen, *Adv. Mater.* **2013**, 3182-3186.
- [48] S. C. Price, A. C. Stuart, L. Yang, H. Zhou, W. You, *J. Am. Chem. Soc.* **2011**, *133*, 4625-4631.
- [49] T. M. Clarke, D. B. Rodovsky, A. A. Herzog, J. Peet, G. Dennler, D. DeLongchamp, C. Lungenschmied, A. J. Mozer, *Adv. Energy Mater.* **2011**, *1*, 1062-1067.

copolymerized with **4a** and **4b** to give PTzBT-EHHDi and PTzBT-BOHDI, and **4b** and **3a** were copolymerized to give PTzBT-BOBOi, respectively.

The polymers were soluble in warm chloroform (CF) and the molecular weight of polymers evaluated by GPC at 140 °C were mostly above 30 kDa (M_n) (**Table 5-1**). Interestingly, the solubility of PTzBTis are quite high. For example, 5mg of PTzBT-BOHD was dissolve in CB at 100°C, however PTzBT-BOHDI was dissolve at room temperature. And PTzBT-BOBO with higher than 16 kDa was not dissolve in hot CF and CB, but PTzBT-BOBOi with 34kDa was dissolve in hot CF and CB.



Scheme 5-1. Synthesis of PTzBT- R^1R^2i

Table 5-1. Polymerization results.

Polymer	M_n (kDa) ^a	M_w (kDa) ^a	PDI ^a
PTzBT-EHHDi	31	61	2.0
PTzBT-BOBOi	34	65	1.9
PTzBT-BOHDI	46	75	1.6

^a Determined by GPC using polystyrene standard and *o*-dichlorobenzene as the eluent at 140 °C.

The HOMO energy level (E_{HOMO}) of the polymers was evaluated by photoelectron spectroscopy in air (PESA) using the polymer thin films (**Figure 5-2b**). All PTzBTis showed similar E_{HOMO} s of around -5.20 eV (**Table 5-2**),

which were almost same as that of PTzBTs. UV-vis absorption spectra of the polymers in the thin film was shown in **Figure 5-2a**. UV-vis absorption spectra of the PTzBTis give absorption maxima at 565-575 and 615-630 nm along with a shoulder at ca. 530 nm in the film. The band gaps (E_g) of the PTzBTis are estimated to be ca. 1.8 eV from the absorption onset in the film spectra and these properties was almost same as PTzBTs.

On the other hands, difference of the PTzBTs and PTzBTis were in UV-vis absorption spectra of polymers in chlorobenzene solution (**Figure 5-3**). In case of PTzBT, absorption spectra was a little shift by raising the temperature, λ_{\max} of 570-580 nm and 610-630 nm shifted to 560-570 nm and 600-610 nm. On the other hands, in case of PTzBTi, raising the temperature induces decrease of the long-wavelength absorption region (at 575-585 nm and 610-620 nm) and increase of short-wavelength absorption region (at 500-520 nm) (**Table 5-3**) indicated that aggregation of the PTzBTs in CB solution is higher than that of PTzBTi.

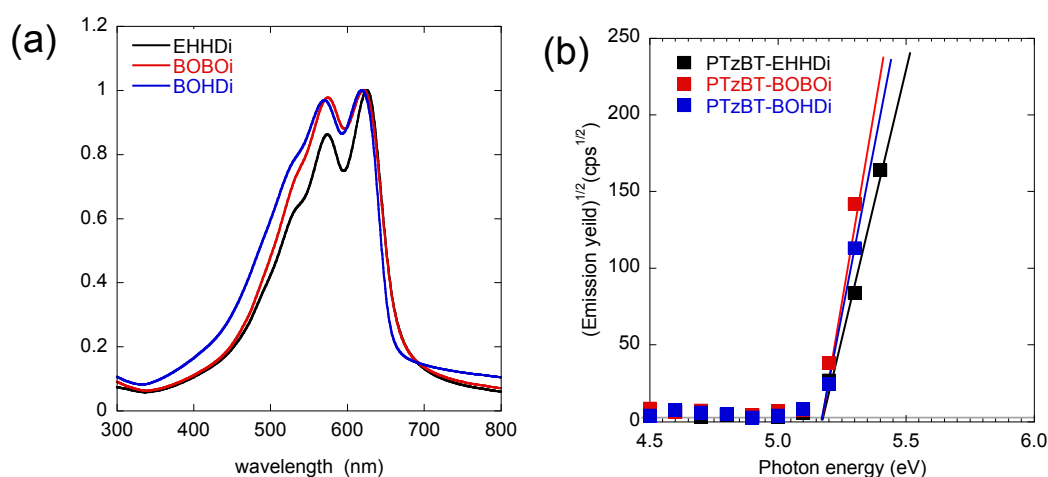


Figure 5-2. UV-vis absorption spectra (a) and Photoelectron spectra (b) of the polymer thin films.

Table 5-2. Electronic properties of the polymers.

	λ_{\max} (nm)	λ_{edge} (nm) / E_g^{opt} (eV) ^a	E_{HOMO} (eV) ^b	E_{LUMO} (eV) ^c
PTzBT-EHHDi	567, 626	671 / 1.85	-5.21	-3.36
PTzBT-BOBOi	570, 616	672 / 1.85	-5.20	-3.35
PTzBT-BOHDi	575, 621	662 / 1.87	-5.21	-3.34

^a λ_{edge} : absorption edge, E_g^{opt} : bandgaps calculated with λ_{edge} . ^b Photoelectron spectroscopy in air (PESA) were used to evaluate HOMO energy levels. ^c LUMO energy levels estimated by adding the band gap (E_g^{opt}) to E_{HOMO} .

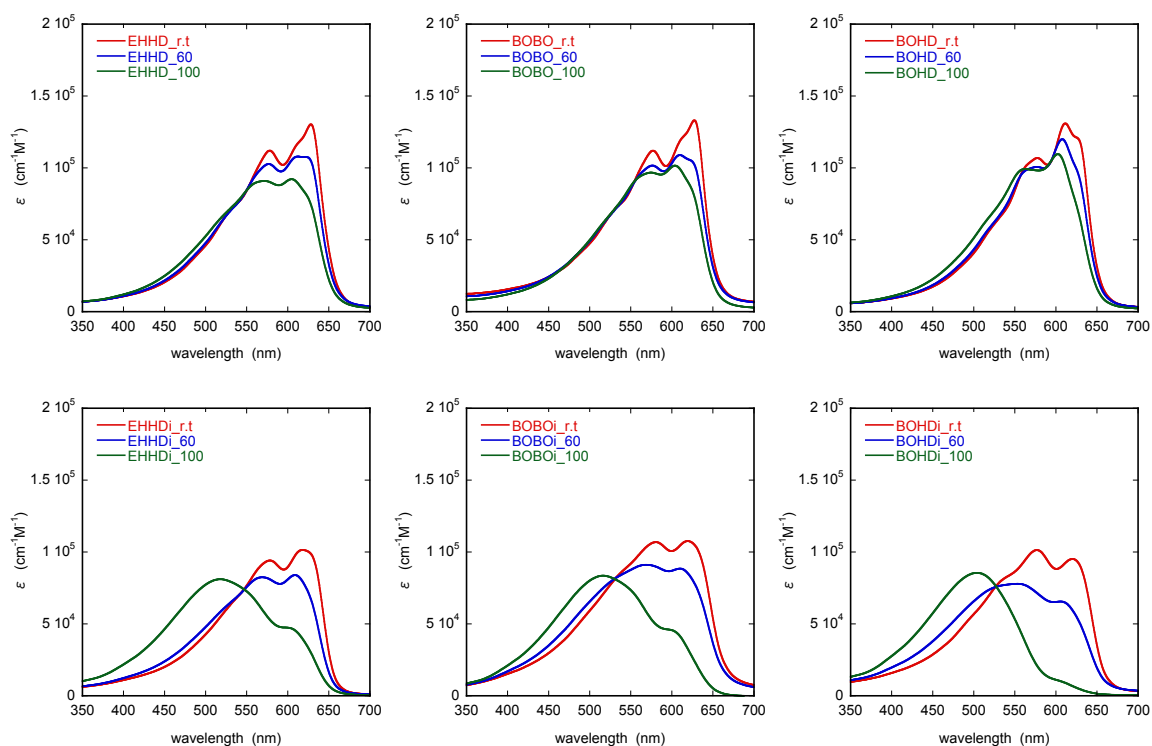


Figure 5-3. UV-vis absorption spectra of PTzBTs and PTzBTis in chlorobenzene solution.

Table 5-3. λ_{\max} (nm) of PTzBTs and PTzBTis in chlorobenzene solution.

polymer	λ_{\max} (nm)			polymer	λ_{\max} (nm)		
	r.t	60°C	100°C		r.t	60°C	100°C
PTzBT-EHHDi	579, 618	569, 609	518	PTzBT-EHHD	578, 629	577, 622	572, 605
PTzBT-BOBOi	581, 620	568, 610	517	PTzBT-BOBO	577, 628	576, 610	575, 604
PTzBT-BOHDi	577, 620	553, 606	504	PTzBT-BOHD	578, 612	577,608	563, 603

5-3. Solar Cell Characteristics.

Solar cells were fabricated by spin-coating the solutions of polymer and [6,6]-phenyl-C₆₁-butyric acid methyl ester (PC₆₁BM) in chlorobenzene onto the PEDOT:PSS spin-coated ITO glass, followed by vacuum deposition of Ca/Al as the cathode. The optimal polymer-to-PC₆₁BM (p:n) ratio were 1:1 for PTzBT-oBOHD and 1:2 for other polymers. The optimized active layer thickness was around 200 nm for the cells with newly synthesized polymers. External quantum efficiency (EQE) spectra and current density (*J*)-Voltage (*V*) curves of the cells under 1 sun of simulated AM 1.5G solar irradiation (100 mW/cm²) are displayed in **Figure 5-4a**, and photovoltaic parameters are summarized in **Table 5-4**. The PTzBT-R¹R²i-based cell gave short-circuit current density (*J*_{SC}) of 8.92-11.4

mA/cm² and open-circuit voltage (V_{OC}) of 0.83-0.85 V obtained for the cells and as a result, PTzBT-BOBOi-based cells exhibited PCEs of 8.8%. Interestingly, V_{OC} of PTzBTis-based cells are higher than that of PTzBTs-based cells, for example, V_{OC} of PTzBT-BOBOi and -BOHDi were 0.90 and 0.91 V, respectively. On the other hands, V_{OC} of PTzBT-BOBO and -BOHD were 0.88 V (shown in Chapter 4). But cause of difference of V_{OC} was not known so far. And in case of PTzBTs, optimal side chain composition is BOHD, however PTzBTis is BOBO, indicated that side chain position is important factor for OPV parameter.

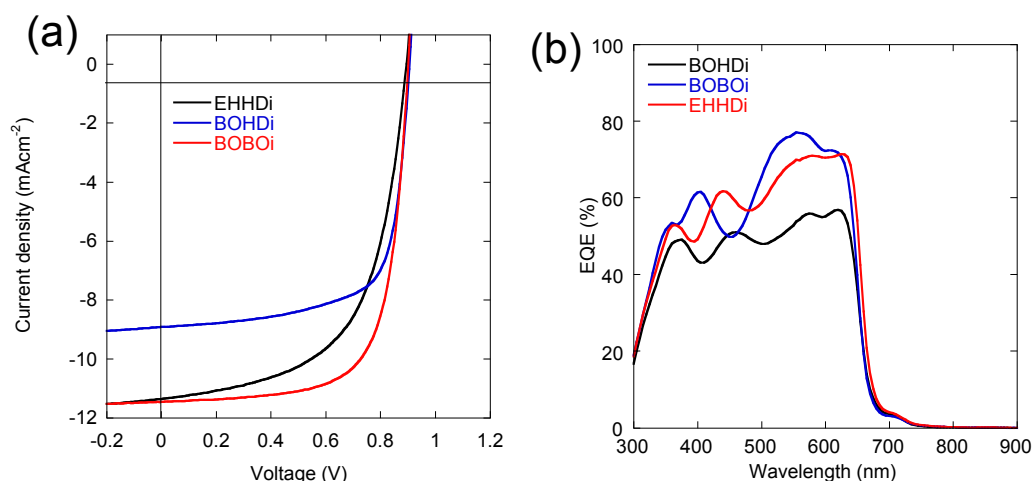


Figure 5-4. J - V curves (a) and EQE spectra (b) of the solar cells based on PTzBT- R^1R^2i .

Table 5-4. Photovoltaic properties of the solar cells based on PTzBT- R^1R^2i .

Polymer	J_{SC} (mA/cm ²)	V_{OC} (V)	FF	PCE_{max} [PCE_{ave}] (%) ^a
PTzBT-EHHDi	11.36	0.89	0.59	6.0 [5.7]
PTzBT-BOBOi	11.40	0.90	0.71	7.3 [6.9]
PTzBT-BOHDi	8.92	0.91	0.70	5.7 [5.4]

^a PCE_{max} : maximum power conversion efficiencies, PCE_{ave} : average power conversion efficiencies.

I also investigated the morphology of the polymer/PC₆₁BM blend films by the atomic force microscopy (AFM) (**Figure 5-5**). PTzBT- R^1R^2 seems to have formed well-phase-separated morphologies, which would ensure the charge generation and the surface roughness (rms) of the blend films were small.

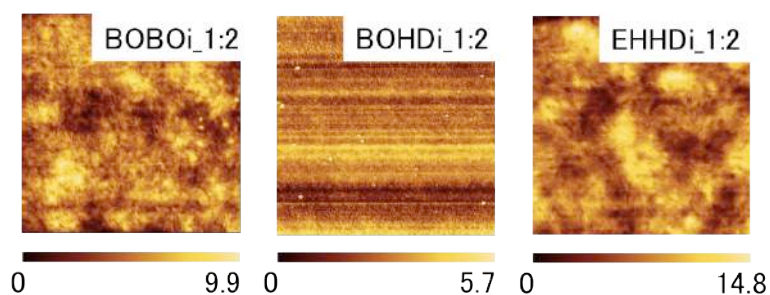


Figure 5-5. AFM image of PTzNTz-R¹R²:PC₇₁BM blend films

In order to understand the photovoltaic performances difference of the cells, polymer ordering structures in the thin film were investigated by X-ray diffraction studies. Two-dimensional grazing incidence X-ray diffraction (2D-GIXD) images of the polymer-only films and the polymer/PC₆₁BM blend films on the ZnO/ITO substrate are shown in **Figure 5-6**. And π -stack distance (d_π), Lamella distance (d_{Lamella}) and Full-Width Half-Maximum ($\text{FWHM}_{\text{Lamella}}$) of PTzBT-R¹R²i are summarized in **Table 5-5**. In polymer-only films, the lamella structure ($q \approx 0.3 \text{ \AA}^{-1}$) and the π - π stacking structures ($q \approx 1.7 \text{ \AA}^{-1}$) appeared and d_π are determined from the diffraction profile along the q_z axis. Both of polymer-only films and polymer/PC₆₁BM blend films, corresponding to the π - π stacking structures appeared along the q_z axes, indicating that the polymers formed face-on orientation on the substrate^[7] (**Figure 5-6**). d_π of PTzBT-EHHDi, -BOBOi and -BOHDi were 3.63, 3.63, and 3.65 \AA respectively (**Table 5-5**) and d_π of PTzBT-R¹R²i was broader than that of PTzBT-R¹R². And $\text{FWHM}_{\text{Lamella}}$ are determined from diffraction profile q_z and q_{xy} axis, $\text{FWHM}_{\text{Lamella}}$ of PTzBT-R¹R²i was broader than that of PTzBT-R¹R. These result indicate that crystallinity of PTzBT-R¹R²i is lower than that of PTzBT-R¹R.

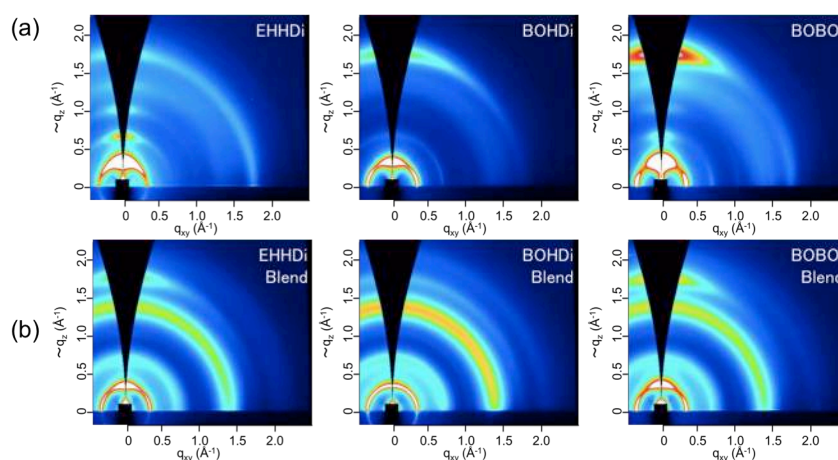


Figure 5-6. 2D-GIXDs images of (a) polymer-only films and (b) polymer/PC₆₁BM blend films for PTzBT-R¹R²i

Table 5-5. π -stack, and Lamella and FWHM of PTzNTz-R¹R²

Polymer	d_{Lamella} (Å) ^[a]	d_{π} (Å) ^[a]	FWHM _{Lamella} ^[b] (out-of-plane)	FWHM _{Lamella} ^[b] (in-plane)
-EHHDi	18.9	3.63	0.056	0.085
-BOBOi	18.4	3.63	0.095	0.050
-BOHDi	19.0	3.67	0.098	0.055
-EHHD	18.9	3.52	0.061	0.064
-BOBO	18.1	3.55	0.079	0.057
-BOHD	19.3	3.54	0.063	0.054
-EHHDi/PC ₆₁ BM	19.1	3.63	0.094	0.067
-BOBOi/PC ₆₁ BM	18.6	3.64	0.102	0.053
-BOHDi/PC ₆₁ BM	19.1	3.67	0.061	0.050

[a] Lamella distance (d_{Lamella}) and π stack distance (d_{π}) are determined from the diffraction profile along the q_z axis (out-of-plane) of the 2D-GIXDs images. [b] Full-Width Half-Maximum (FWHM_{Lamella}) are determined from diffraction profile q_z and q_{xy} axis (in-plane) of 2D-GIXDs images.

5-4. Summary

New thiazolothiazole-based semiconducting polymers with side chain into different position from PTzBTs have been synthesized and investigated. Although electronic structure of PTzBT-R¹R² and PTzBT-R¹R²i were almost the same, optimal side chains of PTzBT-R¹R² and PTzBT-R¹R²i were different for OPV. PTzBT-BOHD was the best polymer in PTzBT-R¹R² series. However, PTzBT-BOBOi was the best polymer in PTzBT-R¹R²i series. And these result caused by crystallinity polymers, PTzBT-R¹R² was higher than that of PTzBT-R¹R²i.

Experimental

Synthesis

General procedure for polymerization

To a reaction tube equipped with a stirring bar, stannylated monomer (0.10 mmol), brominated monomer (0.10 mmol), Pd₂(dba)₃ (1.8 mg, 0.002 mmol), P(*o*-Tol)₃ (2.4 mg, 0.008 mmol), and chlorobenzene (5 ml) were added. Then the tube was purged with argon and sealed. The reaction tube was set into a microwave reactor and heated to 200 °C for 10 min. After cooling to room temperature, the reaction solution was poured into 200 mL of methanol

containing 5 mL of hydrochloric acid, and stirred for 5 hours. Then the precipitated solid was subjected to the sequential Soxhlet extraction with methanol, hexane to remove low molecular weight fractions. The residue was then extracted with chloroform, and reprecipitated in 200 mL of methanol to yield dark purple or dark blue solids (yield = 72-91%).

Instrumentation

UV-vis absorption spectra were measured using a Shimadzu UV-3600 spectrometer. Photoelectron spectra were measured by using a photoelectron spectrometer, model AC-2, in air (Riken Keiki Co., Ltd). Dynamic force-mode atomic force microscopy study was carried out on a Nanoscope scanning probe microscope system (SII Nanotechnology, Inc.). 2D-GIXD experiments were conducted at the SPring-8 on the beamline BL19B2. The sample was irradiated at a fixed incident angle on the order of 0.12° through a Huber diffractometer. The X-ray energy of 12.39 keV ($\lambda = 1 \text{ \AA}$) the 2D-GIXD patterns were recorded with a 2-D image detector (Pilatus 300K). Samples for the X-ray measurements were prepared by spin-casting the polymer and polymer/PC₆₁BM solution on the ITO substrate.

Solar Cell Fabrication and Measurement

ITO substrates were first pre-cleaned sequentially by sonicating in a detergent bath, de-ionized water, acetone, and isopropanol at rt, and in a boiled isopropanol bath each for 10 min, and then baked at 120 °C for 10 min in air. The substrates were then subjected to a UV/ozone treatment at rt for 20 min. The pre-cleaned ITO substrates were coated with PEDOT:PSS (Clevios PVP A14083) by spin-coating (5000 rpm for 30 sec, thickness: ~50 nm). The photoactive layer was deposited in a glove box by spin coating a chlorobenzene solution, containing 3~6 g/L of the polymer sample with respective amount of PC₆₁BM, at 400 rpm for 20 sec and 1500 rpm for 5 sec, in which the solution was kept heated at 100 °C. The thin films were transferred into a vacuum evaporator connected to the glove box, and the Ca layer (20 nm) and the Al layers (100 nm) were deposited sequentially. The active area of the cells was 0.16 cm². *J-V* characteristics for the cells were measured using a Keithley 2400 source-measure unit in nitrogen atmosphere under 1 Sun (AM1.5G) conditions using a solar simulator (SAN- EI Electric, XES-40S1).

The light intensity for the J - V measurements was calibrated with a reference PV cell (KONICA MINOLTA AK-100 certified at National Institute of Advanced Industrial Science and Technology, Japan). EQE spectra were measured with a Spectral Response Measuring System (SOMA OPTICS, LTD., S-9241).

Reference

- [1] (a) G. Yu, J. Gao, J. C. Hummelen, F. Wudl, A. J. Heeger, *Science* **1995**, *270*, 1789-1791. (b) D. Mühlbacher, M. Scharber, M. Morana, Z. Zhu, D. Waller, R. Gaudiana, C. Brabec, *Adv. Mater.* **2006**, *18*, 2884-2889.
- [2] (a) Y. Liang, Z. Xu, J. Xia, S. Tsai, Y. Wu, G. Li, C. Ray, L. Yu, *Adv. Mater.* **2010**, *22*, E135-E138. (b) H. Y. Chen, J. Hou, S. Zhang, Y. Liang, G. Yang, Y. Yang, L. Yu, Y. Wu, G. Li, *Nature Photon.* **2009**, *3*, 649-653. (c) T. Y. Chu, J. Lu, S. Beaupré, Y. Zhang, J. R. Pouliot, S. Wakim, J. Zhou, M. Leclerc, Z. Li, J. Ding, Y. Tao, *J. Am. Chem. Soc.* **2011**, *133*, 4250-4253. (d) S. C. Price, A. C. Stuart, L. Yang, H. Zhou, W. You, *J. Am. Chem. Soc.* **2011**, *133*, 4625-4631. (e) J. You, L. Dou, K. Yoshimura, T. Kato, K. Ohya, T. Moriarty, K. Emery, C. Chen, J. Gao, G. Li, Y. Yang *Nature Commun.* **2013**, *4*, 1446-1456. (f) H. Chen, Y. Chen, C. Liu, Y. Chien, S. Chou, P. Chou, *Chem. Mater.* **2012**, *24*, 4766-4772. (g) I. Osaka, T. Kakara, N. Takemura, T. Koganezawa, K. Takimiya *J. Am. Chem. Soc.* **2013**, *135*, 8834-8837. (h) S. Zhang, L. Ye, W. Zhao, D. Liu, H. Yao, J. Hou *Macromolecules.* **2014**, *47*, 4653-4659. (i) L. Ye, S. Zhang, W. Zhao, H. Yao, J. Hou *Chem. Mater.* **2014**, *26*, 3603-3605.
- [3] I. Osaka, M. Saito, T. Koganezawa, K. Takimiya, *Adv. Mater.* **2014**, *26*, 331-338 .
- [4] Qinghe Wu, Mao W, Xiaolan Q, Yu X, Yangguang H, Xike Gao, Hongxiang Li *Macromolecules.* **2013**, *46*, 3887-3894.

Chapter 6

6. Synthesis and Photovoltaic Properties of Thiophene-Thiazolothiazole Copolymers with Oxygen Containing Functional Groups as The Side Chain

6-1. Introduction

Bulk heterojunction (BHJ) solar cells using semiconducting polymers as the p-type photoactive layer materials together with fullerene derivatives as the n-type materials are of great interest for the development of a low-cost, flexible, and large area renewable energy sources.^[1] During the last decade, a number of new polymers have been reported, and the power conversion efficiencies (PCEs) of polymer-based BHJ solar cells have rapidly improved.^[2] In order to develop high-efficiency solar cells, semiconducting polymers are required to have a wide absorption range, namely a narrow bandgap, to absorb as much sunlight as possible.^[3] They also need to form a highly ordered structure in thin films to ensure high charge carrier transport to better collect the generated charge carriers. Semiconducting polymers consisting of an electron-rich and an electron-poor units, which is so-called donor acceptor (D-A) polymers, are particularly attractive, since they offer facile tunability of the HOMO and LUMO energy levels (E_{HOMO} and E_{LUMO}) and the bandgap (E_{g}), and strong intermolecular interactions.^[4]

Among the many D-A polymer systems studied so far, polymers with thiazolothiazole (TzTz) as the acceptor unit is an interesting system that provides highly ordered structures and thus high charge carrier mobilities.^[4a,5] In fact, several groups have reported on the synthesis of TzTz-based polymers incorporating various donor units in the backbone, which showed good PCEs of ~5.8%.^[6] Independently, I have also reported on a series of TzTz-based polymers with alkylthiophenes as the donor unit (PTzBTs, **Figure 6-1**) and demonstrated that one of the polymers showed quite high PCEs of ~7.5% in conventional single-junction cells.^[7] However, the relatively narrow absorption range of ~680 nm (wide bandgap of ca. 1.8 eV) for PTzBTs limited the light harvesting property, and thus broadening of the absorption range (narrowing of the bandgap) has been an issue for the further improvement of the performances. In this work, I introduced alkoxy and ester groups, which have electron-donating and electron-withdrawing nature, as the side chains of the PTzBT backbone (**Figure 6-1**), since the backbone has already been proven to offer highly ordered structures as mentioned above. It is expected that the combination of these two functional groups would allow us to have polymers with narrow bandgaps with

various HOMO and LUMO levels. I will describe the synthesis, electronic structures, and the ordering structures of new thiophene-TzTz polymers with alkoxy and ester groups as the side chain and their solar cell performances.

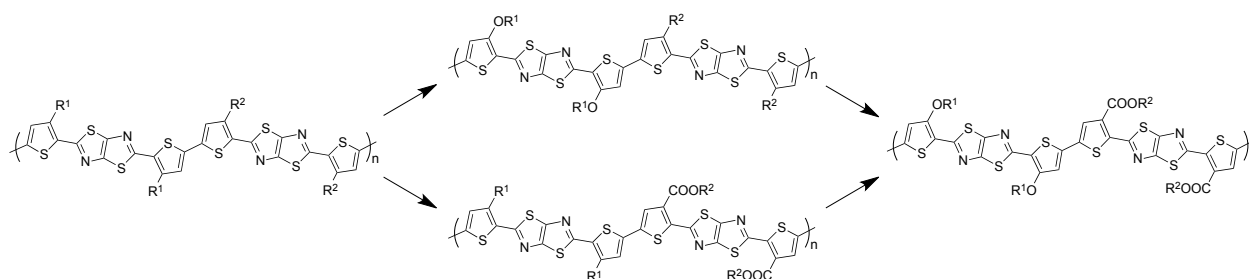
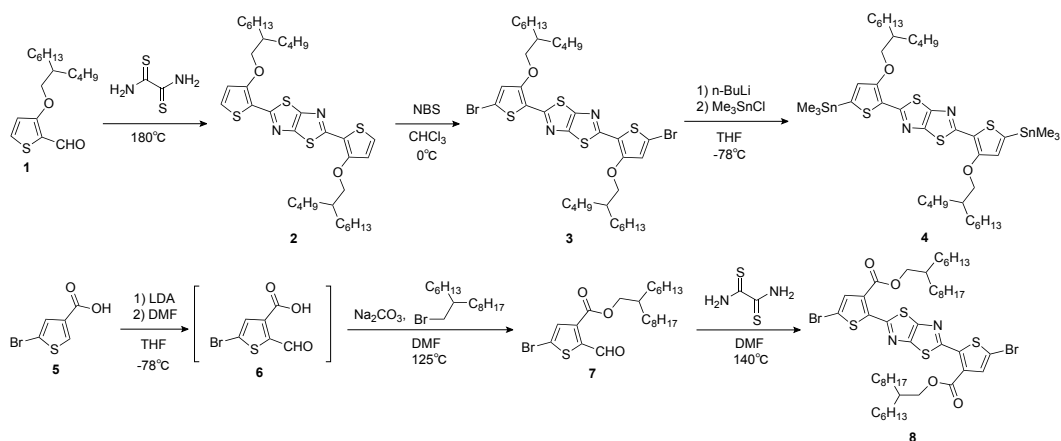


Figure 6-1. Chemical structure of thiophene-thiazolothiazole copolymers studied in this work.

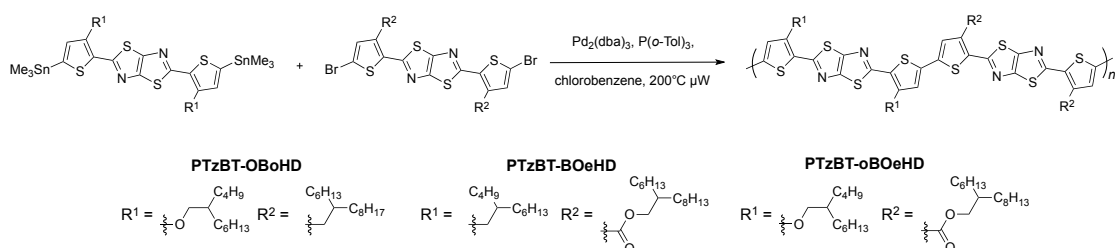
6-2. Results and Discussion

Synthesis

The synthetic routes to the monomer with the alkoxy groups^[8] and the ester groups^[9] are shown in **Scheme 6-1**. First, a TzTz derivative with the butyloctyloxy groups (**2**) was prepared by heating the mixture of **1** and dithiooxamide. **2** was then dibrominated using NBS to give **3**, followed by stannylation via the treatment of *n*-BuLi, which gave the alkoxy monomer (**4**). Second, 5-bromo-thiophene-3-carboxylic acid (**5**) was formylated at the 2-position by the treatment of DMF through lithiation with lithium diisopropylamide (LDA) to yield **6**. However, this reaction gave the 4-formyl-3-thiophene-carboxylic acid as a byproduct, which could not be removed by column chromatography. Therefore, the crude of **6** was subjected to esterification with 2-hexyl-1-bromodecane to afford **7**, which was successfully isolated by column chromatography. The ester monomer (**8**) was prepared by the reaction of **7** and dithiooxamide in DMF. All polymers were synthesized via the Stille coupling reaction using a microwave reactor (**Scheme 6-2**). The alkoxy monomer (**8**) was copolymerized with **3** and **8** to give PTzBT-oBOHD and PTzBT-BOeHD, respectively, and **4** and **8** were copolymerized to give PTzBT-oBOeHD. The polymers were soluble in warm chloroform (CF) and chlorobenzene (CB), and the molecular weight of polymers evaluated by GPC at 140 °C were mostly above 30 kDa (M_n) (**Table 6-1**).



Scheme 6-1. Synthesis of the monomers



Scheme 6-2. Synthesis of PTzBT-oBOHD, BOeHD and oBOeHD

Table 6-1. Polymerization results.^a

polymer	M_n (kDa)	M_w (kDa)	PDI
PTzBT-BOHD	35	110	3.1
PTzBT-oBOHD	32	132	4.0
PTzBT-BOeHD	25	115	4.8
PTzBT-oBOeHD	29	235	8.2

^a Determined by GPC using polystyrene standard and *o*-dichlorobenzene as the eluent at 140 °C.

Physicochemical Properties of the Polymers

To confirm the electronic effect of the side chains, cyclic voltammetry of the dithienyl-TzTz with alkyl (TzBT-BO), alkoxy (TzBT-oBO), and ester groups (TzBT-eHD) (Figure 2a) was carried out in the dichloromethane solution (**Figure 6-2b**). E_{HOMO} of TzBT-BO, TzBT-oBO and TzBT-eHD were estimated from the onset oxidation potentials. While E_{HOMO} of TzBT-BO was -5.59 eV, that of TzBT-oBO was higher by 0.3 eV (-5.29 eV) and that of TzBT-eHD was lower by 0.21 eV (-5.80 eV) (**Table 6-2**), as expected from the electron-donating and electron-withdrawing nature of the alkoxy and the ester groups. E_{LUMO} were estimated by

the addition of E_g determined from the absorption onset. As is the case in E_{HOMO} , E_{LUMO} of TzBT-oBO (-2.58 eV) was higher by 0.24 eV than TzBT-BO (-2.82 eV) and that of TzBT-eHD (-3.22 eV) was lower by 0.40 eV (**Table 6-2**). This trend was in good agreement with the computation using the DFT method at the B3LYP-6-31 g(d) level (**Figure 6-2d**).

E_{HOMO} of the polymers were evaluated by photoelectron spectroscopy in air (PESA) using the polymer thin films (**Figure 6-3a**). E_{HOMO} s of PTzBT-oBOHD and PTzBT-oBOeHD with the alkoxy groups were -5.02 and -5.08 eV, respectively, which were about 0.15-0.2 eV higher than that of PTzBT-BOHD (-5.23 eV) (**Table 6-2**). This indicates that E_{HOMO} s of these polymers were greatly affected by the electron donating nature of the alkoxy group, as is the case in the monomers. Slightly lower E_{HOMO} of PTzBT-oBOeHD compared to PTzBT-oBOHD is likely due to the electron withdrawing nature of the ester group. E_{HOMO} of PTzBT-BOeHD (-5.28 eV) was slightly lower than that of PTzBT-BOHD (**Table 6-2**), which is also attributed to the electron withdrawing nature of the ester groups. E_{LUMO} of the polymers were estimated by adding the band gap (E_g^{opt}), which was determined from the absorption onset in the film, to E_{HOMO} (**Table 6-2**). In PTzBT-oBOHD, E_{LUMO} was elevated to -3.28 eV from that in PTzBT-BOHD (-3.42 eV), being affected by the alkoxy group. On the other hand, E_{LUMO} of PTzBT-BOeHD was lower (-3.51 eV) than that of PTzBT-BOHD owing to the electron-withdrawing nature of the ester group. In PTzBT-oBOeHD, despite having the ester groups, E_{LUMO} was -3.38 eV that is almost the same as that in PTzBT-BOHD. This implies that the electronic effect of the ester groups on the E_{LUMO} is compensated by the effect of the alkoxy groups. These results suggest that the electronic effect of the alkoxy group was more significant than the ester group in this system.

UV-vis absorption spectra of the polymers in the film are shown in **Figure 6-3b**. As expected, all the polymers synthesized here exhibited red-shifted spectra compared to that of PTzBT-BOHD. While the absorption maximum (λ_{max}) of PTzBT-BOHD was 624 nm, those of PTzBT-BOeHD, PTzBT-oBOHD, and PTzBT-oBOeHD were 633, 653 and 675 nm, respectively (**Table 6-2**). The optical bandgap (E_g s) of the polymers determined from the absorption onset are summarized in **Table 6-2**. PTzBT-oBOeHD with both the alkoxy and ester groups showed the smallest E_g of 1.70, which was reduced for about 0.1 eV compared to that of PTzBT-BOHD.

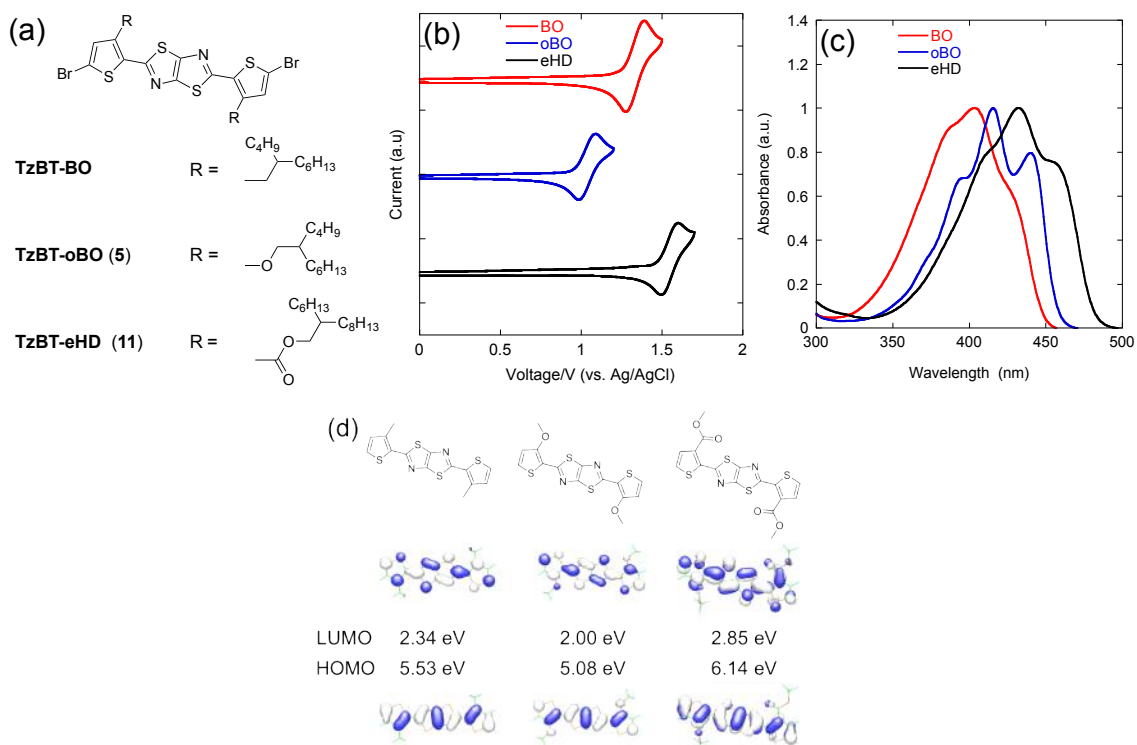


Figure 6-2. Chemical structure (a), cyclic voltammograms (b), UV-vis spectra (c) of the monomer units, and computation of the corresponding model compounds using the DFT method at the B3LYP/6-31 g(d) level

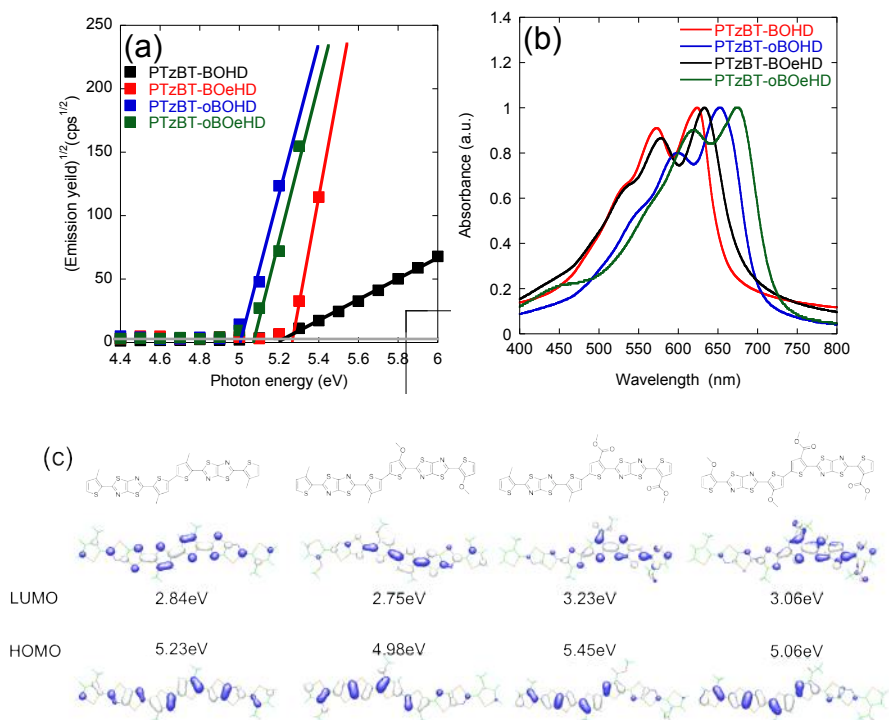


Figure 6-3. (a) Photoelectron spectra of the polymer thin films measured in air. (b) UV-vis absorption spectra of the polymers in the film. (c) HOMO and LUMO geometry calculated of repeating unites by the DFT method at the B3LYP/6-31 g(d) level.

Table 6-2. Electronic properties of the monomers and polymer.

compound	Computation		Experimental			
	E_H^c ^a (eV)	E_L^c ^a (eV)	λ_{\max} (nm)	$\lambda_{\text{edge}}/E_g^{\text{opt}}$ ^b (nm)/(eV)	E_H^c (eV)	E_L^d (eV)
TzBT-BO	-5.53	-2.34	403	448/2.77	-5.59	-2.82
TzBT-oBO	-5.08	-2.00	415, 440	457/2.71	-5.29	-2.58
TzBT-eHD	-6.14	-2.85	432	481/2.58	-5.80	-3.22
PTzBT-BOHD	-5.23	-2.84	573, 624	685/1.81	-5.23	-3.42
PTzBT-oBOHD	-4.98	-2.75	600, 653	709/1.75	-5.02	-3.72
PTzBT-BOeHD	-5.45	-3.23	578, 633	700/1.77	-5.28	-3.51
PTzBT-oBOeHD	-5.06	-3.06	621, 675	730/1.70	-5.08	-3.38

^a HOMO (E_H) and LUMO (E_L) energy levels calculated by the DFT method at the B3LYP/6-31(d) level. ^b λ_{edge} : absorption edge,

E_g^{opt} : bandgap calculated with λ_{edge} . ^c HOMO energy levels, which were determined by cyclic voltammetry for the monomers and

were determined by photoelectron spectroscopy in air (PESA) for polymers. ^d E_{LUMO} estimated by adding the band gap (E_g^{opt}) to

E_{HOMO} .

Solar Cell Characteristics

Solar cells were fabricated by spin-coating the solutions of polymer and [6,6]-phenyl-C₆₁-butyric acid methyl ester (PC₆₁BM) in chlorobenzene onto the PEDOT:PSS spin-coated ITO glass, followed by vacuum deposition of Ca/Al as the cathode. The optimal polymer-to-PC₆₁BM (p:n) ratio were 1:1 for PTzBT-oBOHD and 1:2 for other polymers. The optimized active layer thickness was around 200 nm for the cells with newly synthesized polymers. External quantum efficiency (EQE) spectra and current density (J)-Voltage (V) curves of the cells under 1 sun of simulated AM 1.5G solar irradiation (100 mW/cm²) are displayed in **Figure 6-4a**, and photovoltaic parameters are summarized in **Table 6-3**.

As expected from the absorption spectra, all the cells using the present polymers showed photoresponse in wider spectral ranges compared to that with PTzBT-BOHD (**Figure 6-4b**). However, only the PTzBT-oBOeHD-based cells gave higher short-circuit current density (J_{SC}) of 10.9 mA/cm² than the PTzBT-BOHD-based cell (10.1 mA/cm²), which is also evident from the EQE spectra. Owing to the higher-lying E_{HOMO} for PTzBT-oBOHD and -oBOeHD, their cells showed lower open-circuit voltages (V_{OC}) of 0.71 and 0.78 V than the cells with PTzBT-BOHD and -BOeHD ($V_{\text{OC}} = 0.91\text{-}0.92$ V). Furthermore, all the cells showed lower

fill factors (*FFs*) of below 0.60 than that of the PTzBT-BOHD-based cells (0.68). Overall, modest PCEs of 3.8-4.5% were obtained for the cells with the present polymers.

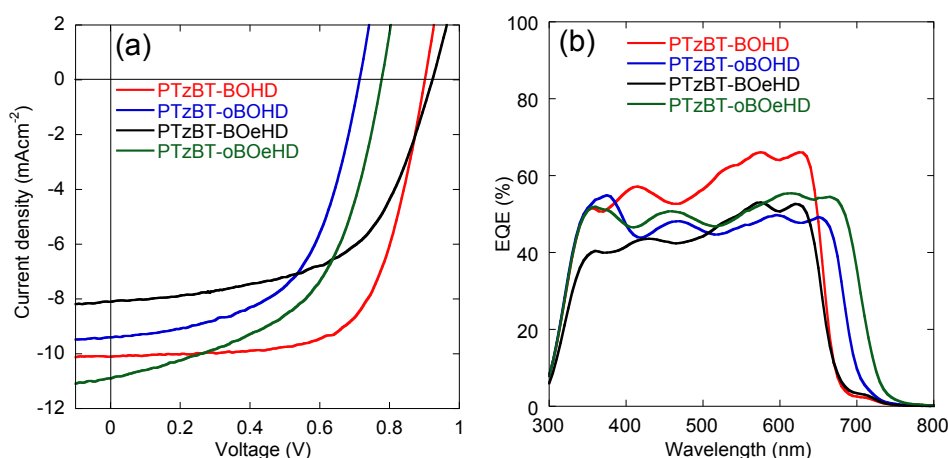


Figure 6-4. *J-V* curves (a) and EQE spectra (b) of BJJ solar cells (ITO/PEDOT:PSS/polymer:PC₆₁BM/Ca/Al)

Table 6-3. Photovoltaic Properties of the Polymer-Based Solar Cells.

Polymer	p:n ratio ^a	thickness (nm)	J_{SC} (mA/cm ²)	V_{OC} (V)	<i>FF</i>	PCE _{max} [PCE _{ave}] (%)
PTzBT-BOHD	1:2	200	10.1	0.91	0.68	6.1 [5.8]
PTzBT-oBOHD	1:1	200	9.4	0.71	0.57	3.8 [3.5]
PTzBT-BOeHD	1:2	160	8.1	0.92	0.57	4.2 [4.0]
PTzBT-oBOeHD	1:2	200	10.9	0.78	0.53	4.5 [4.2]

^a Polymer to PC₆₁BM weight ratio

Thin Film Structure and morphology

In order to further understand the photovoltaic performances of the cells, polymer ordering structures in the thin film were investigated by X-ray diffraction studies. Two-dimensional grazing incidence X-ray diffraction (2D-GIXD) images of the polymer-only films and polymer/PC₆₁BM blend films on the PEDOT:PSS/ITO substrate, are shown in **Figure 6-5a** and **6-5b**, respectively. In all cases, diffractions assignable to the lamellar structure ($q \approx 0.25 \text{ \AA}^{-1}$) and the π - π stacking structures ($q \approx 1.7 \text{ \AA}^{-1}$) appeared along the q_{xy} (in-plane) and q_z axes (out-of-plane), respectively, indicating that the polymers formed face-on orientation on the substrate surface^[10] regardless of with and without PC₆₁BM. Among the newly synthesized polymers, PTzBT-oBOHD and -oBOeHD

with the alkoxy group showed more intense π - π stacking diffractions in the q_z direction, indicating that the face-on orientation is more dominant than PTzBT-BOeHD. π - π Stacking distances estimated from the 2D-GIXD pattern of the polymer-only film were about 3.5 Å for all the polymers, suggesting that the alkoxy and ester groups are not detrimental to the ordering structure. Note that the π - π stacking distance did not change by the addition of PC₆₁BM.

I also investigated the morphology of the polymer/PC₆₁BM blend films by the atomic force microscopy (AFM) (**Figure 6-6**). The polymers with the ester groups (PTzBT-BOeHD and -oBOeHD) showed needle-like textures that are slightly different from the nodule-like textures observed in other polymers. Nevertheless, all the polymer/PC₆₁BM seems to have formed well-phase-separated morphologies, which would ensure the charge generation. On the other hand, the surface roughness estimated by the root mean square (rms) values of the blend of PTzBT-oBOHD, -BOeHD, and -oBOeHD are larger than that of PTzBT-BOHD, which means that the blend films of PTzBT-oBOHD, -BOeHD, and -oBOeHD are less uniform compared to that of PTzBT-BOHD, which could be a reason for the lower hole-mobility and the lower solar cell performances of the new polymers. We believe that the solar cell performances of the new polymers could be improved by optimizing the film morphology.

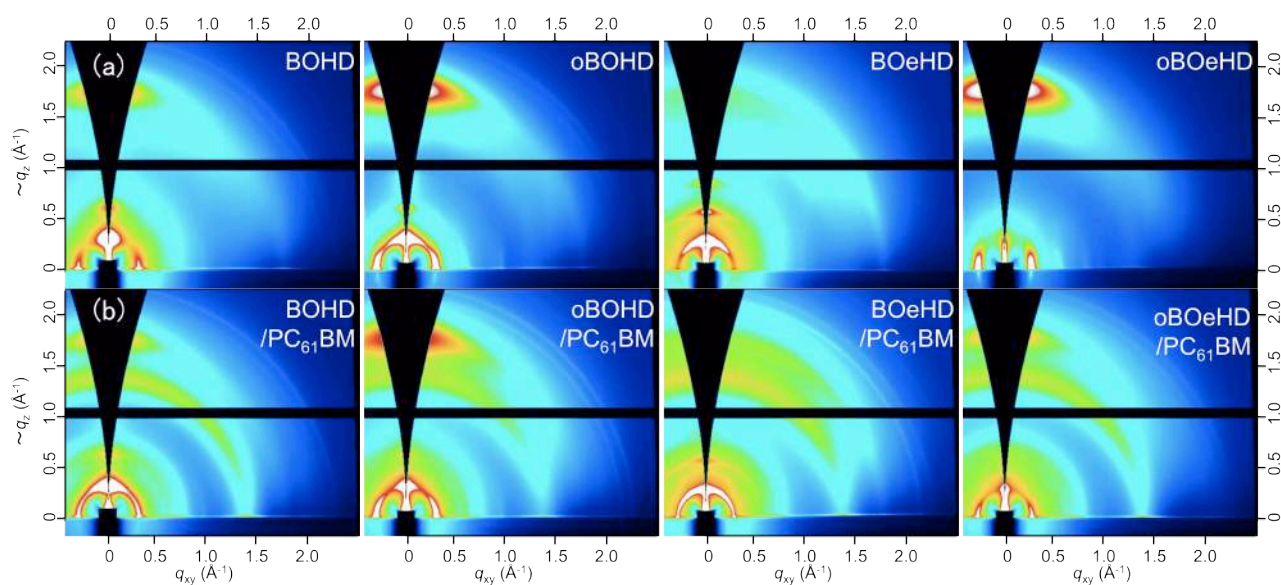


Figure 6-5. 2D-GIXD patterns of (a) polymer-only films (b) polymer / PC₆₁BM blend films

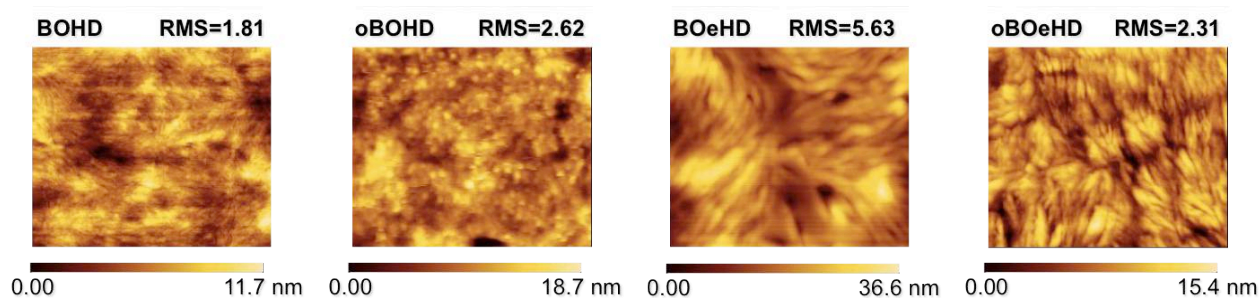


Figure 6-6. AFM images of Polymer / PC₆₁BM blend films

6-3. Summary

New thiazolothiazole-based semiconducting polymers with the alkoxy and ester groups as the side chain have been synthesized and investigated. As expected, introduction of the alkoxy groups raised the HOMO energy level of the polymer, and introduction of the ester groups lowered the LUMO energy levels. Having both the alkoxy and ester groups, PTzBT-oBOeHD gave the most red-shifted absorption spectrum among the polymers studied here. Although the overall efficiencies were lower for the cells using the new polymers compared to the previously synthesized polymer, all the cells using new polymers showed photoresponse in wider spectral regions. Further optimization might lead to the improvement of the efficiency.

Experimental

Synthesis

2,5-Bis(3-((butyloctyl)oxy)thiophen-2-yl)thiazolo[5,4-*d*]thiazole (**2**)

Dithiooxamide (1.1 g, 9.2 mmol) and 3-((2-hexyldecyl)oxy)thiophene-2-carbaldehyde (**1**) (6.0 g, 20.2 mmol) were combined in a round-bottom flask and heated at temperature 200 °C for 12 h. The crude product was purified by column chromatography on silica gel. Recrystallization from hexane gave pure product as yellow solids (1.8 g, 29%). ¹H NMR (400 MHz, CDCl₃) δ 7.32 (d, *J* = 5.5 Hz, 2H), 6.89 (d, *J* = 5.5 Hz, 2H), 4.14 (d, *J* = 4.8 Hz, 4H), 1.85-1.82 (m, 2H), 1.62-1.49 (m, 8H), 1.40-1.20 (m, 24H), 0.86 (t, *J* = 7.0 Hz, 12H). ¹³C-NMR (100 MHz, CDCl₃) δ 159.8, 156.3, 149.9, 126.8, 116.4, 115.5, 74.5, 38.6, 32.0, 31.4, 31.1, 29.8, 29.3, 27.1, 23.2, 22.8, 14.3, 14.3. EI-MS (70 eV) *m/z* = 674 (M⁺); Anal. calcd for C₃₆H₅₄N₂O₂S₄: C, 64.05%; H, 8.06%; N, 4.15%. Found: C, 64.19%; H, 8.36%; N, 4.02%.

2,5-Bis(5-bromo-3-((2-butyloctyl)oxy)thiophen-2-yl)thiazolo[5,4-*d*]thiazole (3)

To a solution of 2,5-bis(3-((2-octyldodecyl)oxy)thiophen-2-yl)thiazolo[5,4-*d*]thiazole (2) (1.5 g, 2.2 mmol) in CHCl₃ (50 mL) and acetic acid (25 mL) solution, NBS (870 mg, 4.9 mmol) solution in CHCl₃/AcOH (20/10 mL) was added dropwise and stirred at 0°C for 2 h. Then the reaction solution was stirred at room temperature overnight. The mixture was washed with water and brine, and the organic layer was concentrated. Purifications with column chromatography on silica gel and recrystallization from hexane gave pure product as yellow solids (1.57 g, 85%). ¹H-NMR (400 MHz, CDCl₃) δ 6.90 (s, 2H), 4.09 (d, *J* = 4.9 Hz, 4H), 1.84-1.82 (m, 2H), 1.60-1.49 (m, 8H), 1.35-1.29 (m, 24H), 0.93-0.86 (m, *J* = 7.0 Hz, 12H). ¹³C-NMR (100 MHz, CDCl₃) δ 158.7, 154.8, 145.0, 119.8, 116.9, 115.5, 74.9, 38.5, 32.0, 31.4, 31.1, 29.8, 29.3, 27.0, 23.2, 22.8, 14.3 EI-MS (70 eV) *m/z* = 830 (M⁺); Anal. calcd for C₃₆H₅₂Br₂N₂O₂S₄: C, 51.91%; H, 6.29%; N, 3.36%. Found: C, 51.70%; H, 6.19%; N, 3.46%.

2,5-Bis(5-trimethylstannyl-3-((2-butyloctyl)oxy)thiophen-2-yl)thiazolo[5,4-*d*]thiazole (4)

To a solution of 2,5-bis(5-bromo-3-((2-butyloctyl)oxy)thiophen-2-yl)thiazolo[5,4-*d*]thiazole (3) (1.2 g, 1.44 mmol) in 50 mL of THF, 1.6 M solution of *n*-butyllithium in hexane (2.25 mL, 3.6 mmol) was added dropwise at -78 °C. The solution was stirred at -78 °C for 1 h and trimethyltin chloride (800 mg, 4.0 mmol) was added. After the solution was warmed to room temperature, 50 mL of water and 50 mL of ethyl acetate were added. The organic layer was washed twice with 50 mL of water and dried over magnesium sulfate. After removing the solvent, recrystallization from hexane gave pure product as yellow solids (1.0 g, 70%). ¹H-NMR (400 MHz, CDCl₃) δ 6.91 (s, 2H), 4.15 (d, *J* = 4.9 Hz, 4H), 1.84-1.82 (m, 2H), 1.61-1.50 (m, 8H), 1.28-1.24 (m, 24H), 0.87-0.84 (m, *J* = 7.0 Hz, 12H), 0.41 (s, 18H). ¹³C-NMR (100 MHz, CDCl₃) δ 159.5, 157.5, 149.9, 141.2, 123.2, 120.7, 74.3, 38.6, 32.0, 31.4, 31.1, 29.8, 29.8, 29.5, 27.1, 22.8, 14.3. EI-MS (70 eV) *m/z* = 1002 (M⁺); Anal. calcd for C₄₂H₇₀N₂O₂S₄Sn₂: C, 50.41%; H, 7.05%; N, 2.80%. Found: C, 50.65%; H, 6.88%; N, 2.98%.

2-Hexyldecyl-5-bromo-2-formylthiophene-3-carboxylate (7)

Lithium diisopropylamide (freshly prepared from diisopropylamine (4.2 mL, 33 mmol) and 1.6 M *n*-butyllithium (20.1 mL, 33 mmol) in tetrahydrofuran (THF) (50 mL)) was added dropwise to a THF (50 mL) solution of 5-bromothiophene-3-carboxylate (5) (2.07 g, 10 mmol) at -30 °C. After stirring the mixture for 1 h, dimethylformamide (2.8 mL, 36 mmol) was added to the mixture at -30 °C, and then the mixture was warmed to

room temperature. The mixture was further stirred for 1 h, and then water (100 mL) was added to the mixture and extracted with ether three times. The organic layer was dried over magnesium sulfate, and the solvent was evaporated under reduced pressure, giving **6** as brown solids (2.2 g). **6** was subjected to the next reaction without further purification. **6** (2.2 g), 2-hexyl-1-bromodecane (3.35 g, 33 mmol), and sodium carbonate (10.5 g, 99 mmol) in DMF (50 ml) were heated to 125 °C for 5 h, and then cooled to room temperature. The reaction mixture was poured into water and extracted with dichloromethane. The crude product was purified by column chromatography on silica gel to give **7** as yellow oil (2.4 g, 52% in 2step). ¹H-NMR (400 MHz, CDCl₃) δ 10.48 (s, 1H), 7.51 (s, 1H), 4.26 (d, *J* = 4.9 Hz, 2H), 1.88-1.78 (m, 1H), 1.62-1.44 (m, 4H), 1.34-1.26 (m, 20H), 0.90-0.86 (m, 6H). ¹³C-NMR (100 MHz, CDCl₃) δ 183.7, 161.5, 148.7, 137.1, 133.5, 122.7, 68.9, 37.7, 37.5, 32.0, 31.9, 31.5, 31.2, 30.0, 29.7, 29.5, 26.8, 22.8, 14.3. EI-MS (70 eV) *m/z* = 458 (M⁺); Anal. calcd for C₂₂H₃₅O₃S: C, 57.51%; H, 7.68%. Found: C, 57.36%; H, 7.46%.

2,2'-(Thiazolo[5,4-*d*]thiazole-2,5-diyl)bis(5-bromothiophene-3-carboxylate)

A mixture of **7** (2.02 g, 4.4 mmol) and dithiooxamide (240 mg, 2 mmol) were heated to 140 °C for 24 h, and then cooled to room temperature. The reaction mixture was poured into water and extracted with dichloromethane. The combined organic layer was dried over magnesium sulfate, and concentrated under reduced pressure. The crude product was purified by column chromatography on silica gel and recrystallization from hexane to give **8** as yellow solids (220 mg, 11%). ¹H-NMR (400 MHz, CDCl₃) δ 7.44 (s, 1H), 4.26 (d, *J* = 4.9 Hz, 4H), 1.78 (m, 2H), 1.60-1.56 (m, 8H), 1.35-1.27 (m, 40H), 0.90-0.86 (m, 12H). ¹³C-NMR (100 MHz, CDCl₃) δ 162.3, 159.6, 153.8, 132.7, 128.8, 115.9, 68.6, 37.5, 32.1, 32.0, 31.5, 30.1, 29.8, 29.7, 29.5, 26.9, 22.9, 22.8, 14.3. EI-MS (70 eV) *m/z* = 998 (M⁺); Anal. calcd for C₄₆H₆₈N₂O₄S₄: C, 55.19%; H, 6.85%; N, 2.80%. Found: C, 54.98%; H, 6.61%; N, 2.91%.

General procedure for polymerization

To a reaction tube equipped with a stirring bar, stannylated monomer (0.10 mmol), brominated monomer (0.10 mmol), Pd₂(dba)₃ (1.8 mg, 0.002 mmol), P(*o*-Tol)₃ (2.4 mg, 0.008 mmol), and chlorobenzene (5 ml) were added. Then the tube was purged with argon and sealed. The reaction tube was set into a microwave reactor and heated to

200 °C for 10 min. After cooling to room temperature, the reaction solution was poured into 200 mL of methanol containing 5 mL of hydrochloric acid, and stirred for 5 hours. Then the precipitated solid was subjected to the sequential Soxhlet extraction with methanol, hexane to remove low molecular weight fractions. The residue was then extracted with chloroform, and reprecipitated in 200 mL of methanol to yield dark purple or dark blue solids (yield = 72-91%).

Instrumentation

UV-vis absorption spectra were measured using a Shimadzu UV-3600 spectrometer. Cyclic voltammograms (CVs) were recorded on a ALS Electrochemical Analyzer Model 612D in dichloromethane containing tetrabutylammonium hexafluoride (Bu_4NF , 0.1 M) as supporting electrolyte at a scan rate of 100 mV/s. Pt counter and working electrodes and a Ag/AgCl reference electrode was used. All the potentials were calibrated with the standard ferrocene/ferrocenium redox couple (Fc/Fc^+ : $E^{1/2} = +0.43$ V measured under identical conditions). Photoelectron spectra were measured by using a photoelectron spectrometer, model AC-2, in air (Riken Keiki Co., Ltd). Dynamic force-mode atomic force microscopy study was carried out on a Nanoscope IIIA MultiMode head on a Nanoscope IIIA MultiMode microscope system (SII Nanotechnology, Inc.). 2D-GIXD experiments were conducted at the SPring-8 on the beamline BL19B2. The sample was irradiated at a fixed incident angle on the order of 0.12° through a Huber diffractometer. The X-ray energy of 12.39 keV ($\lambda = 1 \text{ \AA}$) the 2D-GIXD patterns were recorded with a 2-D image detector (Pilatus 300K). Samples for the X-ray measurements were prepared by spin-casting the polymer and polymer/ PC_{61}BM solution on the ITO substrate.

Solar Cell Fabrication and Measurement

ITO substrates were first pre-cleaned sequentially by sonicating in a detergent bath, de-ionized water, acetone, and isopropanol at rt, and in a boiled isopropanol bath each for 10 min, and then baked at 120 °C for 10 min in air. The substrates were then subjected to a UV/ozone treatment at rt for 20 min. The pre-cleaned ITO substrates were coated with PEDOT:PSS (Clevios P VP A14083) by spin-coating (5000 rpm for 30 sec, thickness: ~50 nm). The photoactive layer was deposited in a glove box by spin coating a chlorobenzene solution, containing 3~6 g/L of the polymer sample with respective amount of PC_{61}BM , at 400 rpm for 20 sec and 1500 rpm for 5 sec, in which

the solution was kept heated at 100 °C. The thin films were transferred into a vacuum evaporator connected to the glove box, and the Ca layer (20 nm) and the Al layers (100 nm) were deposited sequentially. The active area of the cells was 0.16 cm². *J-V* characteristics for the cells were measured using a Keithley 2400 source-measure unit in nitrogen atmosphere under 1 Sun (AM1.5G) conditions using a solar simulator (SAN- EI Electric, XES-40S1). The light intensity for the *J-V* measurements was calibrated with a reference PV cell (KONICA MINOLTA AK-100 certified at National Institute of Advanced Industrial Science and Technology, Japan). EQE spectra were measured with a Spectral Response Measuring System (SOMA OPTICS, LTD., S-9241).

Reference

- [1] (a) G. Yu, J. Gao, J. C. Hummelen, F. Wudl, A. J. Heeger, *Science* **1995**, *270*, 1789–1791. (b) D. Mühlbacher, M. Scharber, M. Morana, Z. Zhu, D. Waller, R. Gaudiana, C. Brabec, *Adv. Mater.* **2006**, *18*, 2884–2889.
- [2] (a) Y. Liang, Z. Xu, J. Xia, S. Tsai, Y. Wu, G. Li, C. Ray, L. Yu, *Adv. Mater.* **2010**, *22*, E135–E138. (b) H. Y. Chen, J. Hou, S. Zhang, Y. Liang, G. Yang, Y. Yang, L. Yu, Y. Wu, G. Li, *Nature Photon.* **2009**, *3*, 649–653. (c) T. Y. Chu, J. Lu, S. Beaupré, Y. Zhang, J. R. Pouliot, S. Wakim, J. Zhou, M. Leclerc, Z. Li, J. Ding, Y. Tao, *J. Am. Chem. Soc.* **2011**, *133*, 4250–4253. (d) S. C. Price, A. C. Stuart, L. Yang, H. Zhou, W. You, *J. Am. Chem. Soc.* **2011**, *133*, 4625–4631. (e) J. You, L. Dou, K. Yoshimura, T. Kato, K. Ohya, T. Moriarty, K. Emery, C. Chen, J. Gao, G. Li, Y. Yang *Nature Commun.* **2013**, *4*, 1446–1456. (f) H. Chen, Y. Chen, C. Liu, Y. Chien, S. Chou, P. Chou, *Chem. Mater.* **2012**, *24*, 4766–4772. (g) I. Osaka, T. Kakara, N. Takemura, T. Koganezawa, K. Takimiya *J. Am. Chem. Soc.* **2013**, *135*, 8834–8837.
- [3] (a) Mühlbacher, D.; Scharber, M.; Morana, M.; Zhu, Z.; Waller, D.; Gaudiana, R.; Brabec, C. *Adv. Mater.* **2006**, *18*, 2884. (b) Hou, J.; Chen, H.-Y.; Zhang, S.; Li, G.; Yang, Y. *J. Am. Chem. Soc.* **2008**, *130*, 16144.
- [4] (a) I. Osaka, G. Sauve, R. Zhang, T. Kowalewski, R.D. McCullough, *Adv. Mater.* **2007**, *19*, 41560–4165. (b) M. Zhang, H. Tsao, W. Pisula, C. Yang, A. Mishra, K. Mullen *J. Am. Chem. Soc.* **2007**, *129*, 3472–3473. (c) M. Wienk, M. Turbiez, J. Gilot, R. Janssen *Adv. Mater.* **2008**, *20*, 2556–2560.
- [5] (a) I. Osaka, R. Zhang, G. Sauve, D.-M. Smilgies, T. Kowalewski, R. D. McCullough *J. Am. Chem. Soc.* **2009**, *131*, 2521–2529. (b) I. Osaka, R. Zhang, J. Liu, D.-M. Smilgies, T. Kowalewski, R.D. McCullough, *Chem. Matter*, **2010**, *22*, 4191–4196.

- [6] (a) J. Peet, L. Wen, P. Byrne, S. Rodman, K. Forberich, Y. Shao, N. Drolet, R. Gaudiana, G. Dennler, D. Waller, *Appl. Phys. Lett.* **2011**, *98*, 043301-043304. (b) I. H. Jung, J. Yu, E. Jeong, J. Kim, S. Kwon, H. Kong, K. Lee, H. Y. Woo, H.-K. Shim, *Chem. Eur. J.* **2010**, *16*, 3743-3752. (c) M. Zhang, X. Guo, Y. Li, *Adv. Energy Mater.* **2011**, *1*, 557-560. (d) Q. Shi, H. Fan, Y. Liu, W. Hu, Y. Li, X. Zhan, *J. Phys. Chem. C* **2010**, *114*, 16843-16848. (e) M. Yang, B. Peng, B. Liu, Y. Zou, K. Zhou, Y. He, C. Pan, Y. Li, *J. Phys. Chem. C* **2010**, *114*, 17989-17994. (f) L. Huo, X. Guo, S. Zhang, Y. Li, J. Hou, *Macromolecules* **2011**, *44*, 4035-4037. (g) S. K. Lee, J. M. Cho, Y. Goo, W. S. Shin, J.-C. Lee, W.-H. Lee, I.-N. Kang, H.-K. Shim, S.-J. Moon, *Chem. Commun.* **2011**, *47*, 1791. (h) M. Zhang, X. Guo, X. Wang, H. Wang, Y. Li, *Chem. Mater.* **2011**, *23*, 4264-4270. (i) Selvam Subramaniyan, Felix Sunjoo Kim, Guoqiang Ren, Haiyan Li, and Samson A. Jenekhe *Macromolecules* **2012**, *45*, 9029-9037.
- [7] (a) I. Osaka, M. Saito, H. Mori, T. Koganezawa, K. Takimiya, *Adv. Mater.* **2012**, *24*, 425-430. (b) I. Osaka, M. Saito, T. Koganezawa, K. Takimiya, *Adv. Mater.* **2014**, *26*, 331-338 .
- [8] (a) S. Subramaniyan, H. Xin, F. Kim, S. Shoaee, J. Durrant, S. Jenekhe, *Adv. Energy Mater.* **2011**, *1*, 854-860. (b) J. Hai, B. Zhao, F. Zhang, C. Sheng, L. Yin, Y. Li, E. Zhu, L. Bian, H. Wu, W. Tang *polymer*, **2013**, *54*, 4930-4939.
- [9] M. Helgesen, M. Madsen, B. Andreasen, T. Tromholt, J. Andreasen. F. Krebs, *Polym. Chem*, **2011**, *2*, 2536-2542.
- [10] H. Sirringhaus, P. J. Brown, R. H. Friend, M. M. Nielsen, K. Bechgaard, B. M. W. Langeveld-Voss, A. J. H. Spiering, R. A. J. Janssen, E. W. Meijer, P. Herwig, D. M. de Leeuw, *Nature*, **1999**, 685-688.

Chapter 7

7. OPV Characteristics of Semiconducting Polymer with Thiazolothiazole and Naphthobisthiadiazole in the Backbone

7-1. Introduction

Bulk heterojunction (BHJ) solar cells composed of semiconducting polymers as the p-type and fullerene derivatives as the n-type materials in the photoactive layer are of great interests as flexible and large-area renewable energy sources that can be produced by solution-processed.^[1]

A number of semiconducting polymers have been developed, which have brought about significant improvement of power conversion efficiencies (PCEs).^[2] In order to improve PEC, semiconducting polymers are desired to have crystalline structures and “face-on” backbone orientation, where the backbone plane lie flat on substrate, facilitating the charge carrier transport along the film thickness. In parallel, they are also required to have a wide absorption range, namely a narrow band gap, to absorb as much sunlight as possible.^[3] They also need to have a low-lying highest occupied molecular orbital (HOMO) energy level to maximized the open circuit voltage (V_{OC}) that is proportional to the energy difference between HOMO of the semiconducting polymer and the lowest unoccupied molecular orbital (LUMO) of the fullerene derivative. To fulfill these requirements, so-called donor-acceptor (D-A) polymers consisting of electron-rich (donor; D) and electron-poor (acceptor; A) have been widely used in this field.^[4]

Recently, I have reported on a D-A copolymer system based on alkylthiophene and thiazolothiazole (TzTz) as the D and A units, respectively (PTzBTs, **Figure 7-1**). These polymers showed relatively high PCE of ~7.5% in conventional cells, most likely originates in the high crystalline structure and favorable face-on orientation.^[5] Although PTzBTs have low HOMO energy levels of -5.20 eV and thus exhibit high V_{OC} of 0.90 V in solar cells, their wide band gap of 1.80 eV, i.e., narrow absorption range of up to 680 nm, limited light harvesting and thus the short-circuit current density (J_{SC}). I have also reported on D-A polymers based on naphthobisthiadiazole (NTz), a stronger A unit, i.e., a more highly electron-poor unit, while other groups also reported on NTz-based polymers.^[2g, 6] An NTz copolymer with simple quaterthiophene as the D unit (PNTz4T) exhibited a narrow band gap of 1.54eV, a wide absorption range of up to 820 nm, and showed quite high PCEs of ~9% and ~10% in conventional and inverted cells, respectively. However, a drawback of PNTz4T-cells is relatively low V_{OC} of around 0.7V.

Despite the fact that the HOMO energy level of PNTz4T is -5.15 eV, which is only about 0.05eV higher than that of PTzBTs, V_{OC} is smaller by ~0.2V. This somewhat large energetic loss is yet unknown, lowering the HOMO energy level is required for the NTz polymer system to further improve the PCE.

In this work, I simply combined TzTz and NTz, giving a D-A polymer with a ternary unit system (PTzNTzs), where alkylthiophene is the D unit and TzTz and NTz are the A unit, to compensate the low J_{SC} of PTzBT-cells and low V_{OC} of PNTz4T-cells. I describe the synthesis, electronic structure, and the ordering structures of PTzNTzs and their solar cell performances. I also note that, unexpectedly, the solar cells based on PTzNTzs showed high thermal stability as compared to the cells based on PTzBTs and PNTz4T.

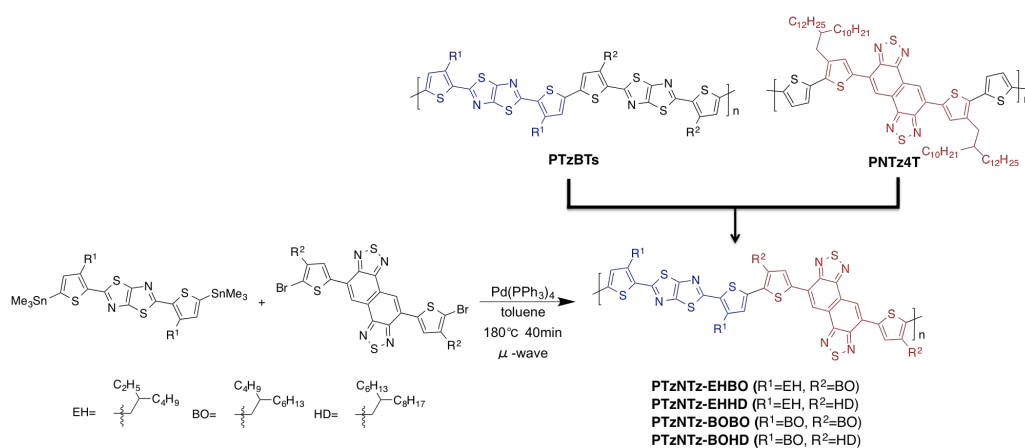


Figure 7-1. Chemical structure of PTzBTs, PNTz4T and PTzNTz- R^1R^2 and polymerization of PTzNTz- R^1R^2

7-2. Result and discussion

All polymers were synthesized via the Stille coupling reaction using a microwave reactor (**Scheme 7-1**). Stannylated TzTz monomers (**1a-1b**) were copolymerized with brominated NTz monomers (**2a-2b**) to give PTzNTzs with four different combinations of alkyl groups (PTzNTz-EHBO, -EHHD, -BOBO, -BOHD). Whereas PTzNTz-EHBO was soluble in hot chlorobenzene (CB), or *o*-dichlorobenzene (DCB), PTzNTz-EHHD, -BOBO, and -BOHD showed quite good solubility even in chloroform (CF) below ca. 40°C. Interestingly, the solubility of PTzNTzs is quite high. For example, 5mg of PTzBT-BOHD was dissolve in CB at 100°C, however PTzNTz-BOHD was dissolve at room temperature. The number-average molecular weight (M_n), evaluated by

GPC at 140 °C, of PTzNTz-EHBO, -EHHD, -BOBO and -BOHD were about 32, 47, 51, 29 kDa, respectively (**Table 7-1**).

The thermal property of polymers was studied by differential scanning calorimetry (DSC). It was revealed that whereas PTzNTz-EHHD, -BOBO and BOHD showed transition peaks between 250-300 °C, PTzNTz-EHBO did not show transition peaks below 350 °C. This implies that PTzNTz-EHBO has a more rigid backbone most likely due to the shorter alkyl groups on the side chain (**Figure 7-2**).

The HOMO energy level (E_{HOMO}) of the polymers was evaluated by photoelectron spectroscopy in air (PESA) using the polymer thin films. All polymers showed similar E_{HOMO} s of around -5.25 eV (**Table 7-1**), which were even lower than that of PTzBTs. **Figure 7-3** displays the UV-vis absorption spectra of the polymers in the thin film. All the polymers exhibited broad spectra with the absorption maximum (λ_{max}) of ca. 690 nm and the absorption edge (λ_{edge}) of ca. 800 nm, which corresponds to the band gap of 1.55-1.60eV. The absorption range of PTzNTzs was similar to that of PNTz4T. Thus as expected, PTzNTzs are found to have both the narrow band gap and low HOMO energy level.

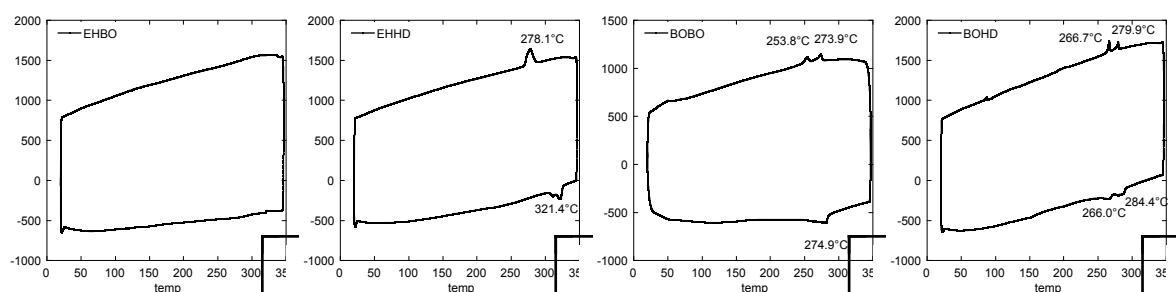


Figure 7-2. DSC thermograms of polymers PTzNTz-EHBO, EHHD, BOBO and BOHD at a temperature ramp rate of 10 °C min⁻¹

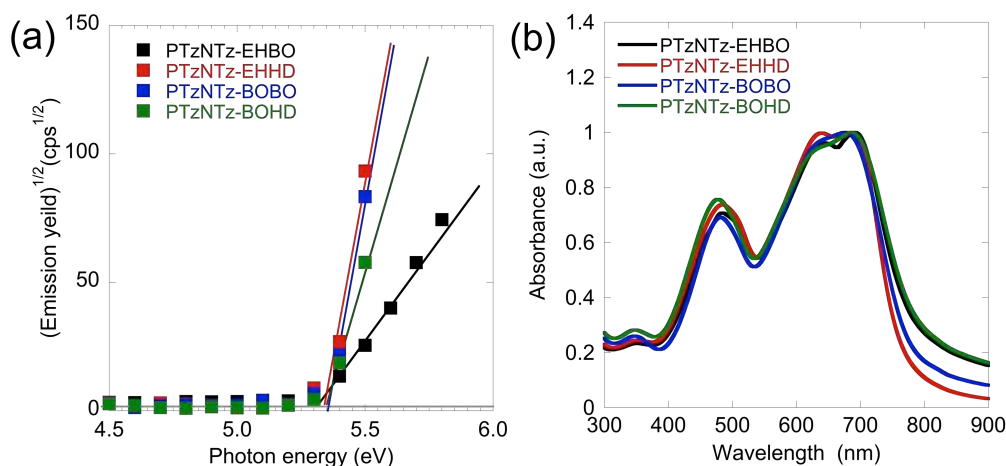


Figure 7-3. Photoelectron spectra (a) and UV-vis absorption spectra (b) of the polymer thin films.

Table 7-1. Polymerization results.^a

Polymer	M_n (kDa)	M_w (kDa)	PDI	λ_{max} (nm)	$\lambda_{edge}^{opt} / E_g^{opt}$ (nm/eV) ^b	E_{HOMO} (eV) ^c
PTzNTz-EHBO	32	64	2.0	484, 691	802 / 1.55	-5.26
PTzNTz-EHHD	47	91	2.0	484, 644, 693	789 / 1.57	-5.25
PTzNTz-BOBO	51	113	2.2	483, 679	795 / 1.56	-5.27
PTzNTz-BOHD	29	54	2.2	479, 688	806 / 1.61	-5.28

^a Determined by GPC using polystyrene standard and *o*-dichlorobenzene as the eluent at 140 °C. ^b λ_{edge}^{opt} : absorption edge, E_g^{opt} :

bandgaps calculated with λ_{edge}^{opt} . ^c Photoelectron spectroscopy in air (PESA) were used to evaluate HOMO energy levels.

Solar cells with an inverted structure, indium tin oxide (ITO)/ZnO/active layer/MoO_x/Ag, were used to investigate the photovoltaic properties of the polymers. [6,6]-phenyl-C₇₁-butyric acid methyl ester (PC₇₁BM) was used as the n-type materials, and the active layer was fabricated from the CB solution. The optimal polymer to PC₇₁BM weight was 1:1.5 for all polymers. The current density (*J*)-Voltage (*V*) curves and the external quantum efficiency (EQE) spectra of the cells under 1 sun of simulated AM 1.5G solar irradiation (100 mW/cm²) are displayed in **Figure 7-3a** and **b**, respectively. The photovoltaic parameters are summarized in **Table 7-2**. While V_{OC} was similar for all the polymer-cells (0.84-0.85 V), significant difference was seen in J_{SC} , where the PTzNTz-EHBO gave much higher J_{SC} of 15.97 mA/cm² than the other polymers (2-4 mA/cm²). It is found that the fill factor (FF) was also higher for PTzNTz-EHBO (0.67) than the other polymers (<0.6). As a result, PTzNTz-EHBO-based cells exhibited the highest PCEs of 9.0%, and those of the other polymer-based cells were

1.2-2.1%. Note that, however, PCEs were markedly improved for the cells that used PTzNTz-EHHD, -BOBO and -BOHD when the active layer was fabricated from CB/ 1% of 1,8-diiodooctane (DIO) solution (**Figure 7-4c**). In particular, the DIO-aided cells of PTzNTz-EHHD and -BOBO showed significant increase in J_{SC} to above 15-16 mA/cm², being consistent with the EQE (**Figure 7-4d**), along with the increase of FF to around 0.60, which resulted in PCEs of 8.8% (**Table 7-2**). In contrast, PCEs of PTzNTz-EHBO-based cells was slightly decreased to 8.5% by the use of DIO.

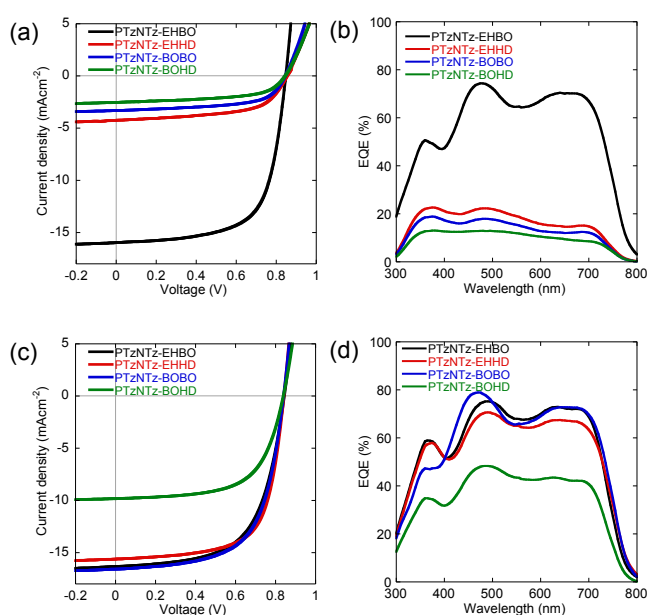


Figure 7-3. J - V curves (a, c) and EQE spectra (b, d) of the solar cells based on PTzNTz-R¹R². (a, b) The active layer was spun from the CB solution. (c, d) The active layer was spun from CB/DIO (1v/v%).

Table 7-2. Photovoltaic properties of the solar cells based on PTzNTz-R¹R².

Polymer	DIO	J_{SC} (mA/cm ²)	V_{OC} (V)	FF	PCE _{max} [PCE _{ave}] ^a (%) ^d
PTzNTz-EHBO		15.97	0.84	0.67	9.0 [8.7]
	1%	16.33	0.84	0.62	8.5 [8.2]
PTzNTz-EHHD		4.25	0.85	0.58	2.1 [1.9]
	1%	15.62	0.84	0.67	8.8 [8.5]
PTzNTz-BOBO		3.31	0.85	0.60	1.7 [1.5]
	1%	16.58	0.84	0.63	8.8 [8.5]
PTzNTz-BOHD		2.52	0.84	0.58	1.2 [1.1]
	1%	9.83	0.84	0.63	5.2 [4.8]

^a PCE_{max}: maximum power conversion efficiencies, PCE_{ave}: average power conversion efficiencies.

In order to understand the difference in the photovoltaic performances, the ordering structures in the polymers in the thin film was investigated by X-ray diffraction studies. Two-dimensional grazing incidence X-ray diffraction (2D-GIXD) images of the polymer-only films and the polymer/PC₇₁BM blend films on the ZnO/ITO substrate are shown in **Figure 7-5**. In polymer-only films, a diffraction corresponding to the π - π stacking structures ($q \approx 1.7 \text{ \AA}^{-1}$) was dominant for PTzNTz-EHBO and -BOBO, indicating that they form crystalline domains with a favorable face-on orientation. The π - π stacking distance (d_π) of these polymers was calculated to be 3.69 and 3.72 \AA , respectively (**Table 7-3**). In the meantime, the π - π stacking diffraction for PTzNTz-EHHD and -BOHD appeared weaker as diffuse ring, indicating that the crystallinity is very weak. The d_π was also wider for PTzNTz-EHHD and -BOHD with 3.77 and 3.80 \AA , respectively (**Table 7-3**). The difference in d_π clearly indicates that in this system the use of the HD group as the side chain diminishes the intermolecular interaction. It is also noted that these d_π , even for PTzNTz-EHBO having the smallest value, is wider than PTzBTs (3.5 \AA) and PNTz4T (3.5 \AA). This is probably explained by the placement of the alkyl groups. In PTzBTs, for example, all the alkyl groups are attached at the 3-position of the thiophene rings neighboring TzTz. In PNTz4T, on the other hand, while the alkyl groups on the thiophene rings neighboring TzTz is attached at the 3-position, those neighboring NTz is attached at the 4-position. This difference could somehow weaken the intermolecular interaction.

In the polymer/ PC₇₁BM blend films fabricated from CB solution (**Figure 7-5b**), PTzNTz-EHBO only showed a clear π - π stacking diffraction along the $\sim q_z$ axis. The PTzNTz-BOBO blend film also showed π - π stacking diffraction, but the intensity was very weak. In contrast, when DIO was used for the film fabrication, all the blend films exhibited a diffraction corresponding to the π - π stacking of the face-on crystallite (**Figure 7-5c**). These GIXD results clearly rationalize the fact that PTzNTz-EHBO-based cells exhibit the best performance when the active layer was fabricated only by CB, and that PTzNTz-EHHD, -BOBO and -BOHD-based cells showed significant improvement in the performance by the association of DIO at the time of active layer fabrication.

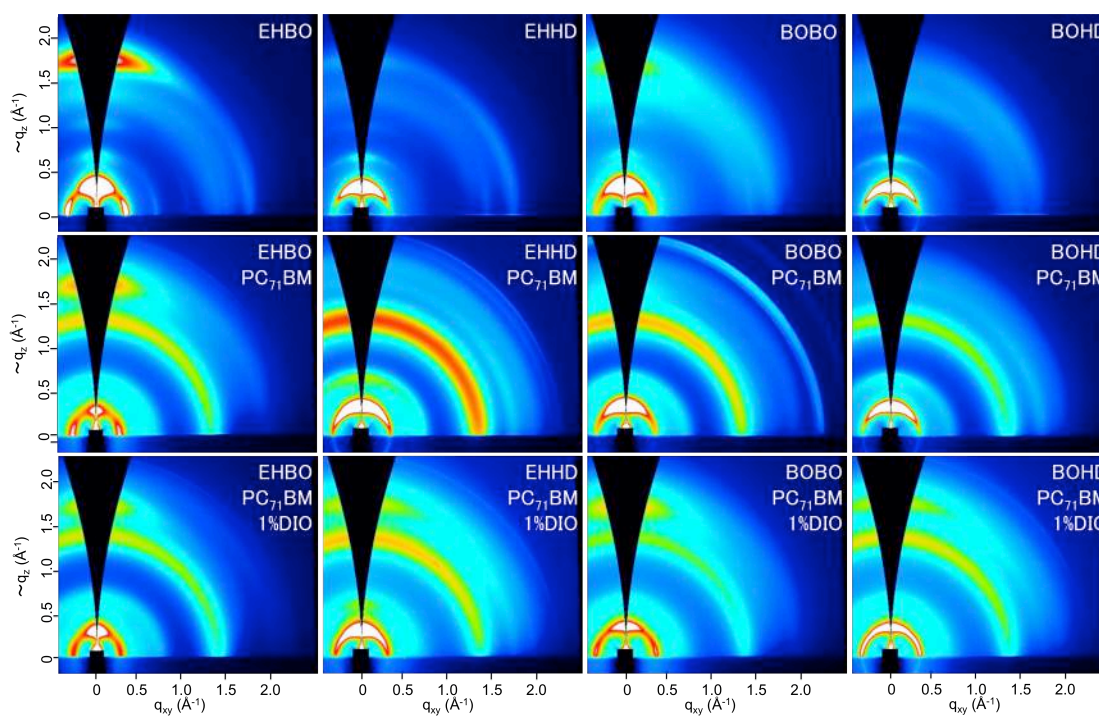


Figure 7-5. 2D-GIXD patterns (a) of the polymer-only film, (b) of the polymer/PC₇₁BM blend films and (c) of the polymer/PC₇₁BM 1% DIO added blend films.

Table 7-3. π -stack, and Lamella and FWHM of PTzNTz-R¹R²

Polymer	d_{Lamella} (Å) ^[a]	d_{π} (Å) ^[a]	FWHM _{Lamella} ^[b] (out-of-plane)	FWHM _{Lamella} ^[b] (in-plane)
-EHBO	16.9	3.69	0.054	0.042
-EHHD	18.5	3.77	0.055	0.087
-BOBO	17.5	3.72	0.089	0.059
-BOHD	18.6	3.80	0.117	0.063
-EHBO/PC ₇₁ BM	17.1	3.69	0.045	0.040
-EHHD/PC ₇₁ BM	18.6	3.78	0.104	0.097
-BOBO/PC ₇₁ BM	18.0	3.73	0.111	0.089
-BOHD/PC ₇₁ BM	19.0	3.81	0.101	0.089
-EHBO/PC ₇₁ BM DIO	17.0	3.69	0.049	0.045
-EHHD/PC ₇₁ BM DIO	18.6	3.78	0.079	0.091
-BOBO/PC ₇₁ BM DIO	17.7	3.73	0.078	0.083
-BOHD/PC ₇₁ BM DIO	18.9	3.81	0.107	0.091

[a] Lamella distance (d_{Lamella}) and π stack distance (d_{π}) are determined from the diffraction profile along the q_z axis (out-of-plane) of the 2D-GIXDs images. [b] Full-Width Half-Maximum (FWHM_{Lamella}) are determined from diffraction profile q_z and q_{xy} axis (in-plane) of 2D-GIXDs images.

I also investigated the morphology of the polymer/PC₇₁BM blend films by the atomic force microscopy (AFM) (**Figure 7-6**). In the blend films fabricated by CB, whereas the PTzNTz-EHBO film formed well phase-separated morphologies, which would enlarge the polymer/PC₇₁BM interface area and thus ensure the charge separation, other polymers, in particular PTzNTz-BOBO and -BOHD, formed large domains that is detrimental for the charge separation. In the DIO-aided blend films, whereas no morphological change was observed for PTzNTz-EHBO, drastic improvement of the morphology was observed for other polymers. These results are also in good agreement with the solar cell performances of the polymers.

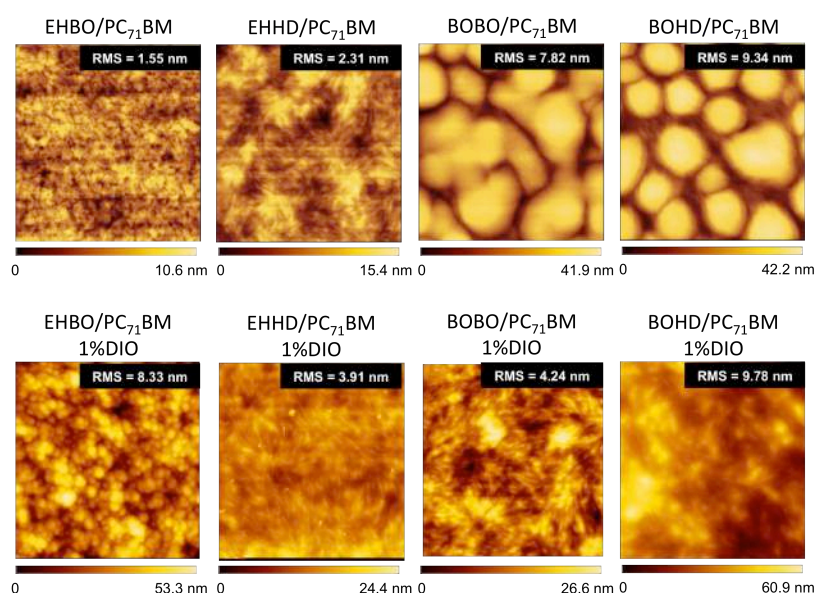


Figure 7-6. AFM image of PTzNTz-R¹R²:PC₇₁BM blend films

I also fabricated OPV device using WO₃ as hole transport layers and investigated OPV stability for PTzNTz-EHHD with and without DIO. Sealed OPV device was monitored with a storage time in 85°C. We compared the degradation trend of the device by evaluating their J_{SC} , V_{OC} , FF, and PCE values as a function of the storage time (**Figure 7-7**). After 1000 hours of storage, we observed J_{SC} and V_{OC} were relatively stable, the FF dropped by 8% and PCE dropped approximately by 8% in PTzNTz-EHBO-based cells with DIO. These results indicate that PTzNTz-EHHD-based cells have high OPV stability and PTzNTzs are desirable polymer for practical application.

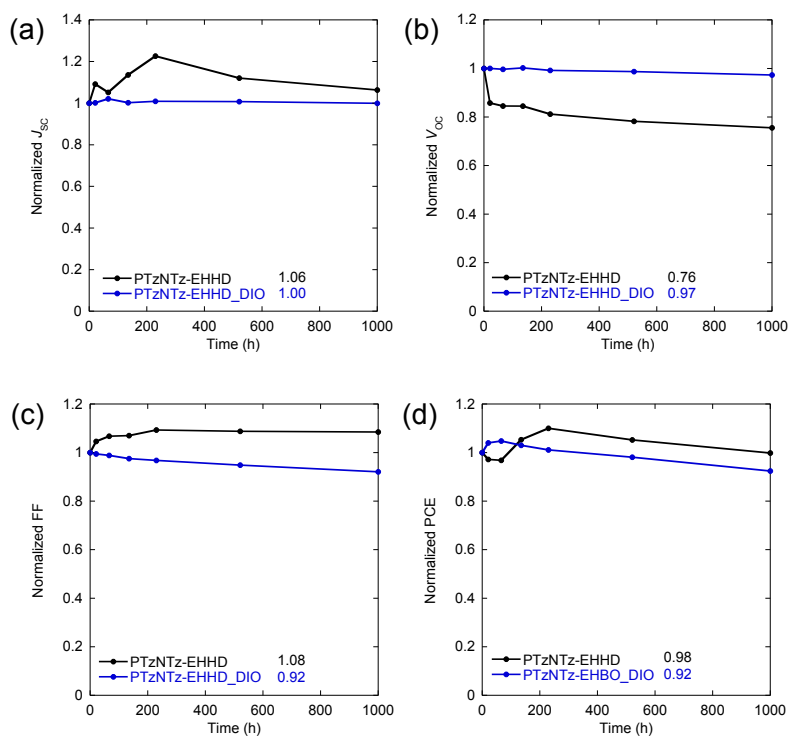


Figure 7-7. Change of organic photovoltaic parameters, (a) J_{sc} , (b) V_{oc} , (c) FF, and (d) PCE, of a PTzNTz-EHHD -based cells with and without of DIO stored 1000 hours at 85°C.

7-3. Summary

New thiazolothiazole-naphthobisthiadiazole-based semiconducting polymers with various side chains have been synthesized and investigated OPV characteristics. PTzNTz-R¹R²s have both of narrow band gap (ca. 1.55 eV) and lower-lying HOMO level (ca. -5.25 eV). Interestingly, PTzNTz-R¹R²s were soluble in warm chlorobenzene in spite of short side chain and could fabricate OPV device in solution process. PTzNTz-EHBO-based cell exhibited PCEs of 9.0% and PTzNTz-BIBO, -EHHD-based cells exhibited PCEs of 8.8%. In addition, PTzNTz-EHHD-based cells have high OPV stability, indicate that PTzNTzs are desirable polymer for practical application.

Experimental

General procedure for polymerization

To a reaction tube equipped with a stirring bar, stannylated monomer (0.10 mmol), brominated monomer (0.10 mmol), Pd(PPh₃)₄ (2.3 mg, 0.002 mmol), and chlorobenzene (5 ml) were added. Then the tube was purged with

argon and sealed. The reaction tube was set into a microwave reactor and heated to 180 °C for 40 min. After cooling to room temperature, the reaction solution was poured into 200 mL of methanol containing 5 mL of hydrochloric acid, and stirred for 5 hours. Then the precipitated solid was subjected to the sequential Soxhlet extraction with methanol, hexane to remove low molecular weight fractions. The residue was then extracted with chloroform, and reprecipitated in 200 mL of methanol to yield dark green solids (yield = 68-89%).

Instrumentation.

UV-vis absorption spectra were measured using a Shimadzu UV-3600 spectrometer. All the potentials were calibrated with the standard ferrocene/ferrocenium redox couple (Fc/Fc^+ : $E^{1/2} = +0.43$ V measured under identical conditions). Photoelectron spectra were measured by using a photoelectron spectrometer, model AC-2, in air (Riken Keiki Co., Ltd). Dynamic force-mode atomic force microscopy study was carried out on a Nanoscope scanning probe microscope system (SII Nanotechnology, Inc.). 2D-GIXD experiments were conducted at the SPring-8 on the beamline BL19B2. The sample was irradiated at a fixed incident angle on the order of 0.12° through a Huber diffractometer. The X-ray energy of 12.39 keV ($\lambda = 1 \text{ \AA}$) the 2D-GIXD patterns were recorded with a 2-D image detector (Pilatus 300K). Samples for the X-ray measurements were prepared by spin-casting the polymer and polymer/ PC_{61}BM solution on the ITO substrate.

Solar Cell Fabrication and Measurement

ITO substrates were first pre-cleaned sequentially by sonicating in a detergent bath, de-ionized water, acetone, and isopropanol at rt, and in a boiled isopropanol bath each for 10 min, and then baked at 120 °C for 10 min in air. The substrates were then subjected to a UV/ozone treatment at rt for 20 min. ZnO layer was prepared by spin-coating (at 5000 rpm) a precursor solution prepared from 0.4 M zinc acetate dihydrate in 0.3M monoethanolamine and 2-methoxyethanol. ZnO substrates were immediately baked in air at 200°C for 30 min then rinsed with acetone, isopropanol and in a boiled isopropanol bath for 10 min. The photoactive layer was deposited in a glove box by spin coating a chlorobenzene solution, containing 5~7 g/L of the polymer sample with respective amount of PC_{71}BM , at 600 rpm for 20 sec, in which the solution was kept heated at 100 °C. The thin films were transferred into a vacuum evaporator connected to the glove box, and the MoOx layer (7.5 nm) and the

Ag layers (100 nm) were deposited sequentially. The active area of the cells was 0.16 cm². *J-V* characteristics for the cells were measured using a Keithley 2400 source-measure unit in nitrogen atmosphere under 1 Sun (AM1.5G) conditions using a solar simulator (SAN- EI Electric, XES-40S1). The light intensity for the *J-V* measurements was calibrated with a reference PV cell (KONICA MINOLTA AK-100 certified at National Institute of Advanced Industrial Science and Technology, Japan). EQE spectra were measured with a Spectral Response Measuring System (SOMA OPTICS, LTD., S-9241).

Reference

- [1] (a) G. Yu, J. Gao, J. C. Hummelen, F. Wudl, A. J. Heeger, *Science* **1995**, *270*, 1789-1791. (b) D. Mühlbacher, M. Scharber, M. Morana, Z. Zhu, D. Waller, R. Gaudiana, C. Brabec, *Adv. Mater.* **2006**, *18*, 2884-2889.
- [2] (a) Y. Liang, Z. Xu, J. Xia, S. Tsai, Y. Wu, G. Li, C. Ray, L. Yu, *Adv. Mater.* **2010**, *22*, E135-E138. (b) H. Y. Chen, J. Hou, S. Zhang, Y. Liang, G. Yang, Y. Yang, L. Yu, Y. Wu, G. Li, *Nature Photon.* **2009**, *3*, 649-653. (c) T. Y. Chu, J. Lu, S. Beaupré, Y. Zhang, J. R. Pouliot, S. Wakim, J. Zhou, M. Leclerc, Z. Li, J. Ding, Y. Tao, *J. Am. Chem. Soc.* **2011**, *133*, 4250-4253. (d) S. C. Price, A. C. Stuart, L. Yang, H. Zhou, W. You, *J. Am. Chem. Soc.* **2011**, *133*, 4625-4631. (e) J. You, L. Dou, K. Yoshimura, T. Kato, K. Ohya, T. Moriarty, K. Emery, C. Chen, J. Gao, G. Li, Y. Yang *Nature Commun.* **2013**, *4*, 1446-1456. (f) H. Chen, Y. Chen, C. Liu, Y. Chien, S. Chou, P. Chou, *Chem. Mater.* **2012**, *24*, 4766-4772. (g) I. Osaka, T. Kakara, N. Takemura, T. Koganezawa, K. Takimiya *J. Am. Chem. Soc.* **2013**, *135*, 8834-8837. (h) S. Zhang, L. Ye, W. Zhao, D. Liu, H. Yao, J. Hou *Macromolecules.* **2014**, *47*, 4653-4659. (i) L. Ye, S. Zhang, W. Zhao, H. Yao, J. Hou *Chem. Mater.* **2014**, *26*, 3603-3605.
- [3] (a) Mühlbacher, D.; Scharber, M.; Morana, M.; Zhu, Z.; Waller, D.; Gaudiana, R.; Brabec, C. *Adv. Mater.* **2006**, *18*, 2884. (b) Hou, J.; Chen, H.-Y.; Zhang, S.; Li, G.; Yang, Y. *J. Am. Chem. Soc.* **2008**, *130*, 16144.
- [4] (a) I. Osaka, G. Sauve, R. Zhang, T. Kowalewski, R.D. McCullough, *Adv. Mater.* **2007**, *19*, 41560-4165. (b) M. Zhang, H. Tsao, W. Pisula, C. Yang, A. Mishra, K. Mullen *J. Am. Chem. Soc.* **2007**, *129*, 3472-3473. (c) M. Wienk, M. Turbiez, J. Gilot, R. Janssen *Adv. Mater.* **2008**, *20*, 2556-2560.
- [5] I. Osaka, M. Saito, T. Koganezawa, K. Takimiya, *Adv. Mater.* **2014**, *26*, 331-338 .
- [6] (a) I. Osaka, M. Shimawaki, H. Mori, I. Doi, E. Miyazaki, T. Koganezawa, K. Takimiya *J. Am. Chem. Soc.* **2012**, *134*, 3498-3507. (b) M. Wang, X. Hu, P. Liu, W. Li, X. Gong, F. Huang, Y. Cao, *J. Am. Chem. Soc.* **2011**,

133, 9638-9641.

[7] H. Sirringhaus, P. J. Brown, R. H. Friend, M. M. Nielsen, K. Bechgaard, B. M. W. Langeveld-Voss, A. J. H. Spiering, R. A. J. Janssen, E. W. Meijer, P. Herwig, D. M. de Leeuw, *Nature*, **1999**, 685-688.

Closing Remarks

In this thesis, I have shown the improvement of photovoltaic properties of polymer-based solar cells, through the design and synthesis of thiazolothiazole-based semiconducting polymers by focusing their ordering structures and electronic structures. I found that the polymer orientation, namely edge-on and face-on, can be altered by and susceptible to the molecular weight, the length and shape of the alkyl side chains and their combination, and blending with fullerene derivatives. I believe here that these parameters affect the intermolecular interaction of the polymer backbones, and in turn affect the polymer orientation. It is likely that polymers tend to orient edge-on when the interaction is strong, and they tend to orient face-on when the interaction become weaker. It should be also noted that in some cases, the polymer orientation is not uniform throughout the film thickness. In the TzTz polymers, although all the polymers formed face-on orientation in the blend film with PC₆₁BM regardless of the primary orientation (in the polymer-only film), in particular, the polymer with the primarily edge-on orientation showed unevenly distributed orientation through the film thickness. The edge-on crystallites were found to be more abundant at the substrate interface. It should be noted that the TzTz polymers also possess higher crystallinity regardless of the orientation. It is also important to note that the polymer orientation motifs significantly affected the properties of the BHJ cells. The BHJ cells that use the polymers with face-on orientation afforded higher J_{SC} with thicker active layers (~300 nm) without a loss of FF, resulting in the increase of PCE. The ability to provide higher PCE with the thick active layers is quite important in terms of processability, and cannot be realized with typical high performance D-A polymers. This means that careful control of the intermolecular interactions by design can control the polymer orientation, and also can improve the solar cell performance..

I found that the introduction of suitable building unit is more effective than the introduction of heteroatom-containing side chains for controlling the electronic structure while maintaining the good ordering structure. PTzNTz synthesized here had both narrow bandgap and lower-lying HOMO level as well as good crystallinity and face-on orientation. Eventually, I realized quite high PCEs of up to 9.0% in PTzNTz-based BHJ cell. It is also noted that PTzNTz-based cells demonstrated very high device stability.

In this thesis, I have shown that I successfully improved the OPV characteristics through the systematic molecular design and synthesis of new semiconducting polymers based on TzTz by focusing on the electronic

structure and, in particular, the ordering structure. Most of the researches in this field have been focused on the control of the electronic structures for the PCE improvement. I therefore believe that these insightful findings regarding the control of polymer orientation and crystallinity by design would open the door for further advances in OPVs.

List of Publication

- 1) “Facile synthesis of [1]benzothieno[3,2-*b*]benzothiophene from *o*-dihalostilbenes” Masahiko Saito, Tatsuya Yamamoto, Itaru Osaka, Eigo Miyazaki, Kazuo Takimiya, Hirokazu Kuwabara, Masaaki Ikeda, *Tetrahedron Letters*, **2010**, 51, 5277-5280
- 2) “One-step synthesis of [1]benzothieno[3,2-*b*]benzothiophene from *o*-chlorobenzaldehyde” Masahiko Saito, Itaru Osaka, Eigo Miyazaki, Kazuo Takimiya, Hirokazu Kuwabara, Masaaki Ikeda, *Tetrahedron Letters*, **2011**, 52, 285-288
- 3) “Drastic Change of Molecular Orientation in a Thiazolothiazole Copolymer by Molecular-Weight Control and Blending with PC₆₁BM Leads to High Efficiencies in Solar Cells” Itaru Osaka, Masahiko Saito, Hiroki Mori, Tomoyuki Koganezawa, Kazuo Takimiya, *Advanced materials*, **2012**, 24, 425-430
- 4) “Thiophene-Thiazolothiazole Copolymers: Significant Impact of Side Chain Composition on Backbone Orientation and Solar Cell Performances” Itaru Osaka, Masahiko Saito, Tomoyuki Koganezawa, Kazuo Takimiya, *Advanced materials*, **2014**, 24, 331-338
- 5) “Small Band Gap Polymers Incorporating a Strong Acceptor, Thieno[3,2-*b*]thiophene-2,5-dione, with P- Channel and Ambipolar Charge Transport Characteristics” Itaru Osaka, Hiroki Mori, Masahiko Saito, Noriko Takemura, Tomoyuki Koganezawa, Kazuo Takimiya, *Journal of Materials Chemistry C*, **2014**, 2, 2307-2312
- 6) “Effect of Oxygen Containing Functional Side Chains on the Electronic Properties and Photovoltaic Performances in a Thiophene-Thiazolothiazole Copolymer System” Masahiko Saito, Itaru Osaka, Tomoyuki Koganezawa, Kazuo Takimiya, *Heteroatom Chemistry*, **2014**, 25, 556-564
- 7) “Enhanced Photovoltaic Performance of Amorphous Copolymers Based on Dithienosilole and Dioxocycloalkene-annelated Thiophene” Jianming Huang, Yutaka Ie, Makoto Karakawa, Masahiko Saito, Itaru Osaka, Yoshio Aso, *Chemistry of Materials*, **2014**, 26, 6971-6978

8) “Thiazolothiazole-based Polymers for Organic Solar Cells” Itaru Osaka, Masahiko Saito, Kazuo Takimiya,
Journal of the Imaging Society of Japan, **2014**, 6, 523-528

謝辞

本研究は広島大学大学院工学研究科応用化学専攻応用有機化学研究室および理化学研究所創発物性科学研究センター創発分子機能研究グループにおいて、2010年から2015年にかけて行われました。研究を行うにあたり瀧宮和男グループディレクター、尾坂格上級研究員、宮碯栄吾博士より懇切丁寧なご指導、ご意見賜りましたことを深く感謝申し上げます。また、共同研究でお世話になりましたJASRIの小金澤智之博士、JX日鉱日石エネルギー株式会社の朝野剛グループマネージャー、劉承訓博士、内田聡一博士、林慎也氏、岡部隆志氏、池田哲氏に感謝いたします。

また、研究室生活でお世話になりました土井伊織博士、樫木友也博士、品村祥司博士、姜明辰博士、中野正浩博士、森裕樹博士、川畑公輔博士、貴志礼文博士をはじめとする諸先輩、同輩、後輩、友人に感謝いたします。

最後に大学生活において経済面、精神面で私を支えてくれた両親に深く感謝いたします。

2015年3月 斎藤慎彦